DISSERTATION ZUR ERLANGUNG DES DOKTORGRADES
DER FAKULTÄT FÜR CHEMIE UND PHARMAZIE
DER LUDWIG-MAXIMILIANS-UNIVERSITÄT MÜNCHEN

Synthesis, Characterization, Scale-up and Investigation of Structure-property Relationships of High Energy Density Materials

Dominik Ernst Dosch

aus

Wertheim, Deutschland

2021

Erklärung:
Diese Dissertation wurde im Sinne von § 7 der Promotionsordnung vom 28. November 2011 von Herrn Professor Dr. Thomas M. Klapötke betreut.

Eidesstattliche Versicherung:
Diese Dissertation wurde eigenständig und ohne unerlaubte Hilfe erarbeitet.

München, den 23 März 2021

_____
Dominik Dosch

Dissertation eingereicht am: 24. März 2021
1. Gutachter: Prof. Dr. Thomas M. Klapötke
2. Gutachter: Prof. Dr. Konstantin Karaghiosoff
Mündliche Prüfung am: 29.04.2021

Danksagung

An erster Stelle gilt mein Dank meinem Doktorvater Prof. Dr. Thomas M. Klapötke für die freundliche Aufnahme in seinen Arbeitskreis und die interessante Themenstellung für meine Promotion. Außerdem möchte ich mich für die stetige finanzielle und fachliche Unterstützung meiner persönlichen Forschungsvorhaben sowie für seine Begeisterung für die Erforschung hochenergetischer Materialien bei ihm bedanken und nicht zuletzt für das Vertrauen, welches er beim EURENCO Projekt in mich und meine Fähigkeiten als Chemiker gesetzt hat.

Herrn Prof. Dr. Konstantin Karaghiosoff danke ich nicht nur für die freundliche Übernahme des Zweitgutachtens dieser Dissertation, sondern auch für seinen unermüdlichen Einsatz für das IT-Team und das X-Ray Team. Seine Anmerkungen und Korrekturen zu diversen Publikationen waren für mich von unschätzbarem Wert und durch seine freundliche und offene Art konnte er mich auch in schwierigen Phasen immer motivieren. Dafür möchte ich dir meinen Dank aussprechen Conny! Ich hoffe, dass das IT Team auch bei künftigen Raubzügen zum LRZ weiterhin fette Beute macht.

Der Prüfungskommission, bestehend aus Prof. Dr. T. M. Klapötke, Prof. Dr. K. Karaghiosoff, Prof. Dr. H. C. Böttcher, Prof. Dr. A. Kornath, Prof. Dr. I. Ivanović-Burmazović und Prof. Dr. O. Trapp danke ich für Ihre Zeit und die Bereitschaft zur Bildung der selbigen.

Herrn Dr. Burkhard Krumm danke ich für die gute Betreuung beim EURENCO Projekt, für interessante Anregungen und Diskussionen auch fernab der Chemie, sowie für die Aufnahme zahlreicher NMR Spektren.

Bei Herrn Dr. Jörg Stierstorfer möchte ich mich vor allem dafür bedanken, dass er mich bei verschiedenen Projekten sowohl fachlich als auch persönlich herausfordern konnte und mir auf diese Weise eine große Hilfe in meiner Entwicklung als Wissenschaftler war. Durch seine unnachahmliche Art, ist er ein elementarer Bestandteil dieses Arbeitskreises und durch niemanden zu ersetzen.

Frau Irene Scheckenbach danke ich für Ihr herausragendes organisatorisches Talent und Ihre Unterstützung bei sämtlichen bürokratischen Angelegenheiten. Eine gute Seele wie Sie im Arbeitskreis zu haben ist Gold wert und ich hoffe für meine Nachfolger, dass sie dieser Funktion noch lange nachgehen kann.

Allen während meiner Promotionsdauer anwesenden Kollegen im Arbeitskreis danke ich für die stets sehr gute und freundschaftliche Arbeitsatmosphäre. In möchte mich bei Herrn Dr. Marco Reichel für die gute Zusammenarbeit bei diversen Projekten und Publikationen bedanken. Allen Mitstreitern aus Labor D.3.103 gilt mein besonderer Dank, namentlich Stefan Huber, Alicia Dufter-Münster, Christin Kirst, Alexander Schweiger, Jonathan Tietze und Dr. Sarah Linert. Wir hatten eine großartige Zeit im Labor und ich hoffe, dass euch die Marschmusikmontage, die Cantina-Band, Sputnik Booster, das Bananaphone und der YEE-Dino in Zukunft fehlen werden.

Bei meinen Mentoren aus den beiden Abschlussarbeiten und meinen F-Praktika möchte ich mich ebenfalls bedanken, namentlich bei Dr. Tomasz Witkowski, Dr. Johann Glück, Dr. Johannes Broichhagen, Dr. Oliver Pham-Schönwetter und Dr. Arno Hahma. Ihr alle habt auf eure individuelle Art und Weise einen Beitrag dazu geleistet meine präparativen und fachlichen Fähigkeiten auszubauen und zu verfeinern – Dafür ein herzliches Dankeschön!

Mein weiterer Dank gilt meinem F-Praktikanten Daniel Bauer sowie meiner Bachelorandin Veronika Fuchs. Durch ihre präparativen Tätigkeiten und die Mitarbeit konnten beide in erheblichem Maße zu meiner letzten Publikation für diese kumulative Dissertation beitragen. Beide werden ihren Weg in der Wissenschaft erfolgreich gehen und ich schätze sie als ausgezeichnete Chemiker & Kollegen.

Bei meinen besten Freunden Max Born, Sebastian Birkholz, Johannes Guilleaume, Christoph Dengel, Thomas Metz, Tobias Fäth und Jörn Dietze möchte ich mich ebenso für Ihre Unterstützung bedanken. Ein Mensch ist nur dann wirklich reich gesegnet, wenn er Freunde wie euch hat, die ihm stets zur Seite stehen, in guten wie in schlechten Tagen!

Nicht zuletzt gilt mein Dank meiner Familie, im Besonderen meinen Eltern Ernst und Gisela, sowie meinen Geschwistern Isabell und Christopher. Durch euren unermüdlichen Glauben daran, dass ich alles schaffen kann was ich mir vornehme und durch euren Einsatz für meinen persönlichen Bildungsweg bin ich euch für immer zum Dank verpflichtet. Nicht zu vergessen sind meine Großeltern Irmgard und Bruno, meine Tante Helga, mein Patenonkel Edgar meine „Kosengine“ Alice und die übrigen Ludwigshäfner. Ihr alle seid mir ein einzigartiger Rückhalt im Leben und habt mich von Kindesbeinen an mit allen euch zur Verfügung stehenden Mitteln gefördert und entwickelt. Ohne euren jeweiligen Einfluss, wäre ich heute nicht der Mensch der ich bin und dafür möchte ich mich bei euch allen bedanken, denn ohne euren individuellen Anteil wäre diese Arbeit nicht möglich gewesen.

Table of Contents

1 Introduction

1.1 Energetic Materials

1.1.1 Classification of high energy density materials (HEDMs)

The research in the field of high energy density materials (HEDMs) with improved properties for various applications is an ongoing project in many research groups around the globe. The definition of a HEDM is “a compound or mixture of substances, which contains both the fuel and oxidizer and which reacts readily under the release of energy and gas”.[1] The subgroup of explosives is further defined as “A material in a metastable state, which has the potential for a fast chemical reaction, which releases a large amount of energy, heat, and pressure. No external reaction partners are required for this reaction, which starts under the influence of an external stimulus such as impact, friction, spark, shock, flame or heating”.[1] Depending on the desired application of an energetic material, the research is always focused on the improvement of various key characteristics, which differ for each application. Therefore, HEDMs are categorized into five major classes with multiple subclasses (**Figure 1**).[1,2]

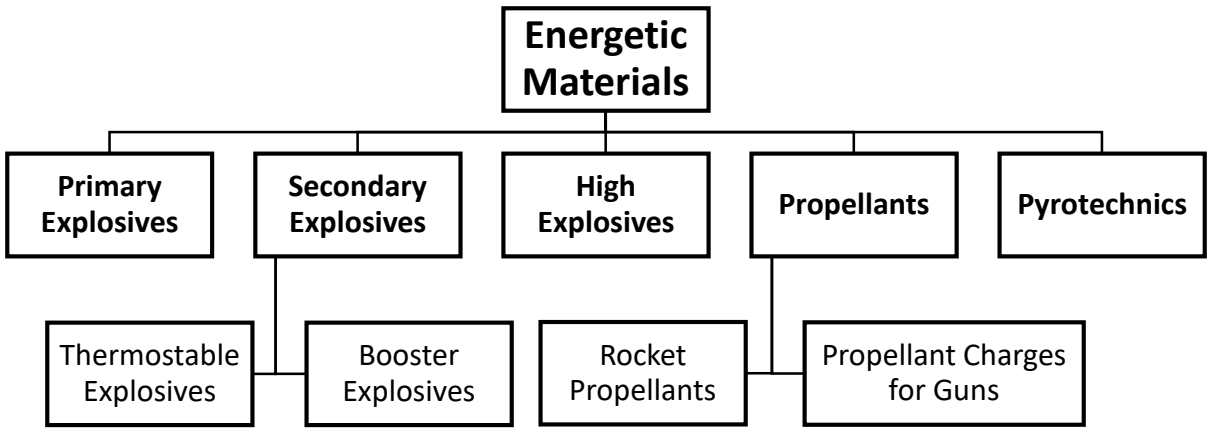

Figure 1. Categories and important subclasses of HEDMs.

Primary explosives, also known as “*primers*” are almost exclusively applied to generate an initial shock wave for the subsequent initiation of booster explosives, secondary explosives, or high explosives.[1-4] For this purpose, primary explosives need to undergo a very rapid deflagration to detonation transition to guarantee a safe initiation of the less sensitive materials. Primary explosives are significantly more sensitive towards external stimuli (i.e. heat, impact, friction, electrostatic discharge) than secondary explosives and in general, they show a lower performance when compared to secondary and high explosives (i.e. detonation velocity, detonation pressure, detonation temperature).[1-4]

Secondary explosives are significantly less sensitive to external stimuli such as impact, friction, electrostatic discharge or heat, but exhibit a higher performance than primary explosives.[1,2,4] They are applied as main charges and/or booster explosives to initiate almost or completely insensitive high explosives. The research in the field of secondary explosives is focused on the following key areas: an increase of the performance of explosives, the development of heat-resistant explosives, and the development of low sensitivity explosives and more eco-friendly materials.[1,4]

High explosives, also known as blasting agents – are a category of explosives that are almost or completely insensitive towards external stimuli like impact, friction, or electrostatic discharge. They require a booster charge (i.e. PETN) to enhance the shockwave of a primary explosive for successful initiation.[1-4] This category of explosives exhibits a relatively large critical diameter and can therefore not be applied in small charges.[2] They are mainly applied in large-scale mining and construction operations or special sectors like oil drilling or stage separation in space applications. Examples are ammonium nitrate fuel mixtures (ANFO), slurry explosives, and special materials like HNS, NONA, or TATB.[4,5]

Propellants are applied for the acceleration of munition (gun propellants) or for the production of thrust in rocket applications (rocket propellants).[1,2,4] For those desired effects a controlled sub-sonic deflagration/decomposition of the material is required and a detonation is not desired.[1,2,4] In contrast to explosives which are mostly homogenous compounds that combine oxidizer and fuel in one molecule, most propellant formulations are heterogenic mixtures of various components (oxidizer, fuel, binder, additives, etc.). Depending on the number of components and the individual composition of the formulation propellants can be further divided into different subcategories (i.e. multi-base powders and composite propellants).

Pyrotechnics are energetic compositions that are applied to generate a wide range of various effects such as heat, light, sound, gas, or smoke.[1,2,4] Usually they undergo subsonic deflagration/decomposition and detonations are unwanted for this class of HEDM.[1,2,4] Similar to propellants, most pyrotechnic formulations are heterogenic mixtures of various components, which are required to achieve the desired effect. However, all pyrotechnic mixtures comprise an oxidizer and at least one fuel to sustain the thermal decomposition of the formulation.

Further details on the requirements for the HEDM classes covered by the research and results within this dissertation are given in the following sections as well as in the introductions of the individual publications.

1.1.2 Thermostable secondary explosives & booster explosives

As stated in the short introduction, the four general goals for the development of new secondary explosives are improvements regarding performance, thermal stability, "green" chemistry, and sensitivity.[1,6] The optimal material would combine all the goals in one molecule. However, especially the combination of higher performance and a low sensitivity proves to be a challenge, as these properties often are contradictory.[7]

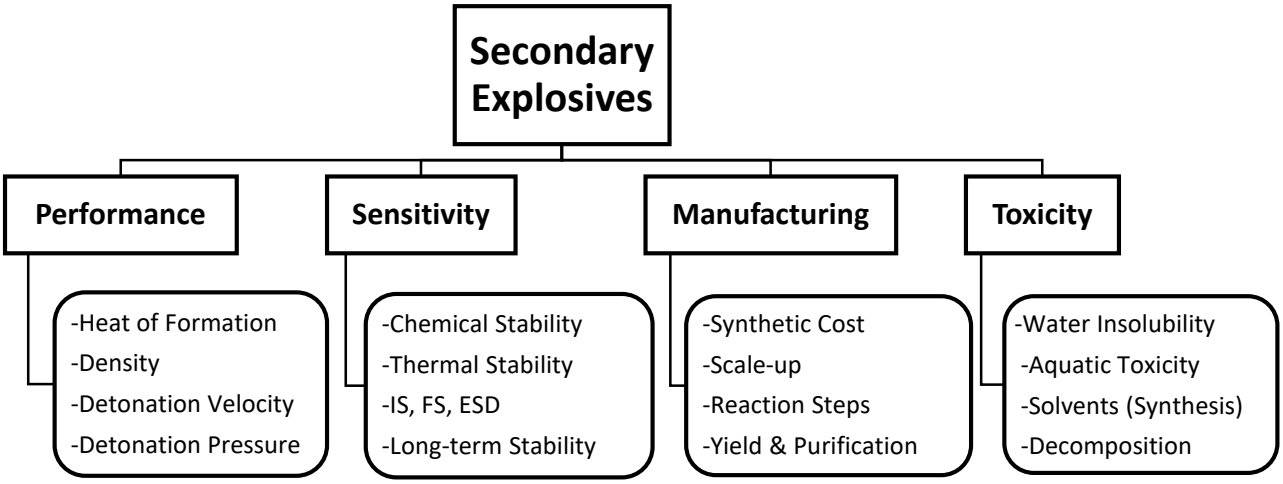

Figure 2. The key requirements for the development of new secondary explosives.

Regarding the performance of a new material for the application as a thermostable secondary explosive or booster explosive the following requirements should be met:

• detonation velocity ≥8500 m s^{-1}

• detonation pressure ≥340 kbar

• heat of formation ≥6000 kJ kg^{-1}

• thermal stability ≥150 °C (booster); ≥250 °C (thermostable)

• low sensitivities (IS ≥7 J, FS ≥120 N, ESD ≥200 mJ)

• convenient, scalable & cost-effective synthesis with less than 6 synthetic steps

• hydrolytic stability

• compatibility with conventional binders and other explosives

In recent times, the environmental and toxicological aspects in terms of "green" chemistry gain more and more relevance. The state-of-the-art materials all exhibit various drawbacks regarding toxicity and environmental compatibility. One of the most commonly applied secondary explosives RDX has been proven to be a carcinogenic material according to EPA.[8] In addition, its decomposition products are highly toxic towards plants, microorganisms, and smaller organisms.[9-11]

Another very common secondary explosive is TNT, which is applied as a melt-castable explosive. It exhibits similar problems to RDX, as it is also carcinogenic and the decomposition products are toxic and associated with problems regarding the liver and the blood system.[12] Another very important secondary explosive is pentaerythritol tetranitrate (PETN). Due to its rather low sensitivity (IS: 4 J, FS: 73 N, ESD: 30 mJ) it is applied as a booster explosive for the initiation of completely insensitive high explosives like TATB or HNS.[12-16] It is applied because of an easy synthesis and good performance, however, the material exhibits a rather low melting point of 142 °C and it is considered toxic and causes problems for the blood system.[12-17] To mitigate the problems regarding sensitivity, PETN is often applied in a mixture with TNT (pentolite).[1] The research regarding new booster explosives is focused on new materials, which show lower sensitivities and higher thermal stability while maintaining the ability to transfer the weak initial shockwave of a primary explosive to an inert high explosive.

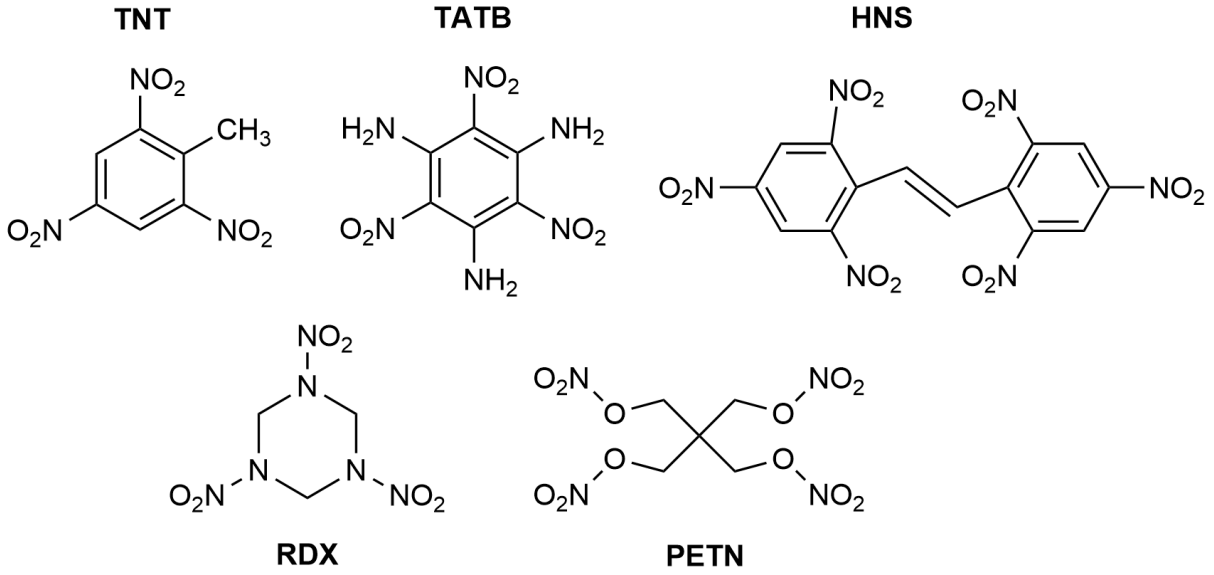

Figure 3. The chemical structure for the most important secondary explosive materials of the past.

Newer developments in the field of secondary explosives follow two main strategies. The first strategy is the introduction of caged compounds which contain ring-strain energy that contributes to the energy released upon detonation (i.e. CL-20 or ONC).[1,18-19] However, the synthesis of those caged compounds comprises multiple reaction steps and therefore they are very expensive and not very common in application. The second strategy focuses on the application of nitrogen-rich energetic heterocycles (i.e. LLM116, TKX50, or TKX55).[20-22] Those materials offer the advantage of a more facile synthesis and therefore a lower price, in combination with similar performance and low sensitivity values.

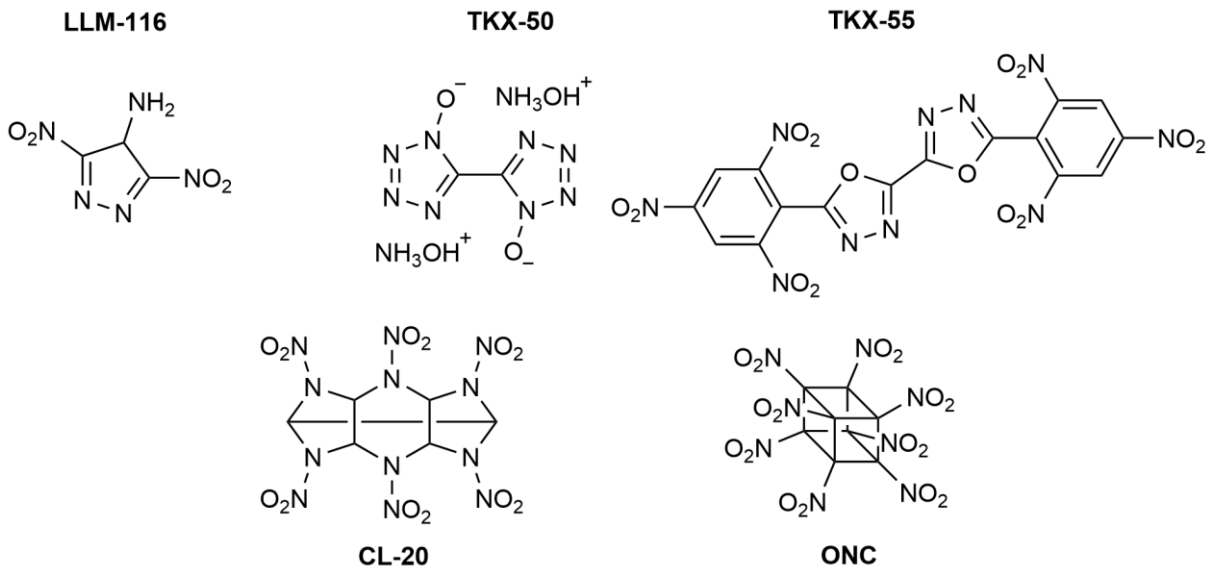

Figure 4. Overview of recent developments in the field of secondary explosives.

Despite the progress already made in the last 50 years, the strife for better secondary explosives for the application as booster explosives, main charges, and high thermostable materials is an ongoing process.

1.1.3 High energy density oxidizers (HEDOs) for propellants

Since the early 1940s, the cheap, accessible, and well-performing material ammonium perchlorate (AP) has been applied as the most important high energy-dense oxidizer (HEDO) for solid rocket composite propellants. The material has maintained relevance until today, as even the newly developed p120 rocket booster for Ariane 6 and Vega E and C are based on AP.[23-25] Despite its various advantages for application, the negative effects on the environment became a focal point for research around the globe. AP is considered to be carcinogenic, mutagenic, and toxic upon long-term exposure.[1, 26-27] Another enormous problem is the fact, that the perchlorate anion itself can compete with iodine for the uptake into the thyroid gland at the sodium/iodide symporter.[28-30] The subsequent interaction with the thyroid hormone synthesis proved to be a problem because it is a crucial mechanism for the development of vertebrates, including unborn and small children.[31-32] Various detrimental effects of AP on aquatic organisms, i.e. an uncommon pigmentation and the delay of the metamorphosis of amphibian embryos was observed in correlation with perchlorate contaminated water.[33] Because the material exhibits a very high solubility, chemical stability, and persistence it is assumed to be widely distributed within groundwater systems,[32] which is directly correlated to the application and release of AP predominately by military operations, aerospace programs, and defense companies.[34-35] This leads to enormous costs of several billion dollars per year to remediate surface and groundwater in the USA.[36]

Figure 5. Lift-off picture of the Ariane 5 utilizing AP-based booster rockets.[37]

The United States Environmental Protection Agency (EPA) released fact sheets regarding the perchlorate levels in drinking water and set a reference of 0.7 µg L^{-1} per kg as the allowed maximum contamination in 2014.[26]

For the European Union and its REACh regulation program (Registration, Evaluation, Authorization, and Restriction of Chemicals), AP has been registered since 2011 with annual production ranging between 1000 t and 10000 t.[38] Since AP is under assessment as an endocrine disruptor it has been listed in the Community Rolling Action Plan (CoRAP) by the Public Activities Coordination Tool (PACT), which coordinates the evaluation of concerning substances.[38-40] The combustion of common AP-based composite solid rocket propellants generates a large quantity of gaseous products, especially CO, CO_2, H_2, H_2O, Al_2O_3 and HCl are produced and emitted into the environment.[1] The corrosive gas HCl is one of the main reasons for the formation of acid rain as well as for the ozone layer depletion.[41]

Multiple research programs have been conducted in the past to substitute AP with a sustainable, chlorine-free alternative. At the moment the two materials ammonium nitrate (AN) and ammonium dinitramide (ADN) are regarded as the most promising AP replacements for HEDO applications.[1] However, both materials exhibit their own drawbacks i.e. hygroscopicity and phase transitions within the desired temperature range for applications in the case of AN and a low decomposition point of 133°C and a detrimental incompatibility with HTPB for ADN.[42-44] Recent projects, therefore, investigated the possibility to combine both HEDOs and achieved some promising results.[23]

Despite being chlorine-free and more eco-friendly, novel HEDOs for composite rocket propellants need to fulfil further requirements:[1,45]

• high density, best case ≥2 g cm^{-3}

• high oxygen balance, Ω_{CO} ≥34% (AP)

• high thermal stability, melting point ≥150 °C

• lower sensitivity towards external stimuli than PETN (IS > 4 J, FS > 80 N)

• low vapor pressure

• convenient, cost-effective synthesis with a minimum number of synthetic steps

• compatibility with various binders (GAP, HTPB, etc.)

• high enthalpy of formation

• long term stable and storable (high shelf-life).

Further research in the field of HEDOs is necessary to match those requirements for a replacement of AP, which is still the most important and most commonly applied oxidizer for composite propellants. Hopefully less toxic and more environmentally benign alternatives can be developed in the future. One potential replacement which is currently under investigation is the compound tris(2,2,2-trinitroethyl) orthoformate TNEF.

1.2 Hirshfeld Surface Analysis

1.2.1 Hirshfeld Surface Analysis (HSA) – A short Introduction

Based on Hirshfelds Stockholder partitioning scheme a novel concept for the definition and visualization of a molecule in a crystal structure was developed and communicated in 1997 by *Spackmann et al.*.[46-47] Subsequently their definition was applied as a new method for crystal analysis and crystal engineering and after further refinements, it was officially named ”Hirshfeld Surface Analysis” (HSA) in 1998.[48] By applying this partitioning model the crystal structure of a molecule is separated into promolecules and procrystals based on the respective electron densities for each region of each molecule in the structure. This creates filled sections as well as voids, which correlate with the distances between the individual atoms of the molecule and its neighbors. This can be visualized with a 3D Isosurface, that represents all interactions between the individual promolecules and therefore the position of all close contacts between all atoms of the crystal. The method is based on experimental crystal structure measurements and offers valuable insight into intermolecular interactions and the distribution and intensity of close contact interactions in the respective crystal structure.

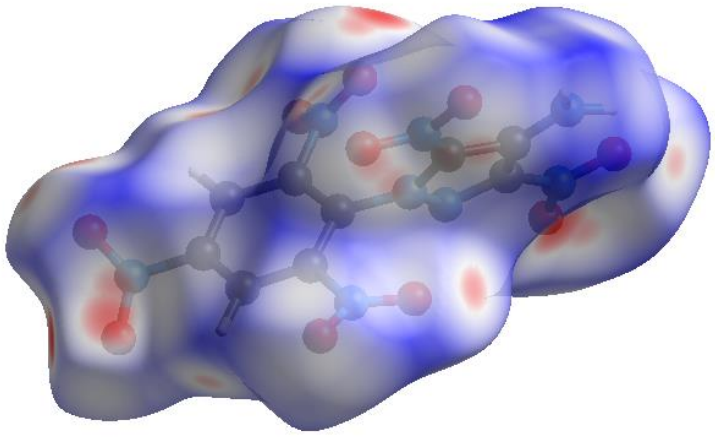

Figure 6. Representation of the Hirshfeld surface of PicADNP.

After the initial success and spread of the method within the crystal engineering community, the complicated 3D Surface provided by HSA was complemented with 2D Fingerprint plot analysis in 2002, which significantly improved and simplified the visualization of intermolecular close contacts in a crystal.[49] By plotting the distance (in *Å*) of any atom at any point on the calculated Hirshfeld surface towards the next internal neighbor (d_i) against the distance of the same spot towards the next external neighbor (d_e) a 2D "heatmap" of the surface – the so-called "Fingerprint plot" can be generated. This visualization resembles every spot of the calculated surface, but it has the advantage, that it can be represented in printed form. Besides, it is a fast and easy tool for the assessment of intermolecular interactions, their quantity, and their relative strength.

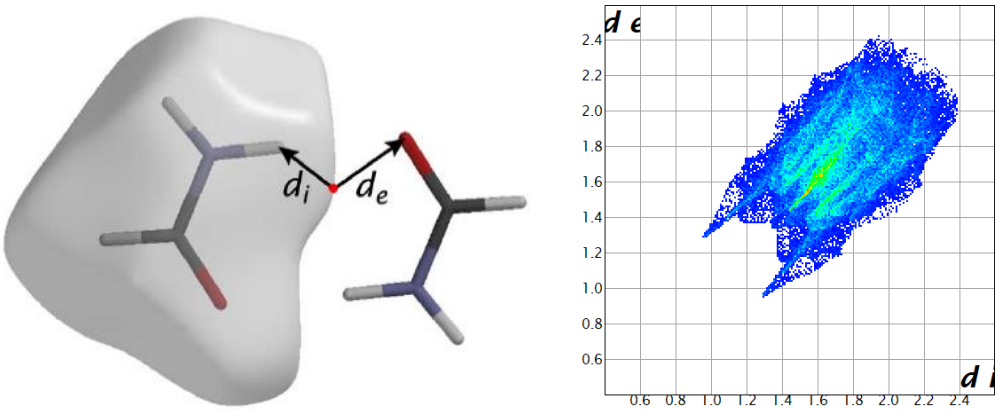

Figure 7. Visualization of d_i and d_e for a hydrogen-bonded dimer of urea[49] and the 2D Fingerprint plot of PicADNP.

In the next step, the development of a software package for both forms of analysis was undertaken by the group of *Spackmann et. al.* between 2004 and 2005.The result of this work is the Crystal Explorer software, which has been continuously improved since then. It can be utilized for close contact analysis.[50] By applying the current version of

Crystal Explorer to a fully solved .cif-file, various important interactions in the crystal can be easily visualized and quantified. The software includes useful features like crystal surface mapping and close contact analysis and therefore resembles a valuable tool for crystal engineering and material design.[51]

The first application of Hirshfeld surface and Fingerprint plot analysis for the analysis and development of energetic materials took place in 2014 when *Zhang et. al.* introduced the method to the energetic materials community.[52] In recent times various groups and authors like *Gozin*[53], *Klapötke*[54], and *Shreeve*[55] started using the Crystal Explorer software and the general methodology for the investigation and design of new energetic materials. One common goal of the mentioned groups is a deeper understanding of the structure-property relationships of energetic materials, especially concerning sensitivity towards mechanical and thermal stability, which is directly correlated to the close-contacts in the crystal structure. A better understanding of those interactions could lead to the detection of advantageous motifs and/or building blocks and therefore to an improvement for the design of new high energetic materials concerning performance and safety. A key advantage of the HSA method is the fact, that one single crystal of material is sufficient to perform the analysis, as the method is solely based on the crystal structure. This increases the safety of energetic material researchers and could lower the cost for research, as no large quantities of new material have to be prepared to get the first idea of a material's sensitivity towards external stimuli.

1.2.2 Safety assessment of energetic materials via HSA

The initial works of *Zhang et. al.*[52,55] as well as the more recent works of *Klapötke*[54,56], *Shreeve*[55], and *Gozin*[53] have shown first general trends for various subgroups of energetic materials regarding their structure-property relationships. One common denominator for all sensitive energetic materials is a Hirshfeld surface exhibiting red dots (representing close-contacts), which are not arranged in a slideable plane, but in a 3D network between the individual layers. When a material with such characteristics is exposed to an external mechanical stimulus like friction or impact the stabilizing interlayer interactions are destroyed. This results in strains, destabilization, and interlayer repulsion, which can subsequently result in the decomposition of the material when the generated strain energy surpasses the energy required to break the weakest bond in the molecule.

Regarding the 2D Fingerprint plots, different categories for stabilizing, destabilizing, and “neutral” interactions could be established for molecules containing energetic moieties like nitro-, nitramino- or azido-groups. Depending on their relative strength and occurrence an assessment of the sensitivity of a material is possible, especially in comparison to other representatives of the respective molecular group (i.e. heterocycles, trinitrobenzenes, etc.). Oxygen-oxygen, nitrogen-nitrogen, nitrogen-oxygen, and hydrogen-hydrogen interactions are considered destabilizing, and

therefore a high occurrence and/or a high relative strength in a crystal is indicative for a sensitive material. In contrary, hydrogen-oxygen and hydrogen-nitrogen interactions (hydrogen bonds) are considered stabilizing and therefore a high occurrence and/or a high relative strength of those interactions is indicative of a less sensitive or insensitive energetic material. Carbon-carbon interactions can be stabilizing in case of π-π or π-C interactions between different layers of molecules in the crystal (π-stacking).

By applying the mentioned methods to further subgroups of energetic materials and subsequent analysis of the HSA results with a global database, an even deeper insight into structure-property-relationships could be gained in the future. Hopefully, this will enable further improvements regarding the search for advantageous structural motifs and for the molecular and crystal design of novel energetic materials.

1.3 Motivation and Objectives

The main objectives of this thesis are the synthesis, characterization, and scale-up of the manufacturing process for materials of different HEDM-classes. The prepared compounds were investigated as potential replacements for state-of-the-art materials of the corresponding HEDM-class like ammonium perchlorate (HEDO), PETN (Booster Explosive), and TNT (Secondary Explosive). For the development and scale-up of syntheses for energetic materials, it is of great importance to focus on compounds that combine the desired properties for application with a cost-effective, high-yielding, and a more environmentally benign manufacturing process.

There is a great need for methods, which can be used for the preliminary testing of promising energetic materials on a small scale for both safety and cost reasons. Therefore, it was another key objective of this thesis to establish Hirshfeld surface analysis (HSA) and 2D Fingerprint plotting as a tool for the assessment of sensitivities for new energetic materials. HSA is a feasible process for the identification, quantification, and comparison of favorable structural motifs for energetic materials research. This goal is especially important because a better insight into structure-property relationships of energetic materials will lead to a better material design in the future.

1.4 References

[1] T. M. Klapötke, *Chemistry of High-Energy Materials*, 5th ed., De Gruyter, Berlin, Germany, **2019**.

[2] J. P. Agrawal, *High Energy Materials Propellants, Explosives and Pyrotechnics*, 1st ed., Wiley-VCH, Weinheim, Germany, **2010**.

[3] R. Matyáš, J. Pachmáň, *Primary Explosives*, Springer, Berlin, Germany, **2013**.

[4] R. Meyer, J. Köhler, A. Homburg, *Explosives,* 7th ed., Wiley-VCH, Weinheim, Germany, **2016**.

[5] E. G. Mahadevan, *Ammonium Nitrate Explosives for Civil Applications: Slurries, Emulsions and Ammonium Nitrate Fuel Oils*, Wiley-VCH, Weinheim, Germany, **2013**.

[6] D. Fischer, T. M. Klapötke, M. Reymann, J. Stierstorfer, *Chem. Eur. J.* **2014**, *20*, p. 6401−6411.

[7] H.-H. Licht, *Propellants, Explos., Pyrotech.* **2000**, *25*, p. 126–132.

[8] United States Environmental Protection Agency (EPA), *Technical Fact Sheet - Hexahydro-1,3,5-trinitro-1,3,5-triazine (RDX)*, **2014**.

[9] Ageny for Toxic Substances and Disease Registry (ATSDR), *Toxicological Profile for RDX*, **2012**.

[10] P. Y. Robidoux, J. Hawari, G. Bardai, L. Paquet, G. Ampleman, S. Thiboutot, G. I. Sunahara, *Arch. Environ. Contam. Toxicol. **2002**, 43*, p. 379–388.

[11] E. L. Etnier, *Regul. Toxicol. Pharmacol.* **1989**, *9*, p. 147–157.

[12] United states States Environmental Protection Agency (EPA), *Technical Fact Sheet - 2,4,6-Trinitotoluene(TNT)*, **2012**.

[13] T. M. Klapötke, *Energetic Materials Encyclopedia*; De Gruyter: Berlin/Boston, Germany/USA, **2018**.

[14] T. M. Klapötke, G. Lemarchand, T. Lenz, M. Mühlemann, J. Stierstorfer, R. Weber, In *PETN - a sensitivity study*, New Trends in Research of Energetic Materials, Pardubice, **2020**.

[15] J. Šelešovsky, J. Pachmaň, M. Hanus, M. In *Proceedings of the Sixth Seminar New Trends in Research of Energetic Materials*, New Trends in Research of Energetic Materials, Pardubice, **2003**, p. 309–321.

[16] R.K. Wharton, J. A: Harding, *J. Energ. Mater.* **1993,** *11* (1), p. 51-65.

[17] https://gestis.dguv.de/data?name=490092 (accessed 17.03.21).

[18] A. T. Nielsen, A. P. Chafin, S. L. Christian, D. W. Moore, M. P. Nadler, R. A. Nissan, D. J. Vanderah, R. D. Gilardi, C. F. George, J. L. Flippen-Anderson, *Tetrahedron* **1998**, 54, *39*, p. 11793-11812.

[19] M.-X. Zhang, P. E. Eaton, R. Gilardi, *Angew. Chem., Int. Ed.* **2000**,39, *2, p.* 1433-7851.

[20] S. Ek, N. V. Latypov, *J. Heterocyclic Chem.* **2014**, 51, *6*, p. 1621-1627

[21] N. Fischer, D. Fischer, T. M. Klapötke, D. G. Piercey, J. Stierstorfer, *J. Mater. Chem.* **2012**, *22*, p. 20418–20422.

[22] T. M. Klapötke, T. G. Witkowski, *ChemPlusChem* **2016**, *81*, p. 357–360.

[23] N. Wingborg, M. Skarstind, M. Sjoblom, A. Lindborg, M. Brantlind, J. Johansson, S. Ek, M. Liljedahl, J. Kjellberg, In *7th European Conference for Aeronautics and Space Sciences(EUCASS)*, EUCASS, Milan, **2017**.

[24] Davenas, *Solid Rocket Propulsion Technology*, Pergamon Press, Oxford (UK), **1993**.

[25] P120c static Fire Test, https://blogs.esa.int/ariane6/2018/07/25/p120c-static-fire-test/ (accessed 17.03.21).

[26] EPA.gov – United States Environmental Protection Agency, Technical Fact Sheet - Perchlorate, EPA 505-F-14-003 01.2014, (accessed 17.03.21).

[27] C. M. Steinmaus, *Curr. Environ. Health Rep.* **2016**, *3*, p. 136–143.

[28] A. Srinivasan, T. Viraraghavan, *Int. J. Environ. Res. Public Health* **2009**, *6*, p. 1418–1442.

[29] Wolff, *Pharmacol. Rev.* **1998**, *50*, p. 89–105.

[30] C. Portulano, M Paroder-Belenitsky, N. Carrasco, *Endocr. Rev.* **2014**, *35*, p. 106–149.

[31] E. D. McLanahan, J. L. Campbell, Jr., D. C. Ferguson, B. Harmon, J. M. Hedge, K. M. Crofton, D. R. Mattie, L. Braverman, D. A. Keys, M. Mumtaz, J. W. Fisher, *Toxicol. Sci.* **2007**, *97*, p. 308–317.

[32] EPA, *Health Risk Reduction and Cost Analysis of the Proposed Perchlorate National Primary Drinking Water Regulation*, **2019**.

[33] The Effects of Ammonium Perchlorate on Reproduction and Development of Amphibians, https://apps.dtic.mil/dtic/tr/fulltext/u2/a495519.pdf (accessed 17.03.21).

[34] E. T. Urbansky, *Environ. Sci. And Pollut. Res.* **2002**, *9*, p. 187–192.

[35] W. Trumpolt, M. Crain, G. D. Cullison, S. J. P. Flanagan, L. Siegel, S. Lathrop, *Remediation* **2005**, *16*, p. 65–89.

[36] P. Waldmann, *The Wall Street Journal, Perchlorate Runoff Flows To Water Supply of Millions,* New York, **2002** (accessed 17.03.21).

[37] https://commons.wikimedia.org/wiki/File:Ariane5_VA221_liftoff2.jpg (accessed 17.03.21).

[38] ECHA – European Chemicals Agency, https://echa.europa.eu/substance-information/-/substanceinfo/100.029.305, (accessed 17.03.21).

[39] ECHA – European Chemicals Agency, https://echa.europa.eu/information-on-chemicals/evaluation/community-rolling-action-plan/corap-table/-/dislist/details/0b0236e1807e9ab1, (accessed 17.03.21).

[40] ECHA – European Chemicals Agency, https://echa.europa.eu/pact, (accessed 17.03.21).

[41] N. Kubota, *Propellants and Explosives*, Wiley-VCH, Weinheim (Germany), **2002**.

[42] A. Larsson, N. Wingborg, *Green Propellants Based on Ammonium Dinitramide (ADN)*,INTECH Open Access Publisher, Rijeka (Croatia), **2011**.

[43] C. Oommen, S. R. Jain, *J. Haz. Mater.* **1999**, *67*, p. 253–281.

[44] S. Lobbecke, H. H. Krause, A. Pfeil, *Propellants, Explos., Pyrotech.* **1997**, *22*, p. 184–188.

[45] NATO, *Manual of Data Requirements and Tests for the Qualification of Explosive Materials for Military Use*, **2003**.

[46] F. L. Hirshfeld, *Theoretica chimica acta* **1977**, *44*, p. 129-138.

[47] M. A. Spackman, P. G. Byrom, *Chem. Phys. Lett.* **1997**, *267*, p. 215-220.

[48] J. J. Mc Kinnon, A. S. Mitchell, M. A. Spackman, *Chem. – Eur. J.* **1998**, *4*, p. 2136-2141.

[49] M. A. Spackman, J. J. McKinnon, *CrystEngComm* **2002**, *4*, p. 378-392.

[50] J. J. McKinnon, M. A. Spackman, A. S. Mitchell, *Acta Crystallogr, Sect. B: Struct. Sci.* **2004**, *60*, p. 627-668.

[51] J. J. McKinnon, D. Jayatilaka, M. A. Spackman, *Chem. Commun.* **2007**, 3814-3816.

[52] Y. Ma, A. Zhang, X. Xue, D. Jiang, Y. Zhu, C. Zhang, *Cryst. Growth & Des.* **2014**, *14*, p. 6101-6114.

[53] H. Li, L. Zhang, N. Petrutik, K. Wang, Q. Ma, D. Shem-Tov, F. Zhao, M. Gozin, *ACS Cent. Sci.* **2020**, *6*, p. 54-75.

[54] M. Reichel M., D. E. Dosch, T. M. Klapötke, K. Karaghiosoff, *J. Am. Chem. Soc.* **2019**, *141*, p. 19911-19916.

[55] C. Zhang, C. Xue, Y. Cao, Y. Zhou, H. Li, J. Zhou, T. Gao, *CrystEngComm* **2013**, p. *15*, 6837.

[56] D. E. Dosch, M. Reichel, M. Born, T. M. Klapötke, K. Karaghiosoff *Crystal Growth & Design* **2021**, *21,* 1, p. 243-248.

2 Summary and Conclusion

Chapters 3–7 have been published in peer-reviewed scientific journals. The content of these chapters is consistent with the list of publications in the Appendix I.[1-5] In order to fit the style of this thesis, the layout of the articles has been modified. A brief summary & conclusion of the results presented in this thesis is given in Chapter 2.

2.1 An Optimized & Scaled-Up Synthetic Procedure for Trinitroethyl Formate TNEF

An optimized and scaled-up synthesis for the high energy-dense oxidizer (HEDO) tris(2,2,2-trinitroethyl) orthoformate (TNEF) is presented. The target molecule was prepared by a $FeCl_3$ catalyzed nucleophilic substitution reaction starting from trinitroethanol (TNE) (**Scheme 1**).

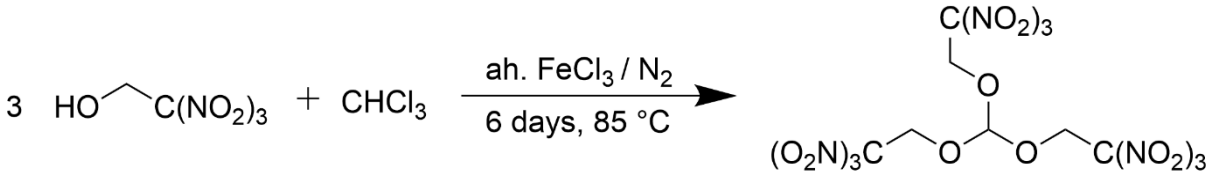

Scheme 1. Reaction equation for the synthesis of TNEF.

From the investigations presented in Chapter 3, it can be concluded, that the described process for the manufacturing of TNEF is suitable for a subsequent scale-up to a technical and/or an industrial scale in the future. With the implemented optimizations like the cheaper protective atmosphere and the improved purification step, a cost-effective and greener synthesis of this high-performing, chlorine-free HEDO is achieved. This could lead to a broader application of TNEF as a HEDO in environmentally benign propellant formulations.

2.2 Scalability of a Time- and Cost-Effective Procedure for the Synthesis of Picryl Bromide

An optimized and scaled-up synthesis for the advanced energetic building block picryl bromide (MBTNB) is presented. Previous synthetic pathways towards this material either comprised of multiple reaction steps, started from expensive starting materials, or were very time-consuming, which are all detrimental factors for large-scale production of an energetic material. In the optimized protocol, the target molecule is prepared by one-pot nitration of bromobenzene using a 5:1 mixed acid consisting of oleum (30%) and white-fuming nitric acid (10 equivalents) and a reaction temperature of 130 °C (**Scheme 1**).

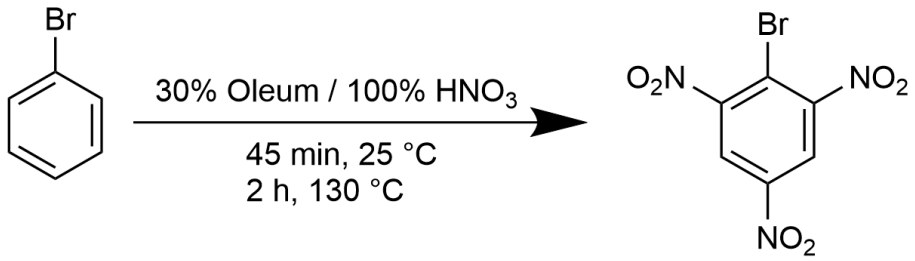

Scheme 1. Optimized synthetic route for MBTNB.[7]

It can be concluded from the results of Chapter 4, that the proposed process for the manufacturing of MBTNB is a scalable, time- and cost-effective way to manufacture the target compound with good yields and high purity. The presented synthetic route is a significant improvement over the state-of-the-art methods and could lead to broader use of MBTNB as a building block for new energetic materials, for example in nucleophilic substitution reactions with energetic heterocycles.

2.3 Correlation between Structure and Energetic Properties of Three Nitroaromatic Compounds: Bis(2,4-dinitrophenyl) Ether, Bis(2,4,6-trinitrophenyl) Ether, and Bis(2,4,6-trinitrophenyl) Thioether

A group consisting of Bis(2,4-dinitrophenyl) ether (**1**), Bis(2,4,6-trinitrophenyl) ether (**2**), and Bis(2,4,6-trinitrophenyl) thioether (**3**), which each comprise an ether or thioether bridge, was synthesized (**Scheme 1**). All three compounds were intensively characterized, including structure elucidation via single-crystal X-ray diffraction.

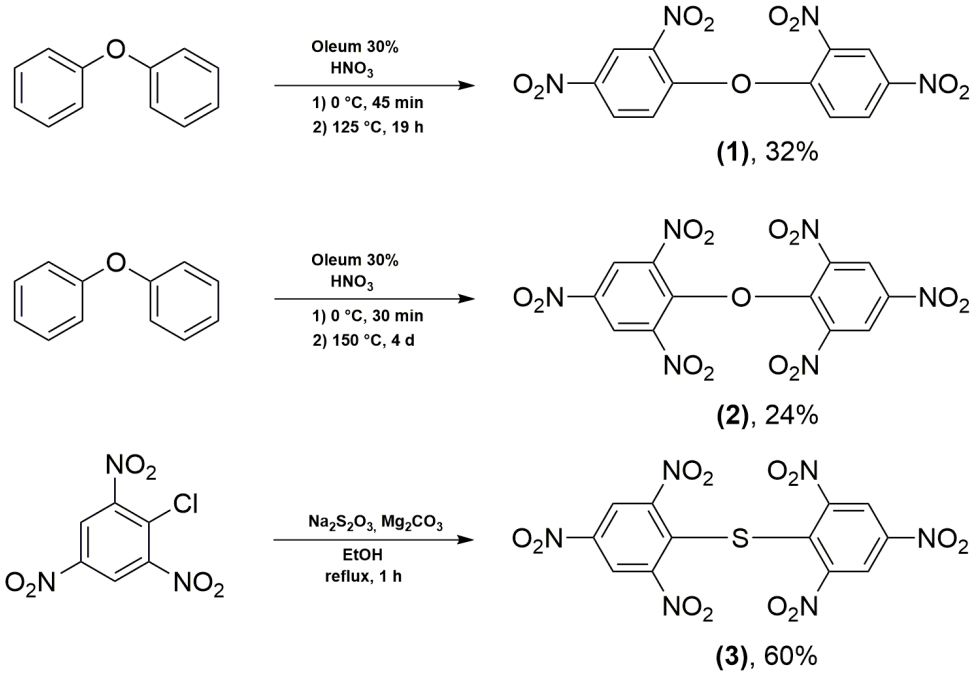

Scheme 1. Reaction schemes for compounds **(1)**–**(3)**.

It can be concluded from the results presented in Chapter 5, that the results of various older prediction models like bond dissociation enthalpy and electrostatic potential (BDE, ESP) for the three model compounds (sensitivity decreasing, **3** > **2** > **1**) did not correspond with the experimentally found trends for the sensitivities (**2** > **3** > **1**). In contrast, the results for newer prediction models based on the crystal structure (Hirshfeld surface and Fingerprint plot analysis) represented the experimentally found trends for the three model compounds correctly. The application of these newer methods could lead to a better understanding and assessment of sensitivity values without the necessity to synthesize large amounts of new energetic materials, which leads to an increase in safety for HEDM researchers.

2.4 Investigation of Structure-Property Relationships of Three Nitroaromatic Compounds: 1-Fluoro-2,4,6-trinitrobenzene, 2,4,6-Trinitrophenyl methanesulfonate, and 2,4,6-Trinitrobenzaldehyde.

A group consisting of 1-Fluoro-2,4,6-trinitrobenzene (**1**), 2,4,6-Trinitrophenyl methanesulfonate (**2**), and 2,4,6-Trinitrobenzaldehyde (**3**), was prepared according to optimized syntheses. All three compounds were intensively characterized, including structure elucidation via single-crystal X-ray diffraction (**Scheme 1**).

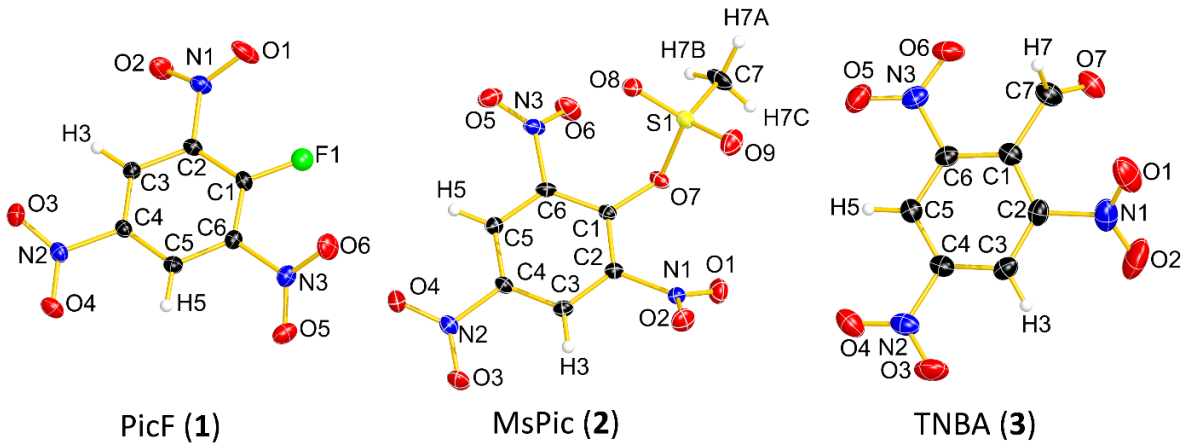

Scheme 1. Single-crystal X-ray structure of the three title compounds.

From the results presented in chapter 6, a deeper insight into structure-property relationships for derivatives of 1,3,5-trinitrobenzene could be gained. A key discovery is the fact, that a combination of very few but strong stabilizing interactions in a crystal can result in the same stability and therefore sensitivity as numerous but significantly weaker stabilizing interactions. The established trends regarding the distribution of stabilizing and destabilizing close-contacts from other publications regarding HSA could be confirmed. The investigated materials were categorized as secondary

explosives comparable to the state-of-the-art material TNT and the calculated EXPLO5 values decrease from **1** over **3** to **2**.

2.5 A Study of 3,5-Dinitro-1-(2,4,6-trinitrophenyl)-1*H*-pyrazol-4-amine (PicADNP) as a New High Energy Density Booster Explosive

Two improved fast, feasible, scalable, and economic synthetic protocols for the laboratory scale manufacturing of 3,5-Dinitro-1-(2,4,6-trinitrophenyl)-1H-pyrazol-4-amine (PicADNP) are described (**Schemes 1** & **2**). The target molecule was prepared from a nucleophilic substitution reaction starting from potassium 4-amino-3,5-dinitropyrazol-1-ide (KADNP) and a picrylation agent in acetonitrile at 70°C.

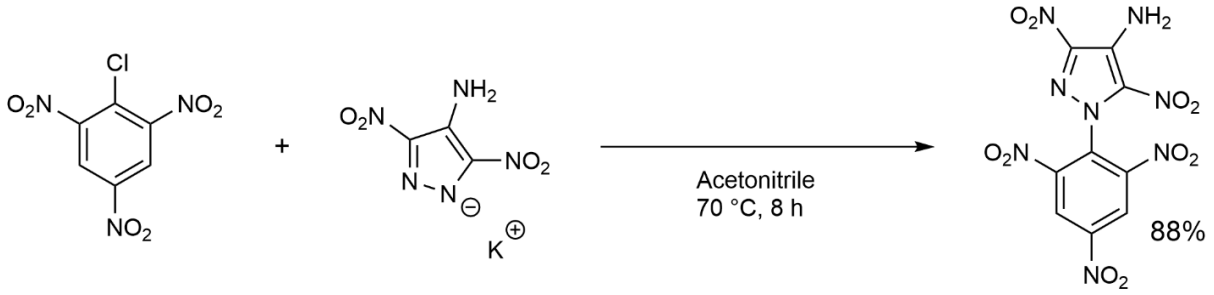

Scheme 1. Reaction Scheme for Synthetic Protocol 1.

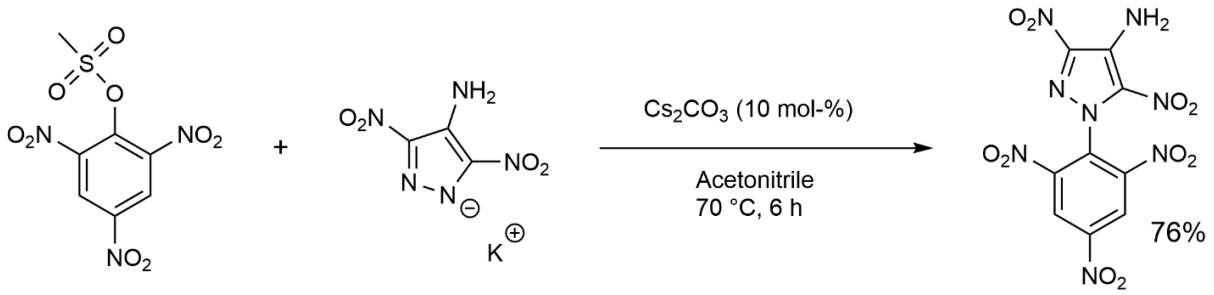

Scheme 2. Reaction Scheme for Synthetic Protocol 2.

From the investigations of Chapter 7, it can be concluded, that the optimized process for the manufacturing of PicADNP is a fast, feasible, and scalable procedure with excellent yields, which resembles an improvement over the state-of-the-art synthesis. The EXPLO5 calculations, SSRT, and booster tests show, that PicADNP resembles a safer alternative to PETN as a booster explosive. The material exhibits a comparable performance, and shows higher sensitivities towards external stimuli as well as an elevated decomposition temperature and therefore an increased handling safety when compared to PETN.

3 An Optimized & Scaled-Up Synthetic Procedure for Trinitroethyl Formate TNEF

Accepted and prepublished in *Propellants, Explos., Pyrotech.* (doi: 10.1002/prep.202000323)

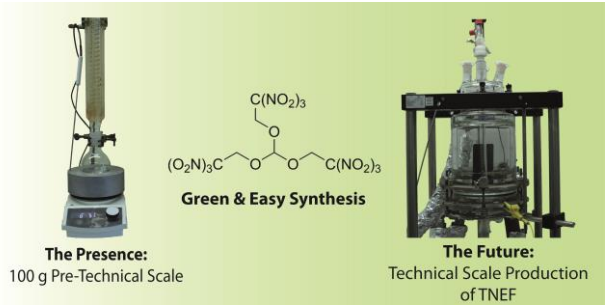

3.1 Abstract

Previous reports showed, that tris(2,2,2-trinitroethoxy)methane, also known as tris(2,2,2-trinitroethyl) orthoformate or trinitroethyl formate (TNEF), exhibits a very high potential for application due to its excellent energetic properties and compatibility with state-of-the-art binder systems for composite propellants. However, TNEF was never produced on a scale exceeding a few grams. In this work, a scaled and optimized synthetic procedure for the manufacturing of elemental analysis pure TNEF in a 100 g pre-technical scale is described. Applied optimizations focus on the cost of the synthesis and improvements regarding a greener purification process. Acceptable yields were achieved in the 100 g scale and the described synthetic procedure could be easily applied in the technical scale in the next step. This could stimulate a broader application of TNEF as an environmentally benign high energy density oxidizer for composite propellants.

KEYWORDS: Oxidizer, Rocket Propellant, HEDO, Scale-up, Green Chemistry.

3.2 Introduction

One of the major research topics within the field of energetic materials research is the development of new high-energy dense oxidizers (HEDOs), especially for the application in composite rocket propellants.[1] Besides factors like good performance, safe handling, and a cost-effective synthesis another main goal is the replacement of the most widely used[2] but toxic[3] oxidizer ammonium perchlorate with more environmentally benign alternatives. Potential replacements that were discussed over the last twenty years are dinitramide salts as well as compounds utilizing the trinitromethyl or trinitroethyl moiety.[4] Various materials from the subsection of polynitrocarbamates and polynitroethers containing those motifs have been extensively studied as potential HEDOs by *Frankel*[5b] and in recent years *by Klapötke et al.*[1b, 1d, 4a, 5a]

One of those molecules tris(2,2,2-trinitroethoxy)methane, also known as tris(2,2,2-trinitroethyl) orthoformate or trinitroethyl formate (TNEF) shows a very high potential for application. This compound was first synthesized in 1967[6], but since then the material was never produced on a scale that exceeded a few grams per batch.[7] TNEF combines a good oxygen balance of 30.4% with regard to carbon monoxide, an acceptable decomposition point of 187–192 °C, moderate sensitivities towards external stimuli (IS: 5 J, FS: 96 N, ESD: 200 mJ), and a rather simple and scalable synthesis. Initial studies regarding formulations, compatibility, and storage stability were conducted between 2017 and 2018.[8] They confirmed its suitability as a HEDO for composite propellant formulations with state-of-the-art binder systems such as HTPB, nitrocellulose, or GAP.[8] Although prepared from trinitroethanol (TNE), which has some toxicity issues, TNEF offers the advantage of a chlorine-free, high-performing oxidizer with less toxic combustion products, when compared to ammonium perchlorate. As the global demand for environmentally benign HEDOs in civil, space, and military applications increases, the development of a scalable and further optimized synthetic procedure for TNEF as well as an improved purification protocol utilizing a less toxic solvent system was mandatory. Therefore, we would like to communicate an optimized pre-technical 100 g scale synthesis for TNEF as well as an improved purification protocol, which is supposed to be further scalable towards a technical or industrial-scale synthetic procedure.

3.3 Experimental Section

General Information. HPLC grade chloroform was purchased from Fisher Chemicals. Anhydrous $FeCl_3$ was purchased from Sigma-Aldrich. Trinitroethanol (TNE) was prepared according to a modified synthesis based on the literature procedure of *Klapötke et. al.*, without the additional sublimation step for purification.[1c]

NMR spectra were recorded on a Bruker Avance III spectrometer operating at 400.1 MHz (^{1}H), 100.6 MHz (^{13}C), and 28.9 MHz (^{14}N). Chemical shifts are referred to TMS (^{1}H, ^{13}C) and $MeNO_2$ (^{14}N). Raman spectra were recorded with a Bruker MultiRam FT Raman spectrometer using a neodymium-doped yttrium aluminum garnet (Nd:YAG) laser (λ = 1064 nm) with 1074 mW. The samples for Infrared spectroscopy were placed under ambient conditions onto an ATR unit using a Perkin Elmer Spectrum BX II FT-IR System spectrometer. Melting and/or decomposition points were detected with a OZM DTA 552-Ex instrument. The scanning temperature range was set from 293 K to 673 K at a scanning rate 5 of °C/min. DSC values were determined on a Mettler-Toledo DSC 822e with an Intracooler (Julabo FT900) and a heating rate of 5 °C/min. Elemental analysis was performed with a Vario EL instrument and a Metrohm 888 Titrando device.

Caution! *The compound TNEF shows partly increased sensitivities toward various stimuli (e.g. higher temperatures, impact, friction, or electrostatic discharge). Therefore, proper safety precautions (safety glasses, Kevlar gloves, and earplugs) have to be applied while synthesizing and handling the described compounds.*

A one-liter round bottom flask was equipped with a magnetic stirrer, an aluminum heating block, and a reflux condenser with a bubble counter for nitrogen inlet. The apparatus was heated to 120 °C, flushed with nitrogen for 30 minutes, and then cooled to 25 °C. It was charged with HPLC grade chloroform (500 mL) and then 100 g trinitroethanol (552.3 mmol, 1 eq) was dispersed under constant stirring at 400 rpm. A total of 8.96 g of anhydrous $FeCl_3$ (55.2 mmol, 10 mol%) was added in small portions, maintaining the temperature at 25 °C. The color of the mixture changed from red over brown to almost black. The temperature was set to 85 °C and the mixture was refluxed under nitrogen conditions for 6 days. The mixture was then cooled to 25 °C and split into two batches. Each batch was extracted with a total of 1.2 L of diethyl ether. The organic phase was washed 3 times with 200 mL of water and the combined aqueous phases were extracted with 200 mL of ether. The combined 1.4 L ether phase was dried over $MgSO_4$ for 15 minutes, and then the solvent was removed *in vacuo* to give the crude product as a beige solid. The crude products of both batches were then dissolved in diethyl ether and filtered over a silica plug to remove any inorganic impurities. The product was precipitated by the addition of *n*-pentane as the precipitating solvent. Repeating this process three times with the obtained solid product afforded 48.7 g (49 %) of a beige-colored solid.

^{1}H NMR (CD_3CN): 5.91 (1H, *H*C($OCH_2R)_3$), 5.11 (6H, OC*H*$_2$R) ppm; **^{13}C{^{1}H} NMR** (CD_3CN): 125.1 *C*$(NO_2)_3$, 112.8 H*C*$(OCH_2R)_3$, 63.8 HC(O*C*$H_2R)_3$ ppm; **^{14}N NMR** (CD_3CN): -34 ppm; **IR** (ATR): $\tilde{\nu}$ = 2986 (vw), 2956 (vw), 2892 (vw), 1579 (vs, *v*as NO_2), 1446 (m), 1401 (w), 1341 (w), 1294 (s, *v*s NO_2), 1184 (w), 1125 (s), 1105 (m), 1075 (s), 1032 (m), 1010 (m), 971 (m), 949 (m), 877 (m), 855 (s), 802 (vs), 778 (s), 728 (m), 644 (m) cm^{-1}; **Raman** (300 mW): $\tilde{\nu}$ = 2989 (14), 2956 (26), 1608 (16), 1448 (8), 1395 (10), 1351 (18), 1308 (19), 1093 (5), 1070 (6), 1030 (5), 881 (6), 859 (51), 804 (5), 782 (8), 543 (22), 488 (22), 400 (49), 374 (60), 268 (44), 204 (52), 103 (100). **Elemental Analysis:** Calculated: C, 15.20; H, 1.28; N, 22.79 Experimental: C, 15.35; H, 1.37; N, 22.66; **Sensitivities:** Impact: 5 J (100–500 µm); Friction: 96 N (100–500 µm); ESD: 200 mJ (100–500 µm). **T**$_{(phase\ transition)}$ **(DTA)**: 121.6 °C, **T**$_{(melt)}$ **(DTA)**: 127.0 °C, **T**$_{(dec.)}$ **(DTA)**: 187.8 °C; **T**$_{(phase\ transition)}$ **(DSC):** 122.9 °C, **T**$_{(melt)}$ **(DSC):** 127.4 °C, **T**$_{(dec.)}$ **(DSC):** 192.5 °C.

3.4 Results and Discussion

3.4.1 Synthesis. Starting from trinitroethanol (as an intermediate available by a two-step procedure from nitroform solution),[1c, 9], TNEF is formed within 6 days in a $FeCl_3$ catalyzed nucleophilic substitution reaction in chloroform under nitrogen atmosphere (**Scheme 1**).

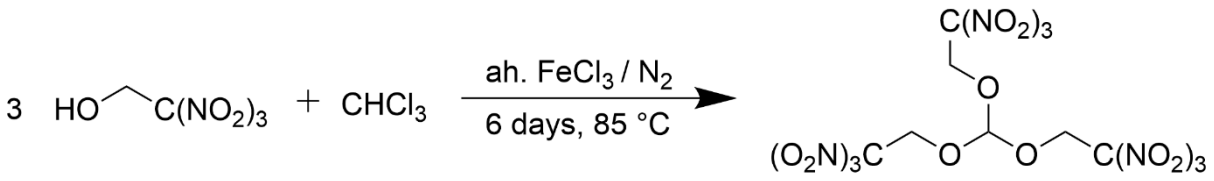

Scheme 1. Reaction equation for the synthesis of TNEF.

The reaction was scaled in multiple steps from 2.5 g, and 10 g over 25 g to the final pre-technical scale of 100 g per batch. The yields for the smaller scales of the reaction varied between 32 and 65%, with the best yield observed for a 25 g scale reaction that proceeded for 5 days in a nitrogen atmosphere. The lowest yield of 32% was obtained for a 25 g scale reaction without protection atmosphere, which is not unexpected regarding the results of older publications. The change from argon to nitrogen for the protection atmosphere did not negatively influence the yields. For the 100 g scale reactions, elongation of the reaction time up to 10 days resulted in a diminished yield of only 30%. A shorter reaction time of 5 days led to a yield of 35%. Therefore, the chosen duration of 6 days is the perfect compromise between yield and consumed time for the 100 g scale synthesis of TNEF.

The application of a nitrogen atmosphere in the 100 g scale, instead of the previously used argon atmosphere is a significant improvement over the older synthetic protocol. This change reduces the costs of the process due to the significantly lower price and the broader availability of nitrogen gas, which has to be considered when scaling this process to a technical scale. The older protocol involved a purification using dichloromethane[7a], which is toxic and was already banned for certain applications according to REACH and is under investigation by the EPA.[10] Therefore, a comparably fast and easy, but less toxic alternative had to be developed for the purification process. We found, that the best purification can be achieved by dissolving the crude material in diethyl ether and precipitation with n-alkanes such as pentane, hexane, or heptane. Subsequent regeneration of the solvents by distillation can facilitate an even more eco-friendly process.

Analysis

3.4.2 Spectroscopic Characterization and Elemental Analysis. The data obtained from NMR and vibrational spectroscopy, as well as elemental analysis, all agree well with those reported.[7a]

3.4.3 Sensitivity Assessment. With regard to the sensitivity towards external stimuli, a small difference was found for the friction sensitivity (96 N) when compared to the literature[7a] (92 N). Impact sensitivity (5 J), as well as sensitivity towards electrostatic discharge (200 mJ), are in agreement with the literature values.

3.4.4 Thermal Analysis. For DTA a phase transition at 121.6 °C with a subsequent melting at 127.0 °C was observed and the TNEF decomposed at 187.8 °C (**Figure 1**).

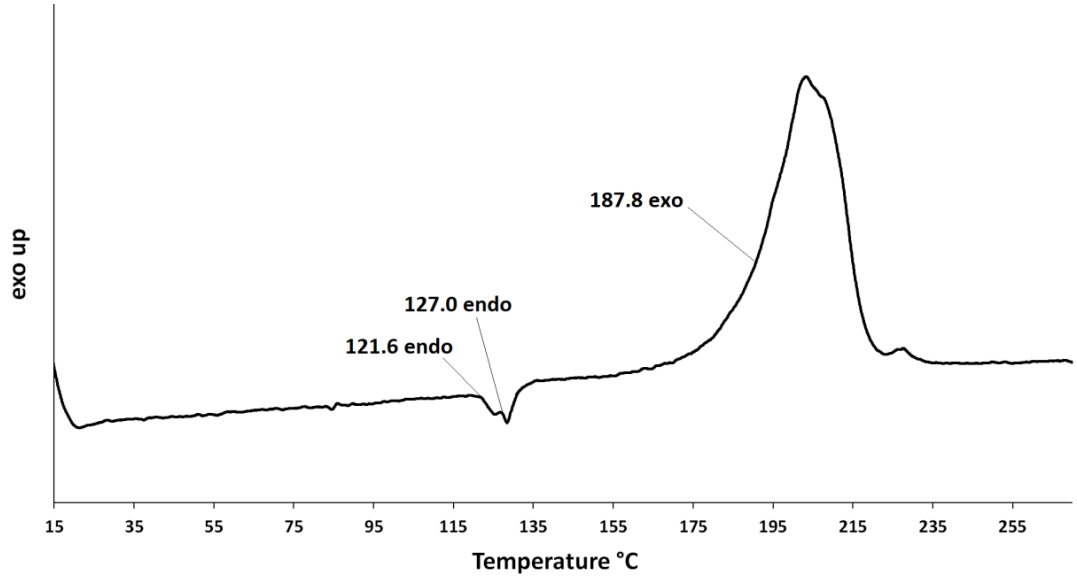

Figure 1. Differential thermal analysis at 5 °C/min heating rate.

This result was reproduced in the DSC measurements, where a phase transition at 122.9 °C with a subsequent melting at 127.4 °C was observed and the material decomposed at a temperature of 192.5 °C (**Figure 2**).

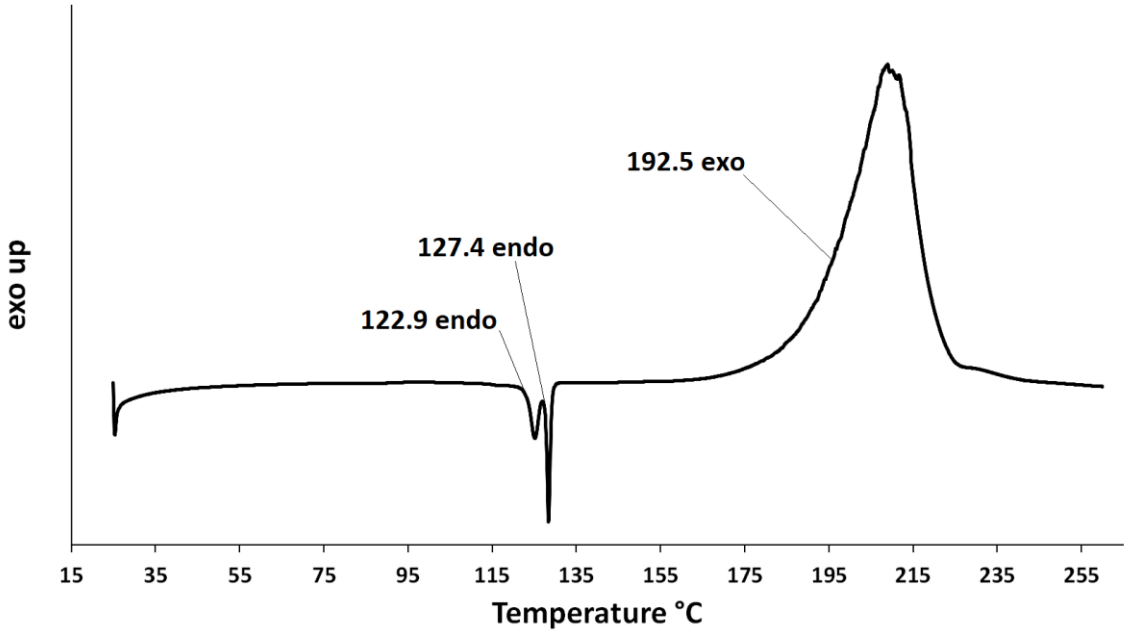

Figure 2. Differential scanning calorimetry at 5 °C/min heating rate.

The values for melting and decomposition are in agreement with older literature values for DSC, however, the observed phase transition has not been described earlier.[6, 7a] Subsequent investigations of formulations with TNEF, as well as aging and long-term stability tests, should take this phase transition into account, as it could lead to problems regarding the shelf-life of industry products with TNEF as the oxidizer.

3.4.5 Storage and Short Term Stability Test. A 10 g sample of TNEF from a batch that was synthesized following the optimized 100 g scale procedure, was stored in a screw-cap plastic container at 20–25 °C for 9 months in a storage room for energetic materials. Samples were taken in 4–6 week intervals and analyzed *via* NMR spectroscopy. After 6 months, a minor decomposition (formation of ~3% nitroform) was observed. However, after another recrystallization from diethyl ether/pentane, the material was stable for further 3 months (until submission of this manuscript). Further analysis of the long-term stability could be pursued by using the vacuum stability test (VST) or computational methods like a simulation with the AKTS Thermodynamics Software package, which is based on DSC measurements with scaling heating rates from 0.1 °C/min to 20 °C/min.[11] The long-term stability of the trinitroethyl building blocks in TNEF should be monitored for formulations, and in case of stability problems, suitable additives must be developed to overcome this issue.

3.5 Conclusion

The proposed optimized route for the synthesis and purification of TNEF is a scalable, cost-effective way to manufacture the target compound with good yields and high purity, which has been confirmed by analytic methods. The optimized purification protocol facilitates a greener synthesis of TNEF in a pure form by replacing dichloromethane with diethyl ether. By applying a nitrogen atmosphere instead of the previously used argon atmosphere costs for the process can be reduced. The presented synthetic procedure is a significant improvement and could stimulate a broader use of TNEF as an environmentally benign HEDO for composite propellants. In the next step, a technical scale synthesis and subsequently the industrial production could be pursued.

3.6 Acknowledgements

We gratefully acknowledge the financial support of this work by Ludwig−Maximilian University (LMU), the Office of Naval Research (ONR) under grant no. ONR.N00014-16-1-2062 and the Strategic Environmental Research and Development Program (SERDP) under contract no. WP19-1287 as well as EURENCO. The authors also thank Mr. Max Born for help with the DSC measurements.

3.7 References

[1] a) T. M. Klapötke, *Chemistry of High-Energy Materials*, 5th Edition, De Gruyter, Boston, USA, **2019**; b) Q. J. Axthammer, B. Krumm, T. M. Klapötke, Synthesis of Energetic Nitrocarbamates from Polynitro Alcohols and Their Potential as High Energetic Oxidizers, *J. Org. Chem.,* **2015**, *80*, 6329; c) T. M. Klapötke, B. Krumm, R. Moll, Polynitroethyl- and Fluorodinitroethyl Substituted Boron Esters, *Chem.- Eur. J.,* **2013**, *19*, 12113; d) Q. J. Axthammer, T. M. Klapötke, B. Krumm, R. Moll, S. F. Rest, The Energetic Nitrocarbamate $O_2NN(H)CO[OCH_2C(NO_2)_3]$ Derived from Phosgene, *Z. Anorg. Allg. Chem.* **2014**, *640*, 76; e) T.M. Klapötke, *Energetic Materials Encyclopedia*, De Gruyter, Berlin / Boston, **2018**.

[2] a) E. W. Price, S. R. Chakravarthy, J. K. Sambamurthl, R. K. Sigman, The Details of Combustion of Ammonium Perchlorate Propellants: Leading Edge Flame Detachment, *Combust. Sci. Technol.,* **1998**, *138*, 63; b) M. R. Sovizi, G. Fakhrpour, A. R. Madram, Comparison of Thermal Degradation Behavior of Epoxy/Ammonium Perchlorate Composite Propellants, *J. Therm. Anal. Calorim.,* **2017**, *129*, 401; c) M. Rodríguez-Pesina, J. García-Domínguez, F. García-Hernández, L. M. Flores-Vélez, O. Domínguez, The Thermal Decomposition of Ammonium Perchlorate-Aluminum Propellants in Presence of Metallic Zinc Particles, *Mater. Sci. Appl.,* **2017**, *08*, 436.

[3] a) B. C. Blount, L. Valentin-Blasini, J. D. Osterloh, J. P. Mauldin, J. L. Pirkle, Perchlorate Exposure of the US Population, 2001–2002, *J. Expo. Sci. Environ. Epidemiol.*, **2007**, *17*, 400; b) M. V. Maffini, L. Trasande, T. G. Neltner, Perchlorate and Diet: Human Exposures, Risks, and Mitigation Strategies, *Curr. Environ. health Rep.*, **2016**, *3*, 107; c) M. R. Sijimol, M. Mohan, D. Dineep, Perchlorate Contamination in Bottled and Other Drinking Water Sources of Kerala, Southwest Coast of India, *Energy, Ecology and Environment,* **2016**, *1*, 148; d) C. Vigreux-Besret, A. Mahé, G. Ledoux, A. Garnier, C. Rosin, A. Baert, M. Joyeux, P.-M. Badot, P. Panetier, G. Rivière, Perchlorate: Water and Infant Formulae Contamination in France and Risk Assessment in Infants, *Food. Addit. Contam.,* **2015**, *32*, 1148.

[4] a) D. Trache, T. M. Klapötke, L. Maiz, M. Abd-Elghany, L. T. DeLuca, Recent Advances in New Oxidizers for Solid Rocket Propulsion, *Green Chem.,* **2017**, *19*, 4711; b) T. M. Klapötke, B. Krumm, R. Scharf, Oxalyl Chloride and Hydrazide Based Energetic Polynitro Derivatives, *Eur. J. Inorg. Chem.,* **2016**, 3086.

[5] a) T. M. Klapötke, B. Krumm, T. Reith, Polynitrocarbamates Derived from Nitromethane, *Z. Anorg. Allg. Chem.,* **2017**, *643*, 1474; b) M. B. Frankel, Polynitro Carbamates and N-Nitrocarbamates, *J. Chem. Eng. Data,* **1962**, *7*, 410.

[6] M. E. Hill*, Orthoesters of 2,2,2-trinitroethanol*, US Patent. 3306939, **1967**.

[7] a) T. M. Klapötke, B. Krumm, R. Moll, S. F. Rest, CHNO Based Molecules Containing 2,2,2-Trinitroethoxy Moieties as Possible High Energy Dense Oxidizers, *Z. Anorg. Allg. Chem.,* **2011**, *637*, 2103; b) A. B. Sheremetev, I. L. Yudin, Synthesis of 2-R-2,2-dinitroethanol Orthoesters in Ionic Liquids, *Mendeleev Commun.,* **2005**, *15*, 204.

[8] a) M. Abd-Elghany, T. M. Klapötke, A. Elbeih, Thermal Behavior and Decomposition Kinetics of Bis(2,2,2-trinitroethyl)-oxalate as a High Energy Dense Oxidizer and its Mixture with Nitrocellulose, *Propellants, Explos. Pyrotech.*, **2017**, *42*, 1373; b) M. Abd-Elghany, T. M. Klapötke, A. Elbeih, Investigation of 2,2,2-Trinitroethyl-nitrocarbamate as a High Energy Dense Oxidizer and its Mixture with Nitrocellulose (Thermal Behavior and Decomposition Kinetics), *J. Anal. Appl. Pyrolysis,* **2017**, *128*, 397; c) M. Abd-Elghany, T. M. Klapötke, B. Krumm, A. Elbeih, Higher Performance and Safer Handling: Formulation Based on 2,2,2-Trinitroethyl Formate and Nitrocellulose, *ChemPlusChem*, **2018**, *83*, 128; d) M. Abd-Elghany, T. M. Klapötke, A. Elbeih, Environmentally Safe (Chlorine-free): New Green Propellant Formulation based on 2,2,2-Trinitroethyl-formate and HTPB, *RSC Adv.,* **2018**, *8*, 11771; e) M. Abd-Elghany, A. Elbeih, T. M. Klapötke, Thermo-analytical Study of 2,2,2-Trinitroethyl-formate as a New Oxidizer and its Propellant Based on a GAP Matrix in Comparison with Ammonium Dinitramide, *J. Anal. Appl. Pyrolysis,* **2018**, *133*, 30.

[9] a) H. Feuer, T. Kucera, Preparation of 2,2,2-Trinitroethanol, *J. Org. Chem.,* **1960**, *25*, 2069; b) N. S. Marans, R. P. Zelinski, 2,2,2-Trinitroethanol: Preparation and Properties, *J. Am. Chem. Soc.,* **1950**, *72*, 5329; c) F. G. Borgardt, A. K. Seeler, P. Noble, Aliphatic Polynitro Compounds. Synthesis of 1,1,1-Trinitrochloroethane and Its Rearrangement to Dipotassium Tetranitroethane, *J. Org. Chem.,* **1966**, *31*, 2806.

[10] a)https://echa.europa.eu/documents/10162/0ea58491-bb76-4a47-b1d2-36faa1e0f290 (01.12.2020). b)https://cfpub.epa.gov/ncea/iris/iris_documents/documents/toxreviews/0070tr.pdf (01.12.2020).

[11] https://akts.com/time-to-maximum-rate-adiabatic/runaway-reactions-akts-thermal-safety-software.html (01.12.2020)

3.8 Supporting Information

1 NMR Spectra

1.1 ^{1}H NMR Spectrum of TNEF

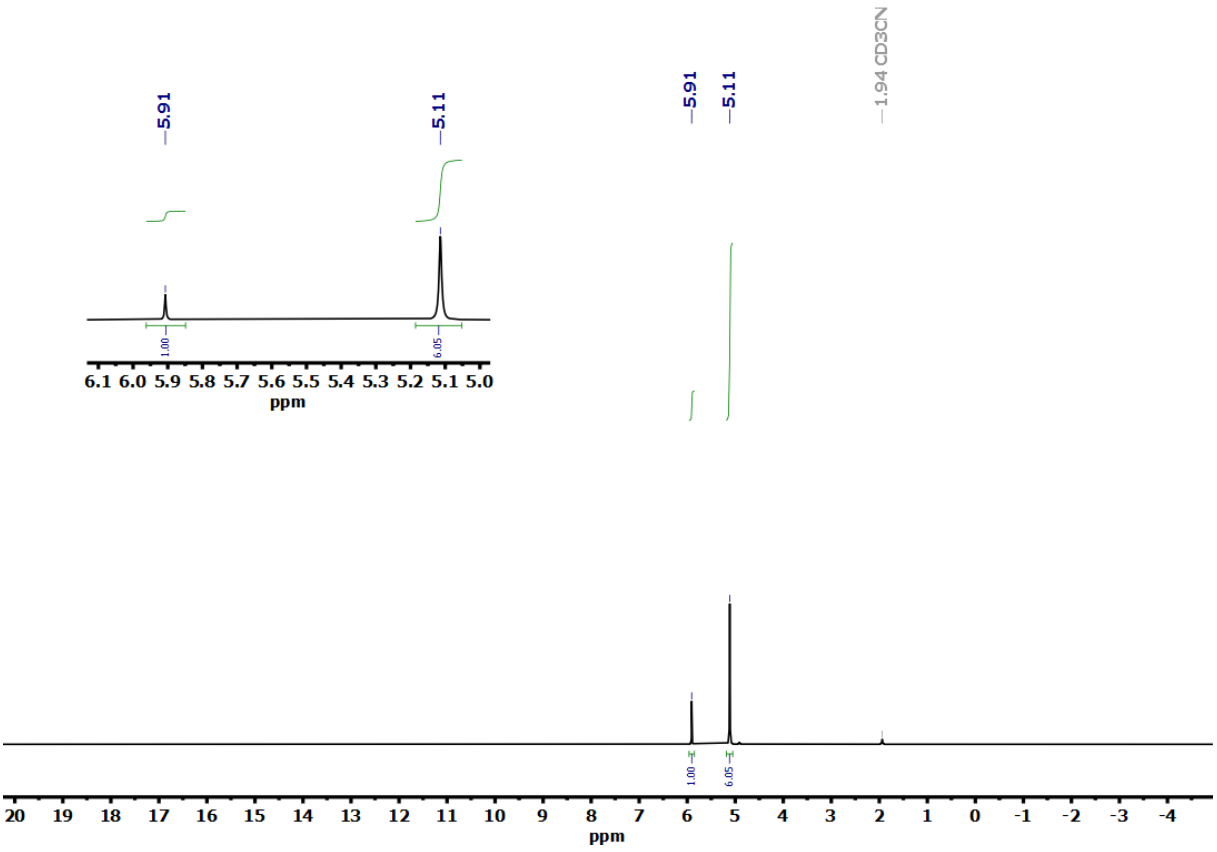

1.2 $^{13}C\{^{1}H\}$ NMR Spectrum of TNEF

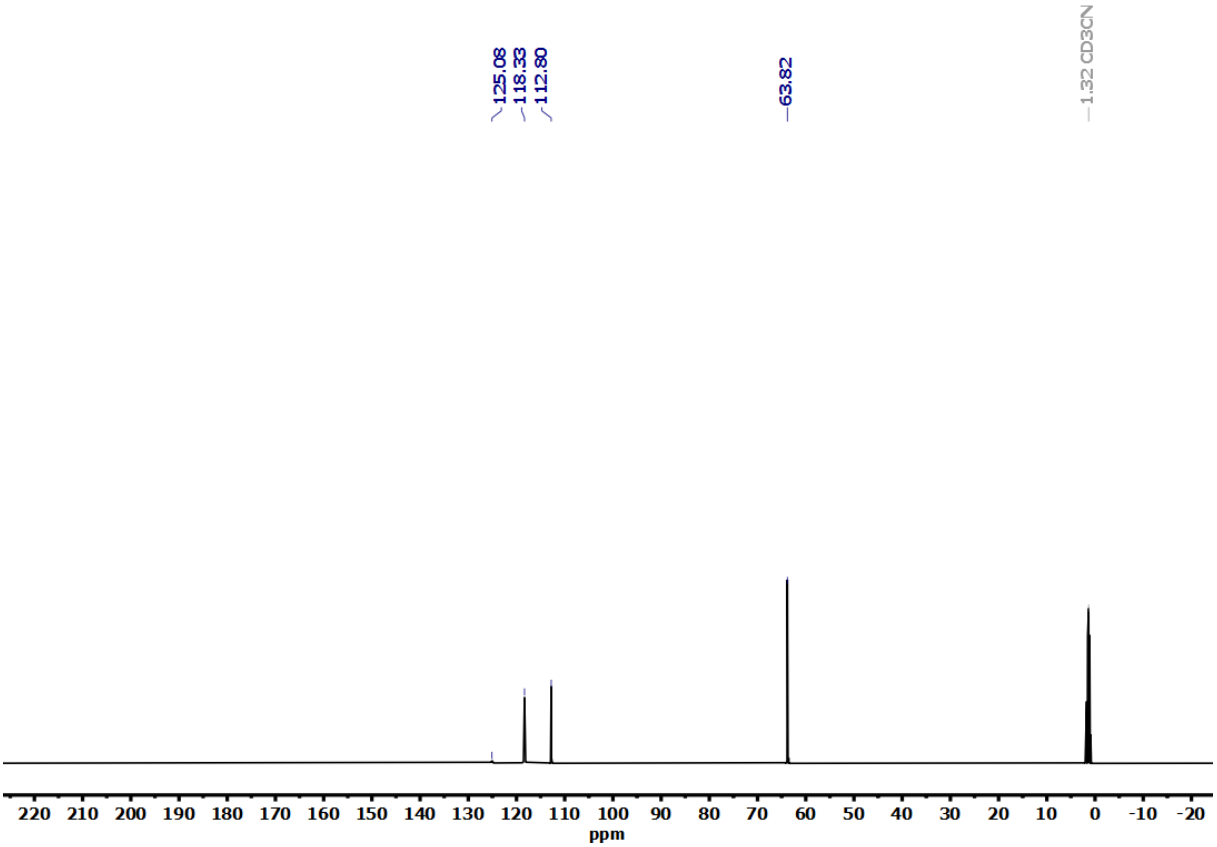

1.3 ^{14}N NMR Spectrum of TNEF

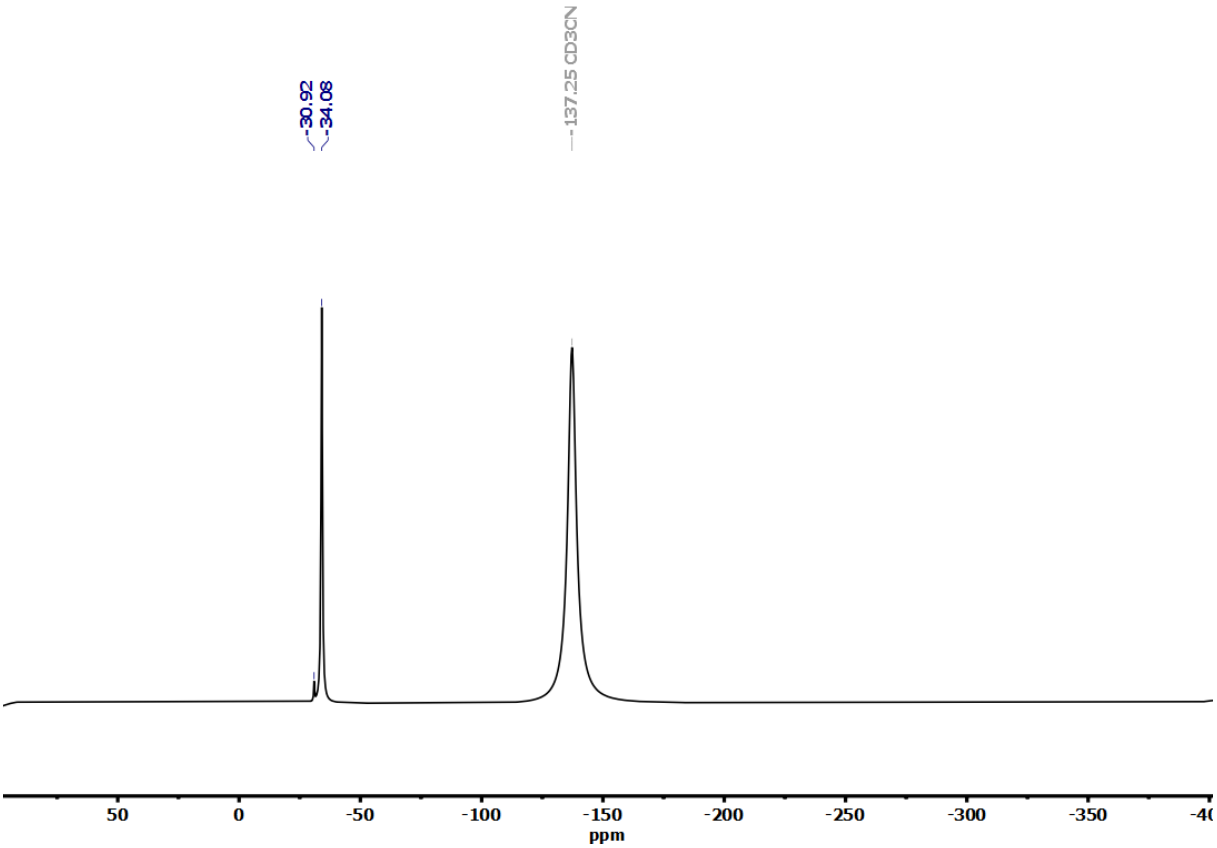

2. IR and Raman data of TNEF

2.1 IR data of TNEF

IR (ATR): $\tilde{\nu}$ = 2986 (vw), 2956 (vw), 2892 (vw), 1579 (vs, *v*as NO_2), 1446 (m), 1401 (w), 1341 (w), 1294 (s, *v*s NO_2), 1184 (w), 1125 (s), 1105 (m), 1075 (s), 1032 (m), 1010 (m), 971 (m), 949 (m), 877 (m), 855 (s), 802 (vs), 778 (s), 728 (m), 644 (m) cm^{-1}.

2.1 Raman data of TNEF

Raman (300 mW): $\tilde{\nu}$ = 2989 (14), 2956 (26), 1608 (16), 1448 (8), 1395 (10), 1351 (18), 1308 (19), 1093 (5), 1070 (6), 1030 (5), 881 (6), 859 (51), 804 (5), 782 (8), 543 (22), 488 (22), 400 (49), 374 (60), 268 (44), 204 (52), 103 (100).

3. Elemental analysis of TNEF

Calculated for TNEF: C, 15.20; H, 1.28; N, 22.79 Experimental: C, 15.35; H, 1.37; N, 22.66.

4. Sensitivity values of TNEF

BAM drop hammer: 5 J; Friction tester: 96 N; ESD: 200 mJ (grain size: 100–500 µm).

5. DSC and DTA data for TNEF

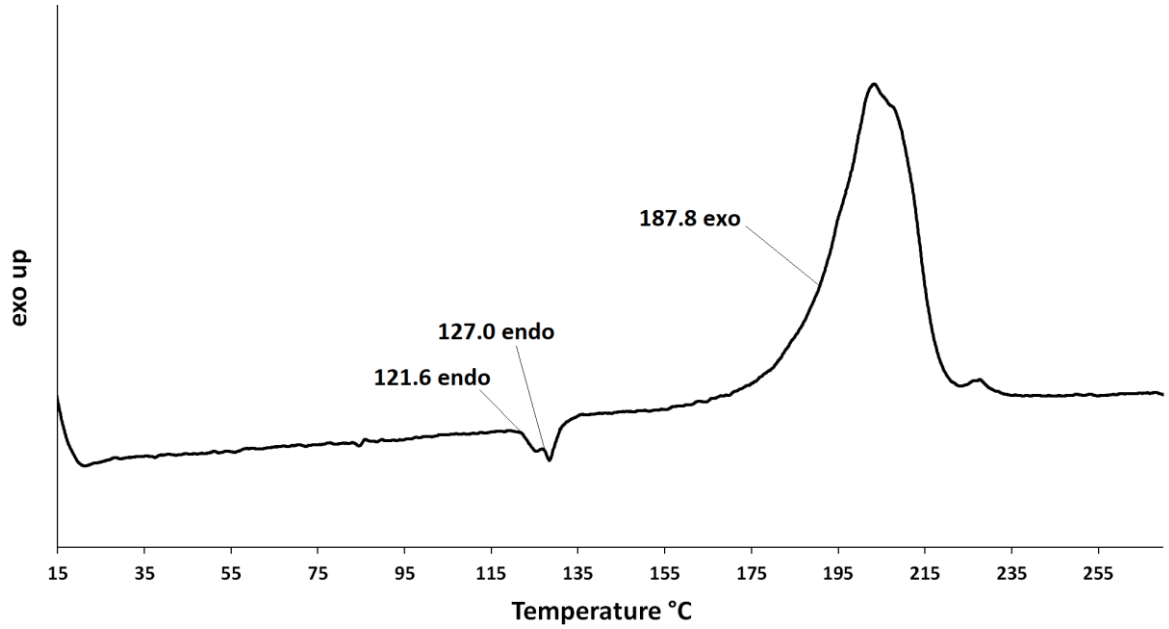

T(phase transition) **(DTA)**: 121.6 °C, **T**(melt.) **(DTA)**: 127.0 °C, **T**(dec.) **(DTA)**: 187.8 °C.

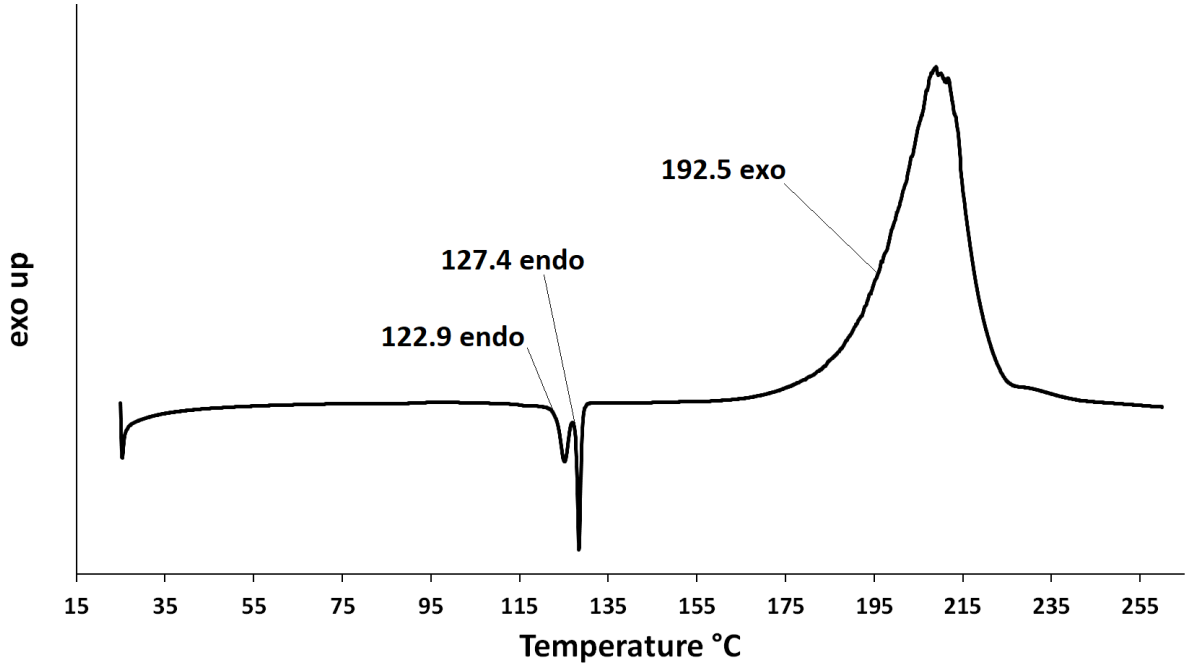

T$_{(phase\ transition)}$ **(DSC)**: 122.9 °C,**T**$_{(melt)}$ **(DSC)**: 127.4 °C, **T**$_{(dec.)}$ **(DSC)**: 192.5 °C.

4 Scalability of a Time- and Cost-Effective Procedure for the Synthesis of Picryl Bromide

Reproduced with permission from *Org. Process Res. Dev*. **2019**, 23, 9, 2096–2098 (doi: 10.1021/acs.oprd.9b00313)

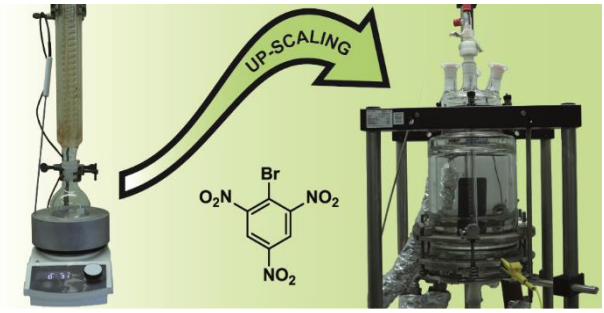

4.1 Abstract

An optimized synthetic procedure for the manufacturing of picryl bromide on a 300 g scale is described. Previous procedures had different drawbacks such as two or more separate nitration steps with varying mixed acids, a complicated workup and purification procedure, expensive starting materials, or very long reaction times. An optimized and time-efficient method on a laboratory scale was described in an earlier conference contribution. The one-pot nitration of bromobenzene using a 5:1 mixed acid, consisting of oleum (30%) and white-fuming nitric acid (ten equivalents) was developed to prove the technical scalability of the reaction. By applying the optimized reaction parameters to a large-scale environment, yields of up to 72% of crude picryl bromide can be achieved. The product contains only a minor picric acid impurity (2-3%), which is formed during the aqueous workup step. It can be removed by a single recrystallization from boiling chloroform, to facilitate the target compound in pure form. This method combines the use of cheap materials with a time-efficient route of synthesis and a simple purification step, which is an improvement compared to the state-of-the-art methods.

KEYWORDS: Picryl bromide, Energetic Materials, 1-Bromo-2,4,6-trinitrobenzene, Synthesis.

4.2 Introduction

Picrylbromide or 1-bromo-2,4,6-trinitrobenzene (MBTNB) is a versatile building block for the synthesis of various energetic materials. Because bromide represents an excellent leaving group, it can be used analogously to picryl chloride to transfer the picryl moiety within a wide variety of nucleophilic substitution reactions. Another relevant application for MBTNB is the manufacturing of highly thermostable explosives belonging to the group of polynitropolyphenylenes like 2,2',2'',4,4',4'',6,6',6''-nonanitro-

1,1':3',1''-terphenyl (NONA) or 2,2',2'',2''',4,4',4'',4''',6,6',6'',6'''-dodecanitro-1,1':3',1'':3'',1'''-quaterphenyl (DODECA). They utilize the copper-mediated *Ullmann* reaction for the formation of carbon-carbon bonds between polynitroarenes, which contain a halogen function as the leaving group.[1, 2] Another relevant use of MBTNB is its application in kinetic and mechanistic studies.[3] In the past various synthetic pathways towards MBTNB were developed and investigated. All of them show significant drawbacks for an industrial-scale application, with the key concerns being the price of the used materials[2, 4], problematic solvents[5], the reaction time[6], or various additional purification steps, which complicate the manufacturing process of larger amounts of high purity MBTNB. The first route of synthesis uses expensive, toxic, and explosive picric acid as a starting material and PBr_3 as bromination agent[2] to yield MBTNB. A mixed solvent system consisting of DMF and toluene is applied, which is problematic for large-scale productions because DMF is on the REACH candidate list.[5] A second synthetic pathway towards MBTNB starts from bromobenzene and a cheap mixed acid system involving two-step nitration. The combined reaction time of 29 hours and the necessity to isolate the intermediate dinitrobromobenzene isomers make this method very inefficient regarding time and workforce.[6] Another synthesis method starts from trinitroanisole, which is not commercially available in larger amounts, which is a disadvantage for large-scale synthesis. It is subjected to a two-step bromo-demethoxylation reaction, using KI/EtOH and PBr_3 as the key reagents.[4] This pathway is therefore not suitable for synthesis exceeding the laboratory scale. The only competitive method for the synthesis of MBTNB starts from bromobenzene and utilizes potassium nitrate and oleum (30%) as the nitration agents at an elevated temperature of 125 °C. According to the literature, the overall yield is 60% and this reaction requires 6 hours and an additional purification step of recrystallization from boiling ethanol to remove byproducts.[2] When considering all the mentioned drawbacks, the development of an optimized and time-efficient synthesis of MBTNB on a technical scale is necessary, to facilitate and stimulate the use of this interesting starting material in the energetic materials community.

4.3 Results and Discussion

4.3.1 Synthetic Approach. To overcome the problems mentioned previously, the synthesis of MBTNB has been optimized according to **Scheme 1** on a laboratory scale. After this procedure had been reproduced several times on a 25 g scale, it was scaled up to a 300 g scale to prove the scalability of the procedure.

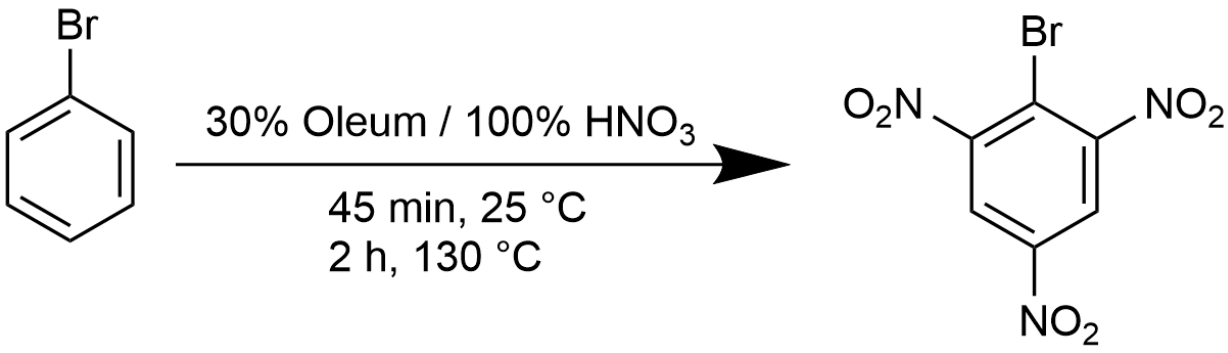

Scheme 1. Optimized synthetic route for MBTNB[7]

Earlier experiments during the optimization process showed unwanted byproducts like dinitrobenzene and multi-brominated benzene derivatives, which formed at temperatures over 140 °C.[7] Their formation is avoided by choosing a programmed temperature. The utilized 5:1 mixed acid is potent enough to introduce the first nitro group at 25 °C and the reaction temperature of 130 °C is optimal for the fast and selective introduction of the two remaining nitro groups. Following this temperature program, the manufacturing of highly pure MBTNB in a time and cost-efficient way with cheap starting materials and a good yield of 72% on a technical scale was realized. Compared to the laboratory scale, using a thermocouple and an aluminum heating-block for temperature control,[7] the yield can be further increased by 9% during scale-up using the 5-liter reactor. Hydrolysis of 2-3% of MBTNB during the workup procedure leads to minor picric acid impurities, which have to be removed by recrystallization from chloroform. No other impurities are formed during synthesis, which is another advantage of the new process.

4.4 Conclusions

It was shown, that the proposed optimized route for the synthesis of MBTNB is a scalable, time- and cost-effective way to manufacture the target compound with good yields and high purity. The presented synthetic route is a significant improvement and can lead to broader use of MBTNB as a building block for new energetic materials.

4.5 Experimental Section

General. Solvents, deuterated solvents for the NMR experiments, and all further chemicals were used as received from the suppliers, without further purification. The reactions were conducted in a Diehm 5 L jacketed glass reactor, equipped with a CAT R100C-T overhead stirrer and a Lauda Integral XT 250 W process thermostat. NMR spectra were recorded with a Bruker 400 or Bruker 400 TR at ambient temperature. The chemical shifts were determined with respect to external standards, Me_4Si (^1H 399.8 MHz; ^{13}C 100.5 MHz) and $MeNO_2$ (^{14}N 28.9 MHz). Infrared spectra were

measured with a PerkinElmer Spectrum BX-FTIR spectrometer equipped with a Smiths DuraSamplIR ATR device. Raman spectra were recorded in a glass tube with a Bruker MultiRAM FT-Raman spectrometer with ND:YAG laser with excitation up to 1000 mW at 1064 nm in the range 4000–400 cm^{-1}. All spectra were recorded at ambient temperature. The C/H/N content was determined with an Elementar vario EL or Elementar vario micro cube instrument. The sensitivities towards impact and friction were determined with a BAM drophammer[8] and a BAM friction tester.[9] The sensitivity towards electrostatic discharge was determined with an electric spark tester from OZM. The melting range was determined with an Büchi Melting Point B-540 device and a heating rate of 1 °C per minute.

Caution! 1-bromo-2,4,6-trinitrobenzene (MBTNB, picryl bromide) itself is considered a sensitive material and therefore should be handled with caution during synthesis or manipulation, and additional protective equipment (leather jacket, face shield, ear protection, Kevlar gloves) is strongly recommended.

4.5.1 300 g reactor scale: A 5 L glass jacketed reactor was charged with oleum (1.3 L, 65% SO_3), which was cooled to 5 °C with external cooling by a process thermostat. Then sulfuric acid (1.6 L, 96%) was added during one hour, whilst the temperature was kept below 40 °C. Afterward white fuming nitric acid (576 mL, 13.8 mol, 10 eq) was added in small portions while keeping the temperature below 25 °C. After cooling to 5 °C, bromobenzene (143.2 mL, 1.38 mol, 1 eq) was slowly added to the mixture and the temperature was kept below 20 °C during the addition. The reaction mixture was then stirred at 25 °C for 45 minutes, followed by heating to 130 °C for two hours. The mixture was cooled to 20 °C and then quenched by adding a total of 5.7 kg of ice. The mixture was separated into five smaller batches and the solid white precipitate was removed by filtration. The product was washed with cold water until the precipitate runs acid-free. After drying, the crude product weighs 287 g (0.98 mol, 72%) with 2–3% of picric acid as a hydrolysis byproduct, which could be easily removed by recrystallization from boiling chloroform.

^{1}H-NMR: 8.75 ppm; **^{13}C-NMR:** 115.1, 122.2, 147.0, 152.1 ppm; **^{14}N-NMR:** -19.8, -24.0 ppm; **Melting Point:** 122–124 °C; **IR (ATR):** $\tilde{\nu}$ = 3082 (m), 1846 (w) 1599 (m), 1532 (s), 1411 (w), 1344 (s), 1197 (m), 1047 (s), 925 (s), 824 (m), 743 (s), 716 (s), 491 (m), 413 (w) cm^{-1}; **Raman (300 mW):** $\tilde{\nu}$ = 3090 (13), 1596 (37), 1542 (16), 1381 (18), 1348 (100), 1199 (12), 1047 (36), 823 (26); **Elemental Analysis:** Calculated: C, 24.68; H, 0.69; N, 14.39 Experimental: C, 24.70; H, 0.75; N, 14.09; **Sensitivities:** BAM drop hammer: 40 J (<100 µm); Friction tester: >360 N (<100 µm); ESD: 0.5 J (<100 µm).

Associated content

Supporting Information

The Supporting Information is available free of charge on the ACS Publications website.

^{1}H, ^{13}C, ^{14}N NMR spectra (PDF)

Author information

Corresponding Author. *E-mail: tmk@cup.uni-muenchen.de

Notes

The authors declare no competing financial interest.

Author Contributions

The manuscript was written through contributions of all authors. All authors have given approval to the final version of the manuscript.

4.6 Acknowledgments

For financial support of this work by the Ludwig-Maximilian University of Munich (LMU), the Office of Naval Research (ONR) under grant no. ONR.N00014-16-1-2062 and the Strategic Environmental Research and Development Program (SERDP) under contract no. WP19-1287 are gratefully acknowledged. The authors also thank Mr. Maurus Völkl, Mr. Stefan Huber, and Dr. Marc Bölter for help regarding the handling of the reactor and Ms. Theresa Küblböck for help with the graphics.

4.7 References

1. Sitzmann, M. E., Method for making nonanitroterphenyl. *US6476280*, **2002**.

2. Bellamy, A. J. H.; P. Nick, Synthesis of Polynitropolyphenyl Compounds. A Strategy for the Construction of Bi-, Ter-, and quater-phenyl Systems Utilising Halogenodemethoxylation and Ullmann Coupling, *J. Chem. Res., Miniprint #4*, **1996**, 959 - 978.

3. Nadar, P. A.; Gnanasekaran, C., Kinetics of reaction of picryl bromide with substituted naphthoate ions, *J. Chem. Soc., Perkin Trans. 2*, **1978**, 7, 671 - 673.

4. Bellamy, A. J.; Hudson, P. N., Chloro- and bromo-demethoxylation of methoxypolynitroaryl systems, *Tetrahedron.*, **1996**, 52, 5639 - 5642.

5. https://echa.europa.eu/candidate-list-table/-/dislist/details/0b0236e1807dec94.

6. Sugden, S.; Willis, J. B., 303. The kinetics of exchange reactions. Part IV. Substituted phenyl and benzyl bromides, *J. Chem. Soc.*, **1951**, 1360 - 1363.

7. Dosch D. E.; Klapötke T. M., A Fast and Feasible Synthesis for Picryl Bromide, *New Trends in Research of Energetic Materials*; Pachmann J. Šelešovský J, Eds.; University of Pardubice: Pardubice Czech Republic, **2018**, 522 - 526.

8. NATO, Standardization Agreement 4489 (STANAG 4489), Explosives, Impact Sensitivity Tests. Brussels, Belgium **1999**.

9. NATO, Standardization Agreement 4487 (STANAG 4487), Explosives, Friction Sensitivity Tests. Brussels, Belgium **2002**.

4.8 Supporting Information

^{1}H, ^{13}C and ^{14}N NMR data of **(1)**

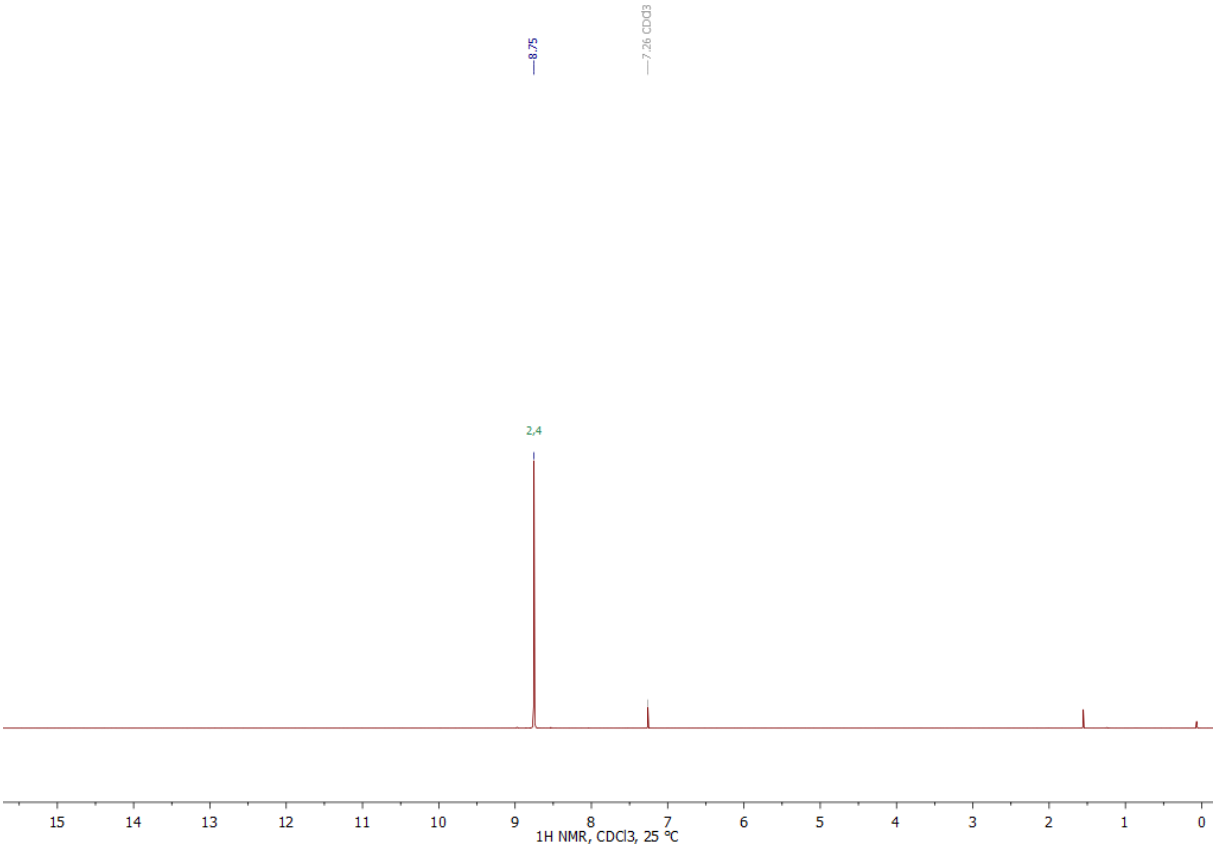

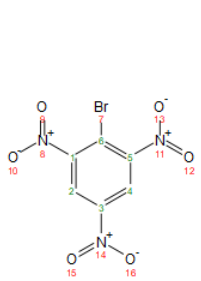

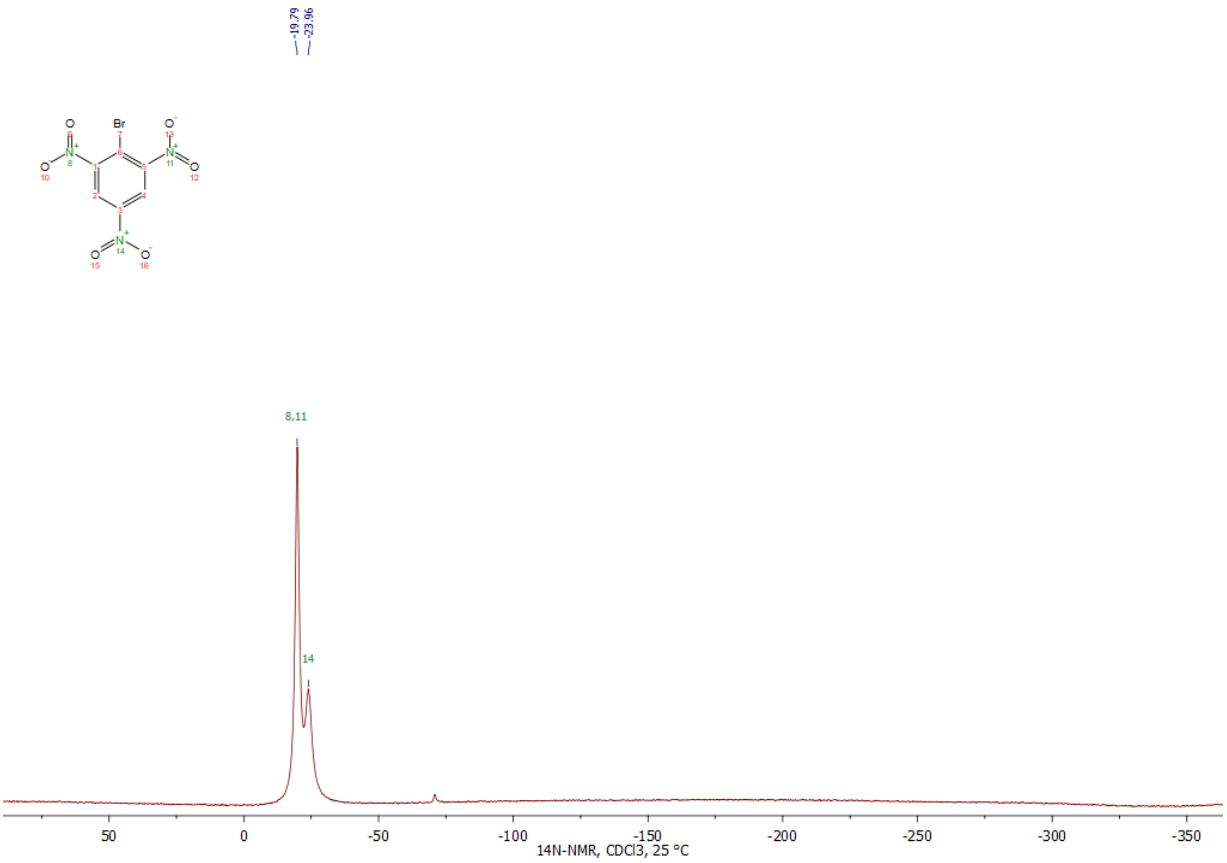
19.79
23.96
Br
8,11
14
50
0
-50
-100
-150
-200
-250
-300
-350
14N-NMR, CDCl3, 25 °C

5 Correlation between Structure and Energetic Properties of Three Nitroaromatic Compounds: Bis(2,4-dinitrophenyl) Ether, Bis(2,4,6-trinitrophenyl) Ether, and Bis(2,4,6-trinitrophenyl) Thioether

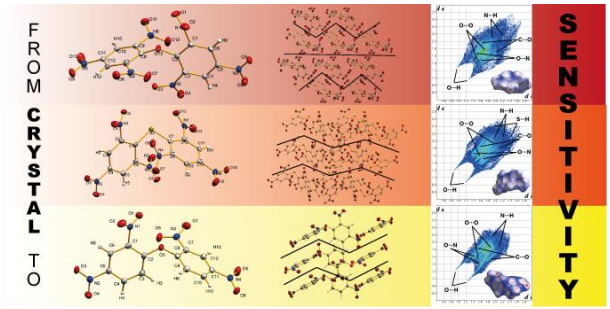

5.1 Abstract

Decades after the initial discovery of is(2,4,6-trinitrophenyl) ether derivatives, the first single-crystal X-ray structures for three members of this compound class could finally be shown and the analytical data could be completed. This group of molecules is an interesting example that illustrates why older predictive models for the sensitivity values of energetic materials like bond dissociation enthalpy and electrostatic potential sometimes give results that deviate significantly from the experimentally determined values. By applying newer models like Hirshfeld surface analysis and Fingerprint plot analysis that utilize the crystal-structure of an energetic material, the experimentally found trend of sensitivities could be understood and the older models could be brought into a proper perspective. In the future, the prediction of structure-property relationships for energetic molecules starting from a crystal structure can be achieved and should be pursued.

5.2 Introduction

About 150 years ago, Alfred Nobel recognized, that the industrialization of “new” synthetic explosives must be accompanied by their safe handling. The development of dynamite was the first step in this direction.[1] Just a quarter of a century later, Dynamit Nobel AG focused on TNT, which replaced its predecessors due to its excellent handling safety and brisance.[2] Although nitroaromatic compounds are no longer the centerpiece of modern explosive investigations,[3] Alfred Nobel's fundamental aim of increased handling safety that was implemented with this group of materials continues to exist.[4] The insensitivity to external stimuli is one of the most important requirements

for the synthesis of new HEDMs, next to other characteristics such as higher environmental compatibility, high density, high thermal stability, and higher detonation velocity/pressure.[3b, 5] The desired high performance of HEDMs can be achieved by using compounds with a high heat of formation, but these candidates tend to be more sensitive towards external stimuli.[4a] The contrary behavior of the desired parameters for HEDMs[4a, 6] leads to the conclusion, that not only the molecular design but also the crystallographic design has to be considered to find a balance between performance and safety for new energetic materials.[7] Better visualization and understanding of the sensitizing properties can be achieved by combining older prediction models - such as the calculation of h_{50} values, electrostatic surface potential (ESP) or E_{ES} values[3b, 4a] - with newer methods like Hirshfeld surface analysis and Fingerprint plot analysis.[8] After many years of uncertainty, a deeper insight into the energetic behavior of the title compounds bis(2,4-dinitrophenyl) ether (**1**), bis(2,4,6-trinitrophenyl) ether (**2**), and bis(2,4,6-trinitrophenyl) thioether (**3**), could be gained. This was achieved by combining theoretical methods with structural investigations of the HEDMs to understand the trends that were found for the experimental sensitivity values.

5.3 Results and Discussion

***5.3.1 Spectroscopic Characterization*.** All three compounds were prepared according to modified and optimized methods (**Scheme 1**).[9]

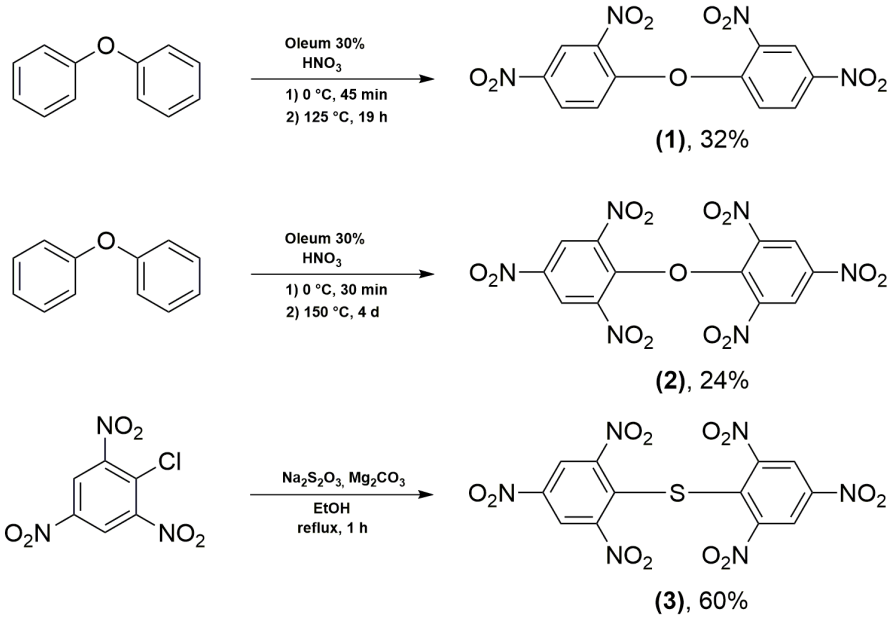

Scheme 1. Reaction schemes for compounds **(1)**–**(3)**.

Although some of these compounds have existed for almost a century and show some importance today, various fundamental analytical data such as NMR or vibrational spectroscopy are still missing.[9a, 10] Therefore all three compounds were characterized

through multinuclear NMR-, infrared-, Raman spectroscopy, elemental analysis, and single-crystal X-ray diffraction. The ^{1}H NMR chemical shifts of the proton in ortho position between the NO_2 groups (**1**: 8.9, **2**: 8.6; **3**: 9.1), correspond well with those of 1-substituted trinitro derivatives such as TNT (8.8 ppm) or picric acid (9.0 ppm).[11] In the ^{13}C NMR spectra, the corresponding chemical shifts are observed between 160 ppm and 120 ppm. In the ^{14}N NMR of **1**, **2** and **3** the differently substituted NO_2 groups are not distinct, due to the signal width of 316 Hz, 280 Hz, and 520 Hz. Characteristic infrared and Raman vibration modes could be assigned according to the literature[12] and are listed in **Table 1**.

Table 1. Characteristic vibration modes of **1**, **2**, and **3**.

	1		**2**		**3**	
	IR	Raman	IR	Raman	IR	Raman
ν(C-H)	3090	3106	3103	3107	3093	3094
$\nu_{as}(NO_2)$	1530	1543	1536	1543	1530	1545
$\nu_{s}(NO_2)$	1342	1361	1339	1362	1332	1354
ν(C-N)	913	940	913	941	911	936
$\delta(NO_2)$	743	796	749	797	748	773

$\nu_{as/s}$ asymmetric/ symmetric vibration mode; δ: deformation vibration

The substitution of the sulfur in **3** by the more electronegative oxygen in **2** and **1** causes a shift to higher wavenumbers, which is observed for the ν(C-N) vibration mode. This displacement can be regarded as a measure of the corresponding bond strength. The greater the shift to higher wavenumbers, the stronger the C-N bond. Thus, the bond strength correlates proportionally with the bond dissociation enthalpy (BDE), which – as many researchers have shown – is associated with the sensitivity of energetic materials.[13] According to this model **3** is expected to have the lowest BDE whereby **2** and **1** should be in a similar range.

In this work, the BDEs were calculated from their crystal structure data using the B3LYP/6-311G+(d,p) method, the found values are depicted in **Figure 1**.

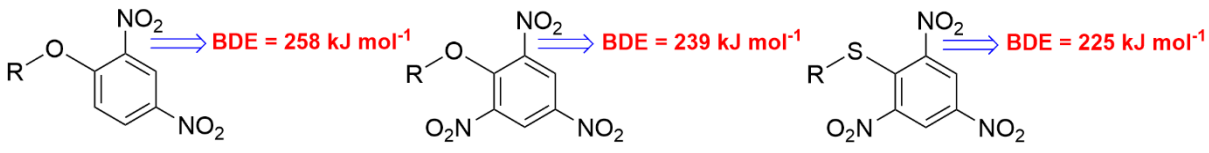

Figure 1. Calculated BDE Values of the weakest Bond in the molecule **1**, **2** and **3**, considering all X-C bonds (X: C, O, N, S)

Since the values of the BDEs for the three compounds all range between RDX (161 kJ mol^{-1}) and TATB (355 kJ mol^{-1}), they can be categorized as sensitive.[14] The calculated trend of decreasing BDEs from **1** to **3** is consistent with the trend of experimental

observation of the shift to higher wavenumbers of the *v*(C–N) vibration mode. As numerous studies have shown, BDEs are considered the most important factor in pyrogenic decomposition for the possible trigger binding that breaks first and can therefore be used to assess the sensitivity of a material.[7] Besides the calculation of h_{50} values or the determination of *volume-based sensitivities*, the electrostatic potential (ESP) is often used to understand changes in the sensitivities and to visualize the bond strength variation.[3b]

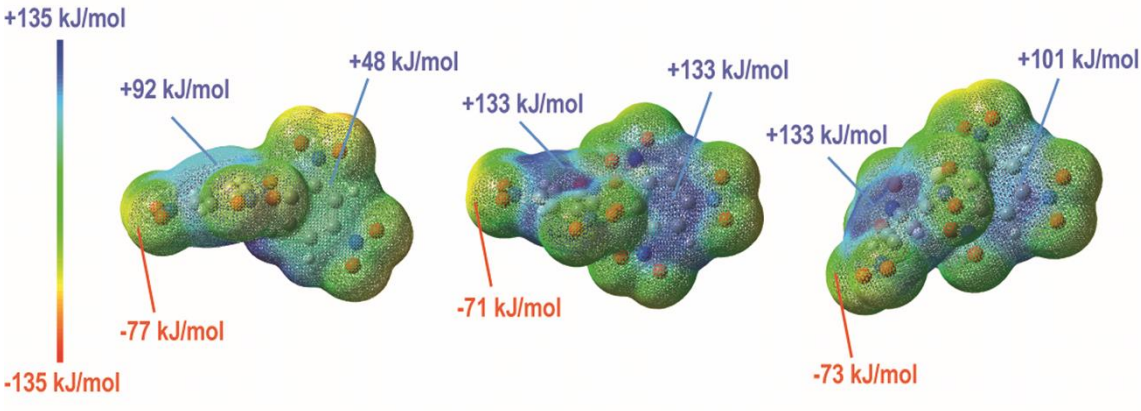

Figure 2. ESP of **1** (left), **2** (center) and **3** (right), calculated on the 0.02 electron bohr^{-3} hypersurface.

The visualization of the ESP for compounds **(1)**–**(3)** is shown in **Figure 2**. For all compounds, the positive range is larger than the negative range. All positive values are significantly stronger than the negative absolute values. In addition to the strongly positive center of the respective molecules, this is a general indication of their sensitive character.[3b-d] According to the BDEs and the ESP, the sensitivity of the compounds should increase from **1** to **3**. However, a different trend is present in experimental observations (**1** < **3** < **2**). Thus, these older prediction models are insufficient to explain the actual sensitivities values that were obtained in experiments. In order to explain this, more modern methods that use the crystal structure and packaging effects have to be applied to correctly assess the structure-property relationships and therefore the sensitivities of this group of nitroaromatic compounds.

***5.3.2 Structure-property relationship*.** In the crystal, an external mechanical stimulus like impact or friction can cause a displacement of the layers, which generates internal strains. If this strain energy is below the lowest BDE, the molecular integrity is not destroyed. If the strain energy is higher than the energy required to break the weakest bond the material is destroyed.[8b] The strain caused by the sliding of the layers depends strongly on the stacking of the layers and other interactions in the crystal, such as hydrogen bridges.[15] It can be seen from the monomers a, b and c, that the phenyl residues in the molecules are twisted against each other to different degrees (**Figure 3**). This results in a different packing behavior in the crystal (d, e, f). The strain energy resulting from a mechanical stimulus should be the greatest for **2** since the gearing of the individual layers is the highest.

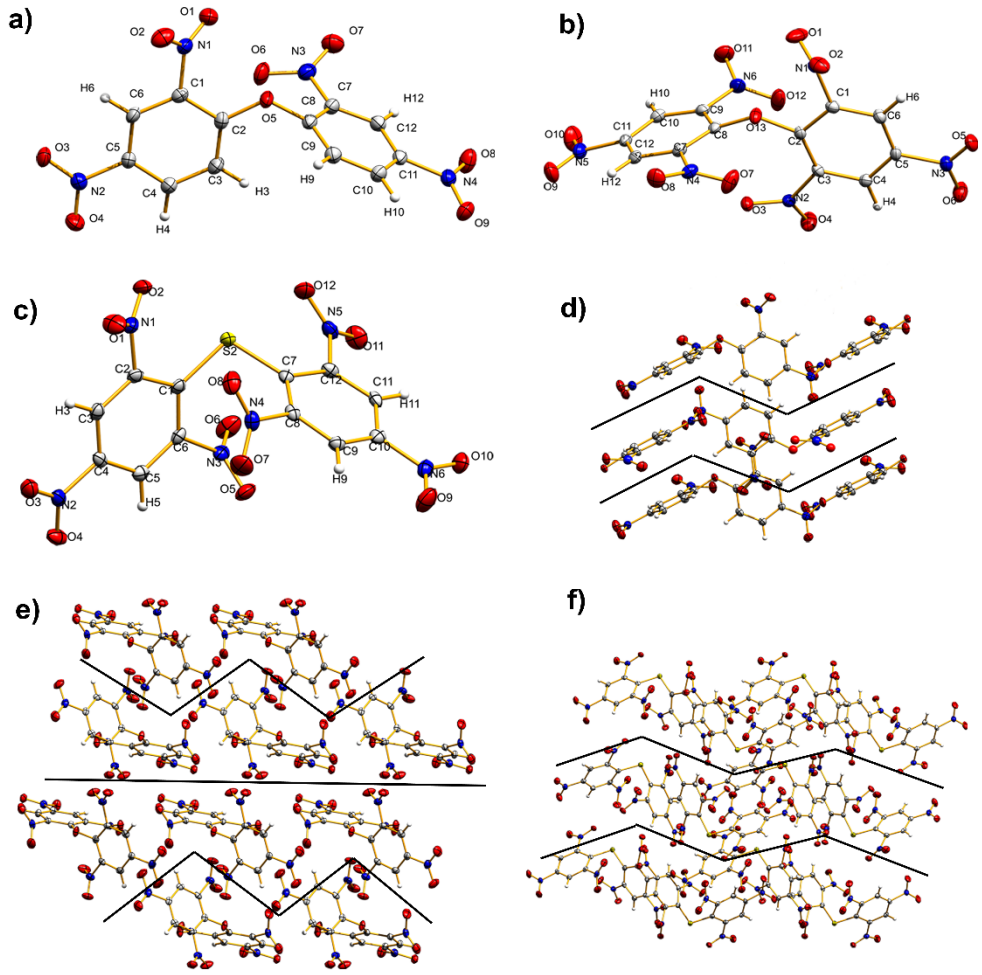

Figure 3. Single-crystal X-ray structure of **1** (a), **2** (b), **3** (c) and the crystal packing of **1** (d), **2** (e), **3** (f).

This effect can reduce the slip barrier to such an extent that it becomes smaller than the BDE.[8b] In addition to the lower gearing of **3** versus **2**, this effect is another indication for the higher sensitivity of compound **2** when compared with compound **3**. In addition to crystal packing, intermolecular interactions contribute significantly to the height of the slide barrier and therefore to the sensitivity to external mechanical stimuli. A feature exhibited by insensitive molecules is, that the Hirshfeld surface on a plane has the most red dots representing close contacts.[15] In the present case, all compounds (**1**, **2,** and **3**) have red dots which point out of a plane (**Figure 4**). The close contacts are not arranged in a slideable plane, which results in interlayer repulsion that can be significantly increased by shifting the plane.

The O···O interaction is a very important close contact interaction. In most cases, a high frequency of O···O contacts indicates a high sensitivity, because more nitro groups are exposed on the molecular surface and that increases the risk of explosion due to the exceeding repulsion via an interlayer sliding.[7, 8b, 14a, 15] Thus, graph d clearly shows that **2** is the most sensitive compound. With 37.9 % of O···O contacts, **2** has the most of those contacts compared to **3** with 33.5 % and **1** with 16.6 %. This distribution can be retrieved from the 2D plot because the marked O···O interactions decrease from a

via c to b in area and color intensity. Furthermore, O···H and N···H contacts, which generate an intermolecular 3D network, can make a compound more sensitive, since an interlayer slide strongly alters these stabilizing interactions. However, the replacement of hard O···O interactions with softer N···H or O···H interactions often leads to better absorption of mechanical stimuli in a material.[14a]

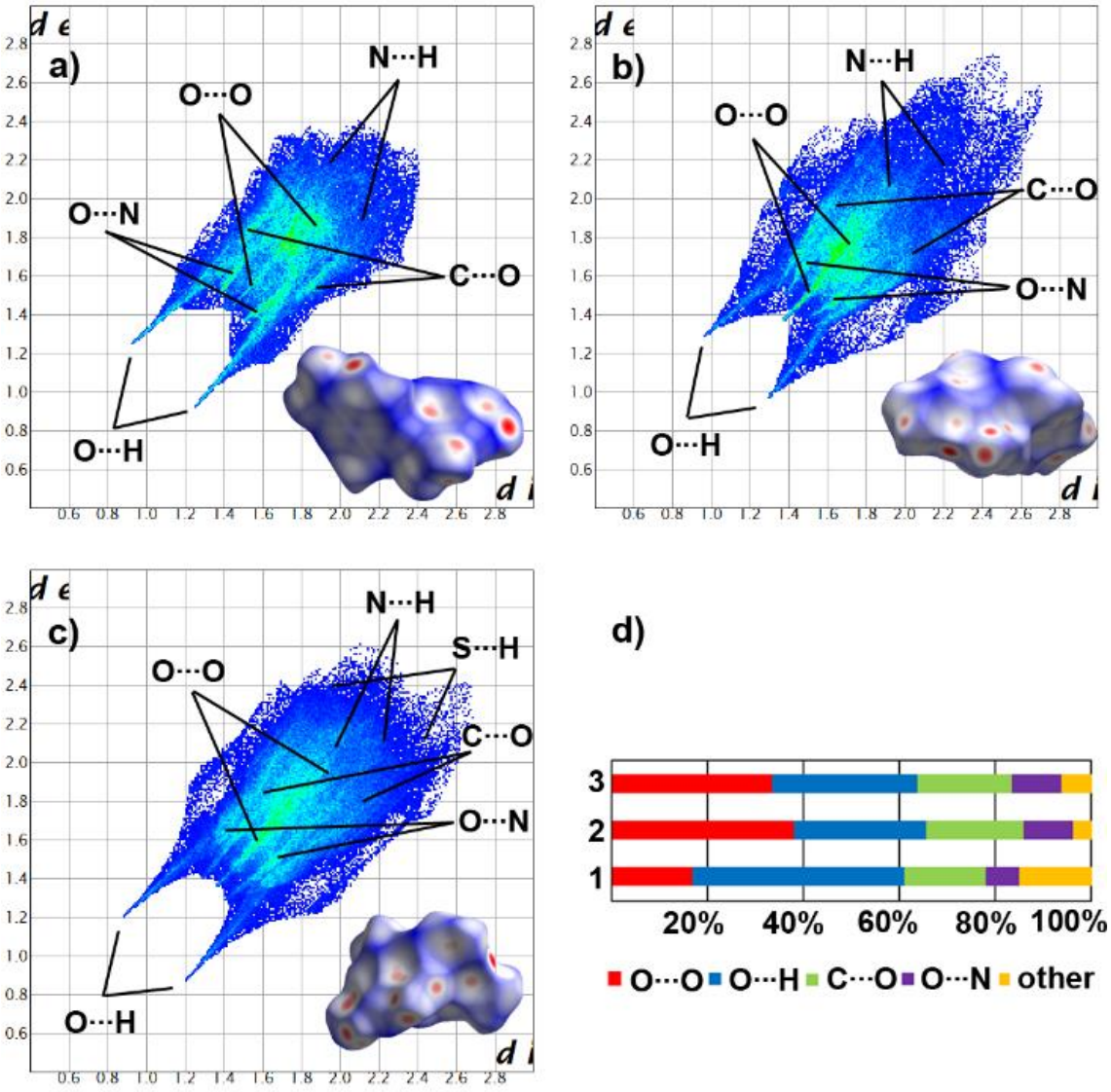

Figure 4. Two-dimensional Fingerprint plot in crystal stacking as well as the corresponding Hirshfeld surface (bottom right in 2D plot) of **1** (a), **2** (b), and **3** (c) (color coding: white, distance d equals VDW distance; blue, d exceeds VDW distance, red, d, smaller than VDW distance). The population of close contacts of **1**, **2**, and **3** in crystal stacking (d).

Strong O···H and N···H interactions are often found in less sensitive compounds because the interlayers are more rigid and can absorb energy better without a shifting of the planes, which would induce a repulsion between the layers.[8b] The 2D Fingerprint plot exhibits two distinctive spikes for strong O···H bonding.[15] With respect to di + de (di: distance from the Hirshfeld surface to the nearest atom interior; de: distance from the Hirshfeld surface to the nearest atom exterior), we can ascertain that

for **1** with a total of 44.3 % the most and strongest hydrogen bonds are present. For **2** the 27.7 % of H-bridges are the fewest and weakest. With a total of 30.1 %, molecule **3** forms more H-bridges than compound **2** but less than molecule **1** while showing similar strong H-bridges than compound **1**. The interlayer contacts of C···O show weak interactions (distances above 3.5 Å) and therefore can be neglected. This also applies to the N···H and N···O contacts.[15] According to this newer model, the frequencies of O···O contacts and the strength and frequency of H-bridges are the most relevant indicator for the impact sensitivity of an explosive material and therefore the order of decreasing sensitivity for the discussed compounds should be **2** > **3** > **1**.

***5.3.3 Heat of formation and detonation parameters*.** Density plays an important role in the performance of energetic materials and is a direct result of the packing in the crystal. With respect to **1**, **2**, and **3**, crystal densities are observed to be 1.73, 1.84, and 1.85 g cm^{-3} at 143 K, and the extrapolated values at room temperature are 1.69, 1.80, and 1.81 g cm^{-3}. These values deviate significantly from the older literature values 1.70 (**2**) and 1.61 g cm^{-3} (**3**).[2]. To gain accurate values for the heat of formation (HOF) it is important to use high precision theoretical methods, as experimental values are often inaccurate.[7] Therefore, the heat of formation was computed by ab initio calculations using the optimized geometry of molecules starting from the X-ray diffraction experiment. According to Trouton´s Rule, the heat of formation (HOF) was calculated by subtracting the enthalpy of sublimation from the HOF of the corresponding gas-phase species.[16] The values for the HOF of the gas phase species were obtained by subtraction of the atomization energies from the total enthalpy of the molecule.[17] Calculations were performed using the CBS-4M level of theory in combination with the crystal structures. By using the specific densities and the EXPLO5 (V6.01) program, the detonation properties of **1**, **2** and **3** could be estimated. They were calculated at the Chapman−Jouguet point (C-J point) with the help of the stationary detonation model using a modified Becker−Kistiakowski−Wilson state equation for gaseous detonation products and the Murnaghan equation of state for condensed products (compressible solids and liquids). By using the first derivative of the Hugoniot curve of the system the C-J point could be found.[18] Given the high density and heat of formation, it is not surprising that compound **2** exhibits a better performance than **1** and **3**. Although **1** has a higher heat of formation, the influence of the increased density of **2** predominates so strongly that **2** has the best performance. As can be seen in **Table 2**, the oxygen balance for **1** is the lowest due to the lower number of NO_2 groups. The substitution of the ether bridge in **2** by a sulfur atom deteriorates the oxygen balance from **2** to **3** as expected. With respect to the detonation velocity, the values of **2** and **3** exceed TNT (6881 m s^{-1}) where **1** falls below it.

Table 2. Physical and Calculated detonation parameters of compounds **1**, **2**, and **3** using EXPLO5 computer code.

	1	**2**	**3**
formula	$C_{12}H_6N_4O_9$	$C_{12}H_4N_6O_{13}$	$C_{12}H_4N_6O_{12}S$
M_r [g mol^{-1}]	350.20	440.19	456.25
IS[a] [J]	>40	9	12.5
FS[b] [N]	>360	>360	>360
ESD [mJ]	50	50	50
N[c] [%]	16.00	19.09	18.42
N+O[d] [%]	57.12	66.34	60.50
Ω_{CO2}[e] [%]	-82.24	-47.25	-56.11
T_{melt}[f] [°C]	246.32	---	253
T_{dec}[g] [°C]	336.73	256	310
$\rho_{143\ K}$[h] [g cm^{-3}] (X−ray)	1.73	1.84	1.85
$\rho_{298\ K}$[i] [g cm^{-3}]	1.68	1.80	1.81
ΔH_f°[j] [kJ mol^{-1}]	-168.1	-132.9	-20.3
EXPLO5 V 6.03			
ΔU_f°[k] [kJ kg^{-1}]	-3934	-4850	-4689
T_{C-J}[l] [K]	2958	3695	2740
P_{C-J}[m] [GPa]	16.7	24.9	15.9
V_{det}[n] [ms^{-1}]	6582	7634	6912
V_o[o] [dm^3 kg^{-1}]	582.5	620.4	427.5

[a] Impact sensitivity[14d] [b] friction sensitivity[14e] [c] nitrogen content [d] combined nitrogen and oxygen content [e] absolute oxygen balance assuming the formation of CO or CO_2 [f] melting point from DTA [g] decomposition from DTA [h] density determined by X−ray experiment at 143 K [i] ambient temperature density, extrapolated from X-ray value [j] Heat of formation calculated at the CBS-4M level of theory for FMN, experimental determined for MN [k] detonation energy [l] detonation temperature [m] detonation pressure [n] detonation velocity [o] volume of detonation gases at standard temperature and pressure conditions

5.4 Conclusions

Bis(2,4-dinitrophenyl) ether, bis(2,4,6-trinitrophenyl) ether, and bis(2,4,6-trinitrophenyl) thioether have been synthesized and characterized. The structures of these three compounds were determined by single-crystal X-ray diffraction. The results of the older prediction models (BDE, ESP) for the sensitivities were compared with results for newer prediction models based on the crystal structure (Hirshfeld surface and Fingerprint plot analysis). The inaccurate trend for the sensitivities that was observed for the older models (**3** > **2** > **1**) could be corrected. The trend for the sensitivities shown by the experimental values (decreasing **2** > **3** > **1**), could be verified by the newer

predictive methods which are based on the crystal structure. The application of these newer methods could lead to a better understanding and assessment of sensitivity values without the necessity to synthesize large amounts of new energetic materials, which leads to an increase in safety. The performance of the compounds was calculated and it was found that it decreases from **2** to **3** to **1** with all three compounds showing similar values as TNT.

5.5 Experimental Section

General Information. Diphenylether, nitric acid, oleum, picryl chloride, and sodium thiosulfate were commercially available. For NMR spectroscopy the solvent DMSO-d_6 was dried using a 3 Å mole sieve. Spectra were recorded on a Bruker Avance III spectrometer operating at 400.1 MHz (^{1}H), 100.6 MHz (^{13}C), and 28.9 MHz (^{14}N). Chemical shifts are referred to TMS (^{1}H, ^{13}C) and $MeNO_2$ (^{14}N). Raman spectra were recorded with a Bruker MultiRam FT Raman spectrometer using a neodymium-doped yttrium aluminum garnet (Nd:YAG) laser (λ = 1064 nm) with 1074 mW. The samples for Infrared spectroscopy were placed under ambient conditions onto an ATR unit using a Perkin Elmer Spectrum BX II FT-IR System spectrometer. Melting and/or decomposition points were detected with a OZM DTA 552-Ex instrument. The scanning temperature range was set from 293 K to 673 K at a scanning rate of 5 K min^{-1}. Elemental analysis was done with a Vario EL instrument and a Metrohm 888 Titrando device.

Caution! *All investigated compounds are explosives, which show partly increased sensitivities toward various stimuli (e.g. higher temperatures, impact, friction, or electrostatic discharge). Therefore, proper safety precautions (safety glass, Kevlar gloves, and earplugs) have to be applied while synthesizing and handling the described compounds.*

***5.5.1 Bis(2,4-dinitrophenyl) ether*.** Diphenylether (2.15 g, 12.65 mmol) was added at 0 °C to a mixed acid consisting of 1.15 mL sulfuric acid, 2.74 mL Oleum (65%), and white fuming nitric acid (2.7 mL, 63.26 mmol). The mixture was stirred for 45 min. After being warmed to room temperature, the solution was heated to 125 °C for 19 hours. The obtained reddish suspension was cooled to room temperature and poured into 750 mL of ice water. The solid was filtered off and washed with water (3 × 100 mL). The filter cake was recrystallized from boiling ethyl acetate and the beige-red powder was dried under ambient conditions (1.4 g, yield: 32%).

^{1}H NMR (DMSO-d_6, 400 MHz): δ 7.67 (d, 2H, J = 2.8 Hz), 8.60 (dd, 2H, J = 9.1, 2.8 Hz), 8.98 (s, 2H, J = 9.1 Hz) ppm. **^{13}C NMR** (DMSO-d_6,100 MHz): δ 151.7, 143.8, 140.3, 130.2, 122.4, 122.3 ppm. **^{14}N NMR** (DMSO-d_6, 29 MHz): δ -20 (s, NO_2) ppm. **FT-IR** (ATR): $\tilde{\nu}$ 3365 (w), 3090 (w), 3076 (w), 2879 (w), 1592 (m), 1530 (s), 1483 (m), 1472 (m), 1422 (w), 1342 (s), 1265 (s), 1155 (w), 1136 (w), 1122 (w), 1067 (s),

972 (w), 928 (m), 913 (s), 867 (s), 834 (s), 787 (w), 762 (w), 743 (s), 721 (s), 687 (w), 661 (m), 639 (m), 603 (w), 521 (w), 499 (w), 458 (w), 435 (w). **Raman** (1064 nm, 300 mW): $\tilde{\nu}$ 3076 (w), 2263 (w), 2217 (w), 2202 (w), 2157 (w), 2137 (w), 2062 (w), 1951 (w), 1611 (m), 1597 (w), 1547 (w), 1352 (s), 1270 (w), 1213 (w), 1156 (w), 1137 (w), 1066 (w), 838 (m), 641 (w). **Elemental Analysis** calcd. (%) for $C_{12}H_6N_4O_9$: C 41.16, H 1.73, N 16.00; found: C 41.09, H 1.82, N 15.82. **DTA**: 246 °C (melting), 336 °C (dec.) **IS**: >40.0 J. **FS**: >360 N. **ESD**: 50 mJ.

***5.5.2 Bis(2,4,6-trinitrophenyl) ether. Diphenylether*.** (1.00 g, 5.88 mmol) was added at 0 °C successively to a mixed acid consisting of 22 mL oleum (30 %) and white fuming nitric acid (4.4 mL, 106 mmol). The mixture was stirred for 30 min. After being warmed to room temperature, the solution was heated to 150 °C for 4 d. The obtained white suspension was cooled to room temperature and poured into 750 mL of ice water. The solid was filtered off and washed with water (3 × 100 mL). The filter cake was recrystallized from boiling chloroform and the colorless powder was dried under ambient conditions (0.53 g, yield: 24%).

^{1}H NMR (DMSO-d_6, 400 MHz): δ 8.60 (s, 4H) ppm. **^{13}C NMR** (DMSO-d_6,100 MHz): δ 160.6, 141.8, 125.2, 124.6 ppm. **^{14}N NMR** (DMSO-d_6, 29 MHz): δ -11 (s, NO_2) ppm. **FT-IR** (ATR): $\tilde{\nu}$ 3103 (m), 1612 (m), 1601 (m), 1536 (s), 1455 (m), 1415 (m), 1339 (s), 1268 (s), 1212 (m), 1191 (m), 1085 (m), 944 (m), 927 (m), 913 (m), 832 (m), 795 (m), 749 (m), 733 (m), 717 (s) 523 (m). **Raman** (1064 nm, 1074 mW): $\tilde{\nu}$ 3107 (w), 1627 (m), 1559 (m), 1543 (m), 1362 (s), 1275 (w), 1214 (m), 1171 (w), 1083 (w), 941 (w), 829 (m), 797 (w), 329 (w), 270 (w), 202 (w). **Elemental Analysis** calcd. (%) for $C_{12}H_4N_6O_{13}$: C 32.74, H 0.92, N 19.09; found: C 32.71, H 1.01, N 18.88. **DTA**: 256 °C (dec.) **IS**: 9.0 J. **FS**: 360 N. **ESD**: 50 mJ.

***5.5.3 Bis(2,4,6-trinitrophenyl) thioether*.** Sodium thiosulfate (0.498 g, 3.15 mmol) was added successively to a reflux heated suspension of picryl chloride (1.00 g, 4.04 mmol) and magnesium carbonate (0.190 g, 2.26 mmol) in absolute ethanol (25 mL). The mixture was heated for 1 h. The mixture turned into a yellow suspension. After being cooled to room temperature the obtained suspension was filtered off and the filter cake washed with ethanol (3 × 15 mL), 1.0 M HCl (3 × 5 mL), and water (3 × 5 mL). The yellow powder was dried under a nitrogen stream (1.1 g, yield: 60%).

^{1}H NMR (DMSO-d_6, 400 MHz): δ 9.17 (s, 4H) ppm. **^{13}C NMR** (DMSO-d_6,100 MHz): δ 151.6, 147.8, 125.6, 124.4 ppm. **^{14}N NMR** (DMSO-d_6, 29 MHz): δ -19 (s, NO_2) ppm. **FT-IR** (ATR): $\tilde{\nu}$ 3093 (m), 2917 (w), 2850 (w), 1598 (m), 1530 (s), 1392 (w), 1332 (s), 1169 (w), 1112 (w), 1047 (m), 931 (m), 911 (s), 822 (m), 748 (m), 726 (s), 718 (s), 687 (m). **Raman** (1064 nm, 1074 mW): $\tilde{\nu}$ 3094 (w), 1601 (m), 1545 (m), 1354 (s), 1301 (w), 1180 (m), 1059 (m), 936 (m), 825 (w), 773 (m), 433 (w), 370 (w), 331 (w), 287 (w). **Elemental Analysis** calcd. (%) for $C_{12}H_4N_6O_{12}S$: C 31.59, H 0.88, N 18.42, S 7.03; found: C 31.48, H 0.94, N 18.34, S 7.17. **DTA**: 253 °C (mp), 310 °C (dec.) **IS**: 12.5 J. **FS**: 360 N. **ESD**: 50 mJ.

5.5.4 X-Ray Measurements. Bis(2,4,6-trinitrophenyl) ether and bis(2,4-dinitrophenyl) ether were solved in ethyl acetate and single crystals have been received after slow solvent evaporation. Single crystals of bis(2,4,6-trinitrophenyl) thioether have been received of the decomposition of fluoromethyl-(2,4,6)-trinitrobenzene sulfonate with triphenylphosphine sulfid in DCM after slow solvent evaporation. Data collection was performed with an Oxford Xcalibur3 diffractometer with a CCD area detector, equipped with a multilayer monochromator, a Photon 2 detector and a rotating-anode generator

were employed for data collection using Mo-Kα radiation (λ= 0.7107 Å). Data collection and reduction were carried out using the Crysalispro software.[19] The structures were solved by direct methods (SIR-2014)[20] and refined (SHELXLE)[21] by full-matrix least-squares on F2 (ShelxL)([22][23]) and finally checked using the platon software[24] integrated with the WinGX software suite.[25] The non-hydrogen atoms were refined anisotropically and the hydrogen atoms were located and freely refined. All Diamond 3 plots are shown with thermal ellipsoids at the 50% probability level and hydrogen atoms are shown as small spheres of arbitrary radius.

ASSOCIATED CONTENT

Supporting Information

The Supporting Information is available free of charge on the ACS Publication website.

^{1}H, ^{13}C, ^{14}N NMR spectra; Detonation parameter calculations (output files) (PDF)

X-ray data for bis(2,4-dinitrophenyl) ether (CIF)

CCDC: 1959182

X-ray data for bis(2,4,6-trinitrophenyl) ether (CIF)

CCDC: 1959183

X-ray data for bis(2,4,6-trinitrophenyl) thioether (CIF)

CCDC: 1959184

AUTHOR INFORMATION

Corresponding Author

* tmk@cup.uni-muenchen.de

ORCID

Konstantin Karaghiosoff: 0000-0002-8855-730X

Thomas Klapötke: 0000-0003-3276-1157

Marco Reichel: 0000-0003-0137-4816

Dominik Dosch: 0000-0003-4804-6473

Author Contributions

‡ Marco Reichel and Dominik Dosch contributed equally to this work.

Notes

The authors declare no competing financial interests.

5.6 Acknowledgment

For financial support of this work by Ludwig−Maximilian University (LMU), the Office of Naval Research (ONR) under grant no. ONR.N00014-16-1-2062 and the Strategic Environmental Research and Development Program (SERDP) under contract no. WP19-1287 are gratefully acknowledged. The authors also thank Ms. Teresa Küblböck for help with the graphics and F−Select GmbH for the generous donation of fluoro-chemicals.

5.7 References

[1] Nobel, A. Dynamit. United Kingdom, **1867**.

[2] a) Köhler, J.; Meyer, R.; Homburg, A. *Explosivstoffe*, Wiley-VCH, **2008**, Weinheim; b) Klapötke, T. M. *Energetic Materials Encyclopedia*, De Gruyter, 1st edn., **2018**, Boston/Berlin.

[3] a) Giles, J. Green explosives: collateral damage. *Nature* **2004**, *427*, 580-581; b) Klapötke, T. M. *Chemistry of High-Energy Materials*, De Gruyter, 5th edn., **2019**, Boston/Berlin c) Reichel, M.; Krumm, B.; Vishnevskiy, Y.; Blomeyer, S.; Schwabedissen, J.; Stammler, H.-G.; Karaghiosoff, K.; Mitzel, N. W. *Angew. Chem. Int. Ed.* **2019**, *in Press* (DOI: 10.1002/anie.201911300*)*; d) Reichel, M.; Krumm, B.; Karaghiosoff, K. Synthesis, and investigation of highly energetic and shock-sensitive fluoromethyl perchlorate. *J. Fluorine Chem.* **2019**, *226*, 109351.

[4] a) Zhi, C.-Y.; Cheng, X.-L.; Zhao, F. The Correlation between Electric Spark Sensitivity of Polynitroaromatic Compounds and Their Molecular Electronic Properties. *Propellants, Explos., Pyrotech.* **2010**, *35*, 555-560; b) Zeman, S.; Krupka, M. New aspects of impact reactivity of polynitro compounds, part III. Impact sensitivity as a function of the intermolecular interactions. *Propellants, Explos., Pyrotech.* **2003**, *28*, 301-307; c) Tan, B.; Li, H.; Huang, H.; Han, Y.; Li, J.; Li, M.; Long, X. Large π-π separation energies of some energetic compounds. *Chem. Phys.* **2019**, *520*, 81-87.

[5] Gao, H.; Shreeve, J. Azole-Based Energetic Salts. *Chem. Rev. (Washington, DC, U. S.)* **2011**, *111*, 7377-7436.

[6] Thottempudi, V.; Gao, H.; Shreeve, J. Trinitromethyl-substituted 5-nitro- or 3-azo-1,2,4-triazoles: synthesis, characterization, and energetic properties. *J. Am. Chem. Soc.* **2011**, *133*, 6464-6471.

[7] Zhang, J.; Zhang, Q.; Vo, T. T.; Parrish, D. A.; Shreeve, J. Energetic Salts with π-Stacking and Hydrogen-Bonding Interactions Lead the Way to Future Energetic Materials. *Journal of the American Chemical Society* **2015**, *137*, 1697–1704.

[8] a) Spackman, M. A.; Jayatilaka, D. Hirshfeld surface analysis. *CrystEngComm* **2009**, *11*, 19-32; b) Ma, Y.; Zhang, A.; Xue, X.; Jiang, D.; Zhu, Y.; Zhang, C. Crystal Packing of Impact-Sensitive High-Energy Explosives. *Cryst. Growth Des.* **2014**, *14*, 6101-6114.

[9] a) Rath, C.; Rost, A.; Rittler, K. W. Hexanitrodiphenyl ether. Chemische Fabrik von Heyden A.-G. . **1936**; b) Sprengstoff-A.-G. Carbonit . **1912**.

[10] a) Isanbor, C.; Emokpae, T. A. Anilinolysis of nitro-substituted diphenyl ethers in acetonitrile: The effect of some ortho-substituents on the mechanism of SNAr reactions. *Int. J. Chem. Kinet.* **2009**, *42*, 37-49; b) Davydov, D. V.; Mikaya, A. I.; Zaikin, V. G. Mass-spectrometric study of substituted trinitrobenzenes. *Zh. Obshch. Khim.* **1983**, *53*, 455-462; c) Desvergnes, L. Some physical properties of nitro derivatives. *Monit. Sci. Doct. Quesneville* **1926**, *16*, 201-208; d) Zhou, J.; Zhang, C.; Wang, Y.;

Zhang, M.; Li, Y.; Huang, F.; Hu, L.; Xi, W.; Wang, Q. 2,2',4,4',6,6'-hexanitrodiphenyl sulfide refining method. Modern Chemistry Research Institute, Peop. Rep. China . **2015**, p. 6pp.

[11] a) Hussain, I.; Tariq, M. I.; Siddiqui, H. L. Structure elucidation of chromogen resulting from Jaffe's reaction. *J. Chem. Soc. Pak.* **2009**, *31*, 937-948; b) Soojhawon, I.; Lokhande, P. D.; Kodam, K. M.; Gawai, K. R. Biotransformation of nitroaromatics and their effects on mixed function oxidase system. *Enzyme Microb. Technol.* **2005**, *37*, 527-533.

[12] Lewis, I. R.; Daniel, N. W.; Griffiths, P. R. Interpretation of Raman spectra of nitro-containing explosive materials. Part I: Group frequency and structural class membership. *Appl. Spectrosc.* **1997**, *51*, 1854-1867.

[13] a) Li, J. Relationships for the Impact Sensitivities of Energetic C-Nitro Compounds Based on Bond Dissociation Energy. *J. Phys. Chem. B* **2010**, *114*, 2198-2202; b) Li, J. A quantitative relationship for the shock sensitivities of energetic compounds based on X-NO2 (X = C, N, O) bond dissociation energy. *J. Hazard. Mater.* **2010**, *180*, 768-772.

[14] a) Tang, Y.; Zhang, J.; Mitchell, L. A.; Parrish, D. A.; Shreeve, J. Taming of 3,4-Di(nitramino)furazan. *J. Am. Chem. Soc.* **2015**, *137*, 15984–15987; b) Test methods according to the UN Manual of Tests and Criteria, Recommendations on the Transport of Dangerous Goods, N. Y. United Nations Publication, Geneva, 4th revised ed., 2003: Impact: insensitive >40 J, less sensitive ≥35 J, sensitive ≥4 J, very sensitive ≤3 J; friction: insensitive >360 N, less sensitive: 360 N, sensitive <360 N and >80 N, very sensitive ≤ 80 N, extremely sensitive ≤ 10 N; c) www.reichel-partner.com; d) NATO, Standardization Agreement 4489 (STANAG 4489), Explosives, Impact Sensitivity Tests. Brussels, Belgium **1999**; e) NATO, Standardization Agreement 4487 (STANAG 4487), Explosives, Friction Sensitivity Tests. Brussels, Belgium **2002**.

[15] Zhang, C.; Xue, X.; Cao, Y.; Zhou, Y.; Li, H.; Zhou, J.; Gao, T. Intermolecular friction symbol derived from crystal information. *CrystEngComm* **2013**, *15*, 6837-6844.

[16] Klapötke, T. M. *Chemie der hochenergetischen Materialien*, De Gruyter, **2009**, Boston/Berlin.

[17] a) Curtiss, L. A.; Raghavachari, K.; Redfern, P. C.; Pople, J. A. Assessment of Gaussian-2 and density functional theories for the computation of enthalpies of formation. *J. Chem. Phys.* **1997**, *106*, 1063–1079; b) Byrd, E.; Rice, B. M. Improved Prediction of Heats of Formation of Energetic Materials Using Quantum Mechanical Calculations. *J. Phys. Chem. A* **2006**, *110*, 1005–1013.

[18] a) Suceska, M. *EXPLO5 6.01* **2013**, *Brodarski Institute: Zagreb, Croatia*; b) Klapoetke, T. M.; Krumm, B.; Steemann, F. X.; Umland, K.-D. Bis(1,3-dinitratoprop-2-yl) nitramine, a new sensitive explosive combining a nitrate ester with a nitramine. *Z. Anorg. Allg. Chem.* **2010**, *636*, 2343-2346.

[19] CrysAlisPRO (Version 171.33.41), **2009**, Oxford Diffraction Ltd.

[20] Burla, M. C.; Caliandro, R.; Carrozzini, B.; Cascarano, G. L.; Cuocci, C.; Giacovazzo, C.; Mallamo, M.; Mazzone, A.; Polidori, G., Crystal structure determination and refinement via SIR2014. *J. Appl. Crystallogr.* **2015**, *48*, 306.

[21] Hübschle, C.B., Sheldrick, G.M., Dittrich B. ShelXle: a Qt graphical user interface for SHELXL. *J. Appl. Cryst.* 2011, *44*, 1281.

[22] Sheldrick, G. M., SHELXL-97, Program for the Refinement of Crystal Structures., **1997** University of Göttingen, Germany.

[23] Sheldrick, M. A short history of SHELX. *Acta Crystallogr. Sect. A* **2008**, 112.

[24] Spek, A. L., PLATON, A Multipurpose Crystallographic Tool., **1991**, Utrecht University, The Netherlands.

[25] Farrugia, L. J., WinGX and ORTEP for Windows: an update. *J. Appl. Cryst.* **2012**, 849.

5.8 Supporting Information

1 NMR Spectra

1.1 Compound 1

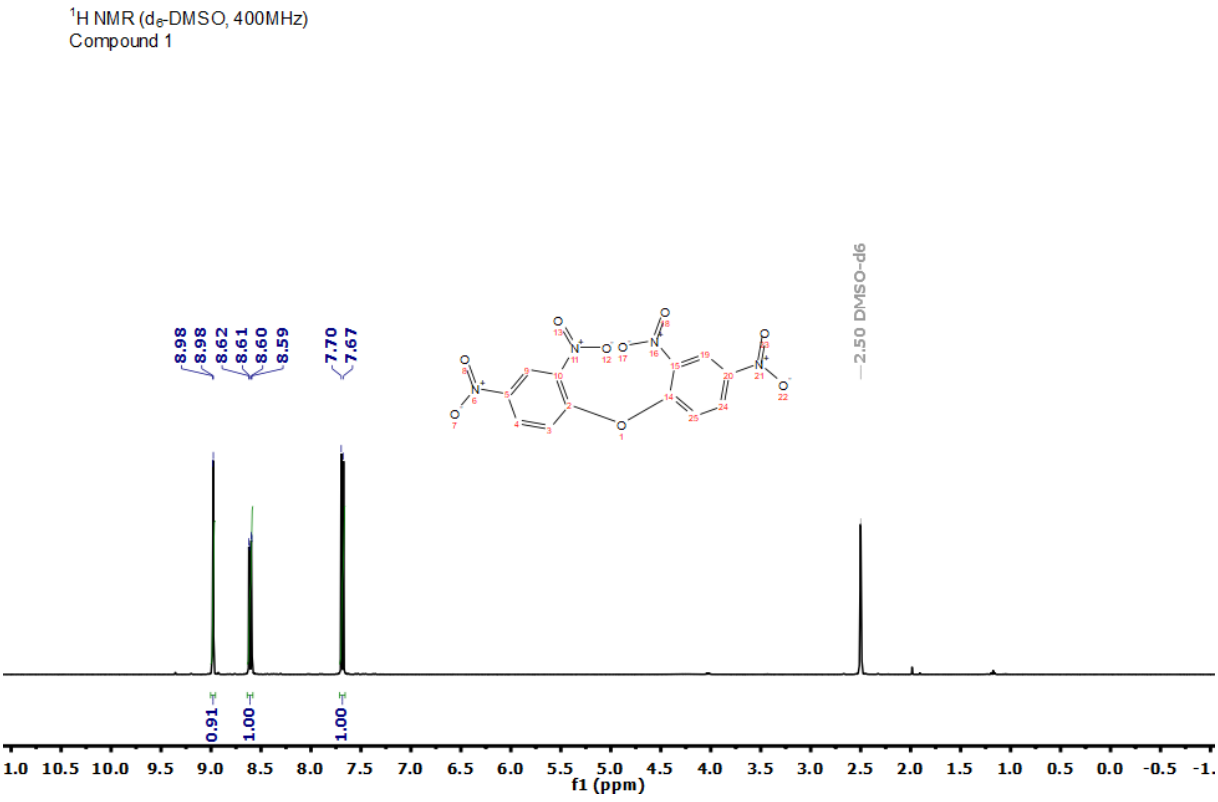

$^{13}C\{^{1}H\}$ NMR (d_6-DMSO, 101 MHz)
Compound 1

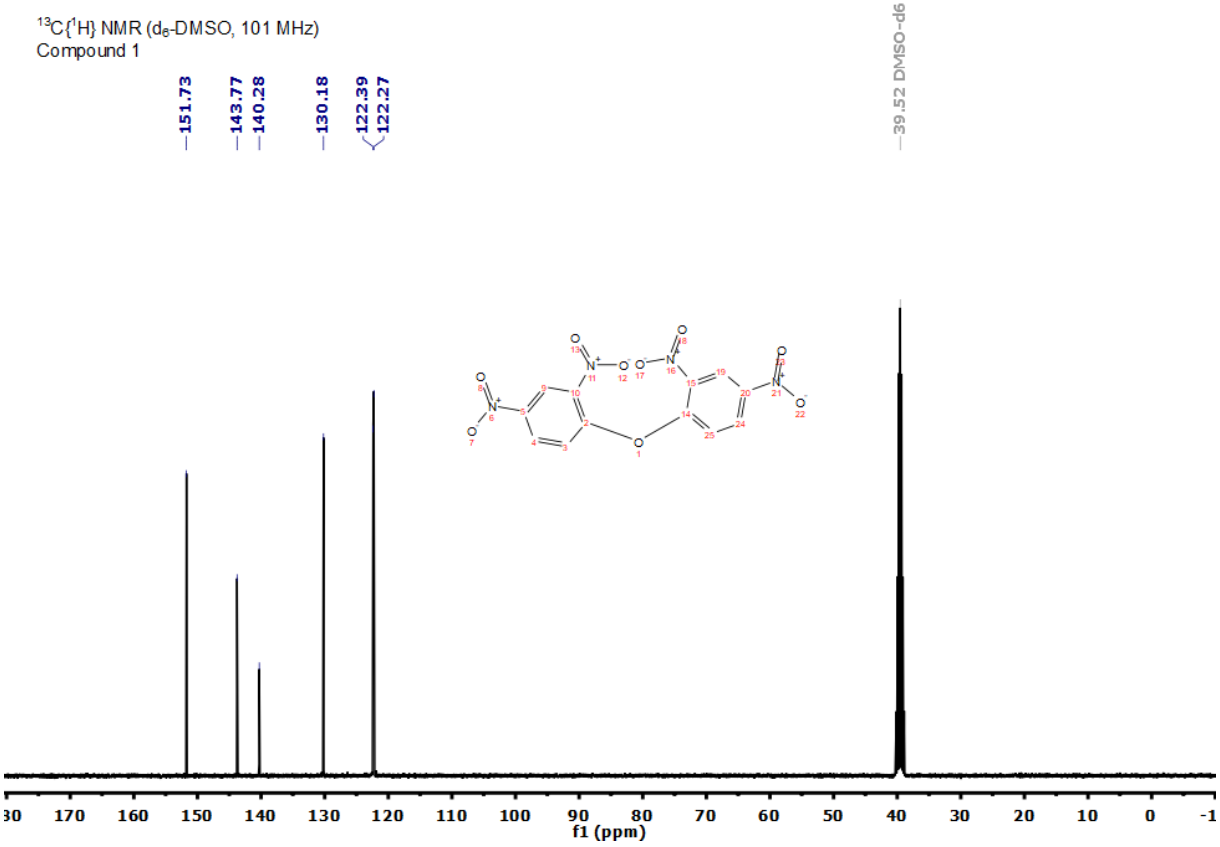

$^{14}N\{^{1}H\}$ NMR (d_6-DMSO, 29 MHz)
Compound 1

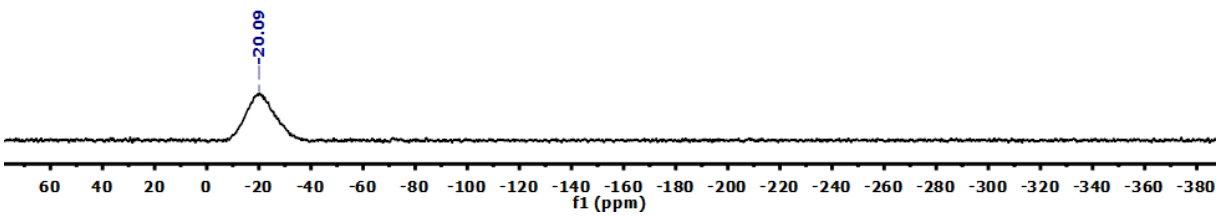

1.2 Compound 2

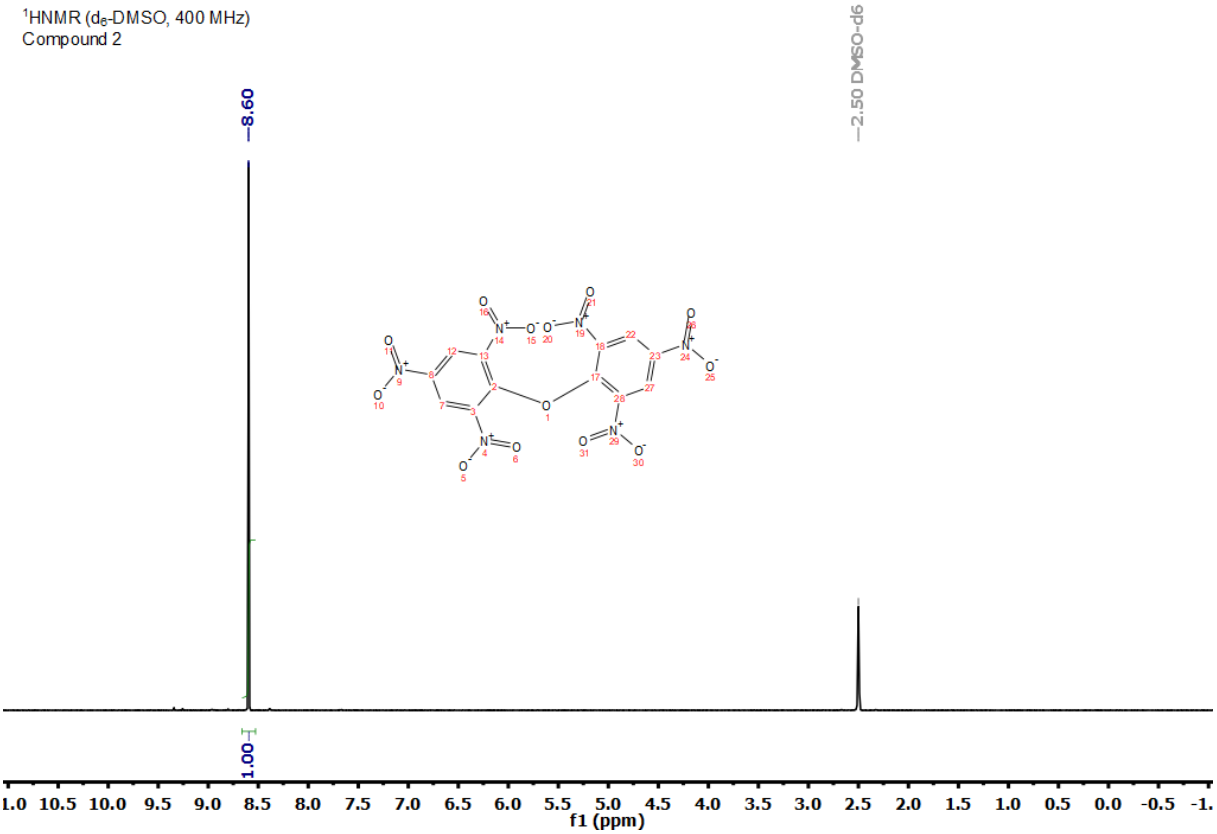

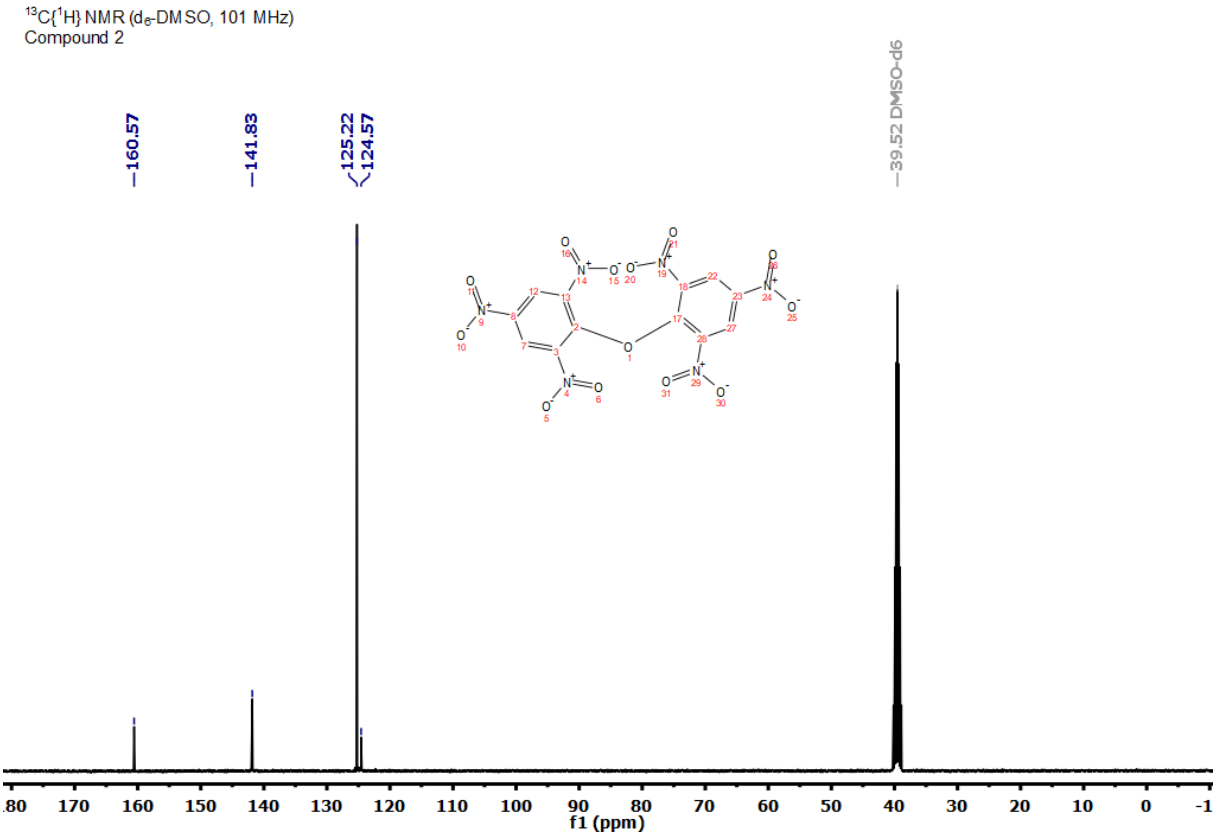

$^{14}N\{^{1}H\}$ NMR (d_6-DMSO, 29 MHz)
Compound 2

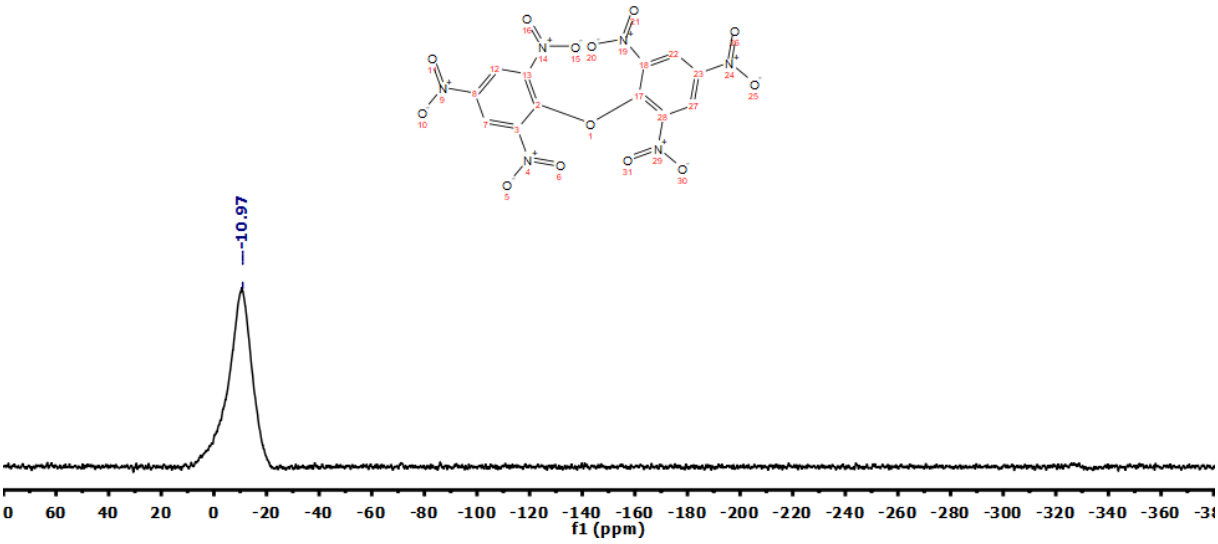

1.3 Compound 3

^{1}H NMR (d_6-DMSO, 400MHz)
Compound 3

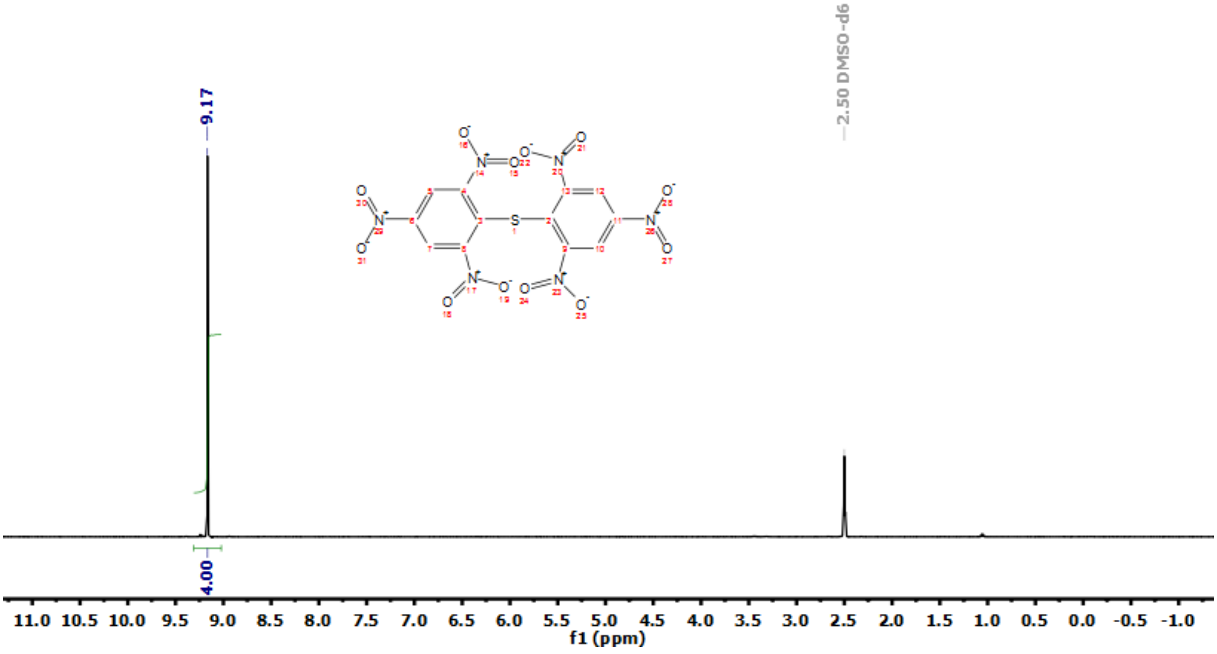

$^{13}C\{^{1}H\}$ NMR (d_6-DMSO, 101MHz)
Compound 3

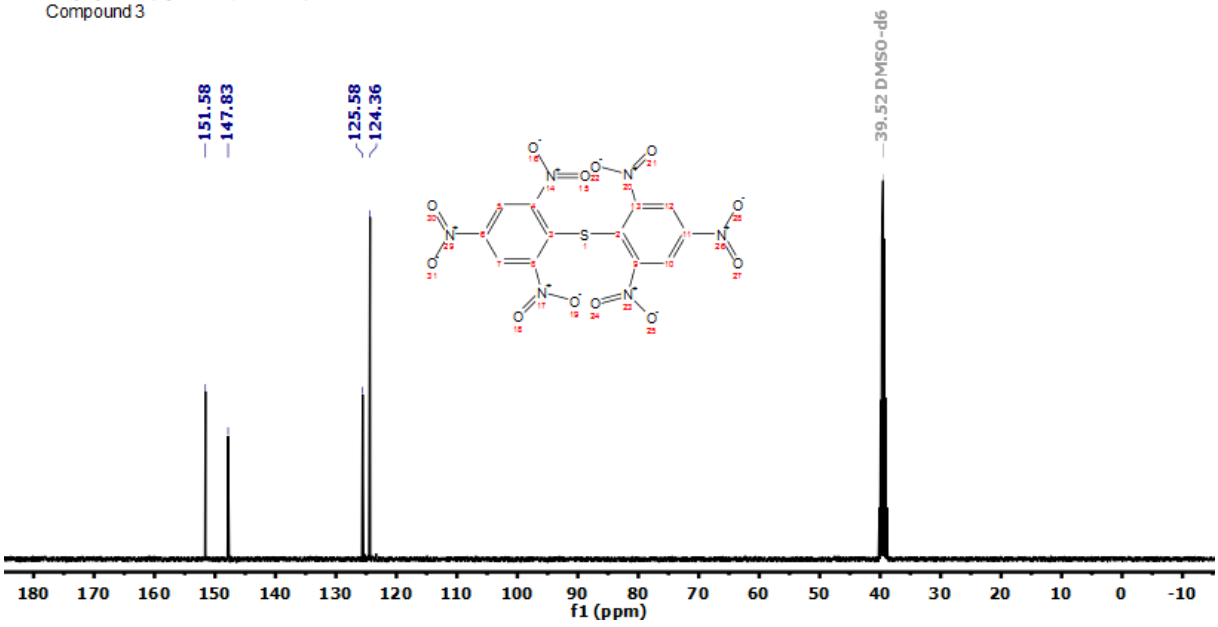

$^{14}N\{^{1}H\}$ NMR (d_6-DMSO, 29 MHz)
Compound 3

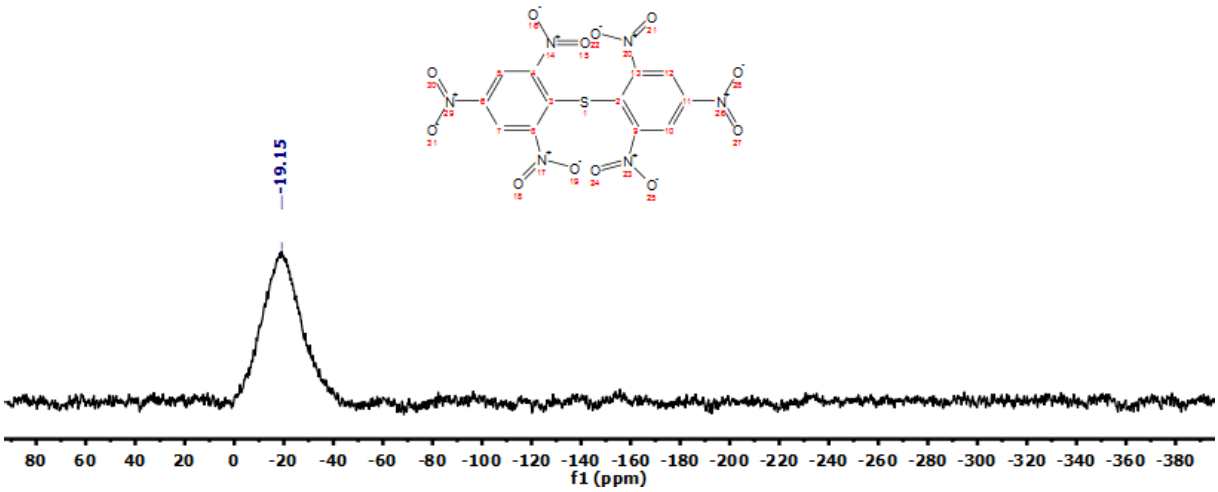

2 Detonation Parameter

2.1 Compound 1

C(12,000) H(6,000) N(4,000) O(9,000)

Molecular weight = 350,19

Density of explosive = 1,689 g/cm^3

Oxygen balance = -82,23569 %

Enthalpy of formation = -480,02 kJ/kg

Internal energy of formation= -412,78 kJ/kg

Detonation parameters (at the C-J point):

Heat of detonation = -3934,204 kJ/kg

Detonation temperature = 2958,848 K

Detonation pressure = 16,76195 GPa

Detonation velocity = 6582,22 m/s

Particle velocity = 1507,727 m/s

Sound velocity = 5074,493 m/s

Density of products = 2,190834 g/cm^3

Volume of products = 0,4564473 cm^3/g

Exponent 'Gamma' = 3,365658

Moles of gaseous products = 8,341371 mol/mol explosive

Moles of condensed products = 7,721982 mol/mol explosive

Volume of gas at STP = 582,5294 dm^3/kg

Mean molecular mass of gas. prod. = 30,86434 g/mol

Mean molecular mass of cond.prod.= 12,011 g/mol

Mean molecular mass of all prod. = 21,80115 g/mol

Entropy of products = 6,020409 kJ/kg K

Internal energy of products = 5070,83 kJ/kg, i.e. 8,564632 kJ/cm^3

Compression energy = 1136,627 kJ/kg, i.e. 1,919762 kJ/cm^3

Total heat energy = -3934,204 kJ/kg, i.e. -6,64487 kJ/cm^3

Composition of detonation products:

Products	mol/mol	mol/kg	Mol %
C(d) =	5,478155	15,64333	34,10344
C(gr) =	2,243827	6,407437	13,96861
H_2O =	1,994153	5,694471	12,4143
N_2 =	1,969661	5,624534	12,26183
CO_2 =	1,95825	5,591948	12,19079
CO =	1,462114	4,175191	9,102175
CH_2O_2 =	0,8133489	2,322587	5,063383
H_2 =	0,05551904	0,1585393	0,3456255
NH_3 =	0,04892552	0,1397109	0,3045785
CH_4 =	0,0221407	0,06322464	0,1378336
HCN =	0,01168588	0,03337	0,07274867
C_2H_4 =	0,002493494	0,007120383	0,01552287
C_2H_6 =	0,002478281	0,00707694	0,01542817
CH_3OH =	0,0004634941	0,001323547	0,002885414
CH_2O =	4,890695E-05	0,0001396579	0,0003044629
H =	3,28261E-05	9,373769E-05	0,000204354
NH_2 =	2,222998E-05	6,347959E-05	0,0001383894
CHNO =	1,900792E-05	5,427872E-05	0,000118331
N_2H_4 =	1,040695E-05	2,971792E-05	6,478691E-05
CNO =	3,961135E-06	1,131136E-05	2,465946E-05
N =	4,6288E-08	1,321793E-07	2,88159E-07
N_2O =	4,094651E-08	1,169262E-07	2,549064E-07
NO_2 =	1,861445E-08	5,315513E-08	1,158815E-07

2.2 Compound 2

C(12,000) H(4,000) N(6,000) O(13,000)

Molecular weight	= 440,19
Density of explosive	= 1,799 g/cm^3
Oxygen balance	= -47,24968 %
Enthalpy of formation	= -301,92 kJ/kg
Internal energy of formation	= -237,16 kJ/kg

Detonation parameters (at the C-J point):

Heat of detonation	= -4850,189 kJ/kg
Detonation temperature	= 3695,919 K
Detonation pressure	= 24,96996 GPa
Detonation velocity	= 7634,488 m/s
Particle velocity	= 1818,054 m/s
Sound velocity	= 5816,435 m/s
Density of products	= 2,361317 g/cm^3
Volume of products	= 0,4234925 cm^3/g
Exponent 'Gamma'	= 3,199264
Moles of gaseous products	= 11,16658 mol/mol explosive
Moles of condensed products	= 4,726592 mol/mol explosive
Volume of gas at STP	= 620,3951 dm^3/kg
Mean molecular mass of gas. prod.	= 34,33665 g/mol
Mean molecular mass of cond.prod.	= 12,011 g/mol
Mean molecular mass of all prod.	= 27,69705 g/mol
Entropy of products	= 6,145839 kJ/kg K
Internal energy of products	= 6502,856 kJ/kg, i.e. 11,69864 kJ/cm^3
Compression energy	= 1652,667 kJ/kg, i.e. 2,973148 kJ/cm^3
Total heat energy	= -4850,189 kJ/kg, i.e. -8,725491 kJ/cm^3

Composition of detonation products:

Products	mol/mol	mol/kg	Mol %
C(d) =	4,726592	10,73769	29,73977
CO_2 =	3,786484	8,601991	23,8246
N_2 =	2,986187	6,783905	18,78912
CO =	2,392444	5,435062	15,05328
CH_2O_2 =	1,07583	2,44403	6,769136
H_2O =	0,8826873	2,005255	5,553878
HCN =	0,01661758	0,03775118	0,104558
H_2 =	0,013704	0,03113222	0,08622571
NH_3 =	0,0108196	0,02457956	0,06807706
CH_4 =	0,001098652	0,002495876	0,006912731
C_2H_4 =	0,0002984355	0,0006779744	0,00187776
CNO =	0,000100776	0,000228939	0,0006340835
CH_3OH =	8,147198E-05	0,0001850849	0,0005126225
H =	7,172149E-05	0,0001629341	0,0004512724
C_2H_6 =	5,110326E-05	0,0001160944	0,0003215423
NH_2 =	3,75623E-05	8,533259E-05	0,0002363424
CHNO =	2,574001E-05	5,847517E-05	0,0001619564
CH_2O =	2,539377E-05	5,768858E-05	0,0001597778
N_2H_4 =	9,059019E-06	2,057993E-05	5,699944E-05
NO_2 =	2,321328E-06	5,273503E-06	1,460582E-05
N =	2,160263E-06	4,907602E-06	1,359239E-05
N_2O =	1,014494E-06	2,304689E-06	6,383209E-06
C(gr) =	7,000778E-10	1,59041E-09	4,404897E-09

2.3 Compound 3

C(12,000) H(4,000) N(6,000) O(12,000) S(1,000)

Molecular weight	= 456,25
Density of explosive	= 1,807 g/cm^3
Oxygen balance	= -56,10583 %
Enthalpy of formation	= -44,49 kJ/kg
Internal energy of formation	= 15,27 kJ/kg

Detonation parameters (at the C-J point) :

Heat of detonation	= -4689,054 kJ/kg
Detonation temperature	= 2740,172 K
Detonation pressure	= 15,89516 GPa
Detonation velocity	= 6912,697 m/s
Particle velocity	= 1272,505 m/s
Sound velocity	= 5640,192 m/s
Density of products	= 2,214684 g/cm^3
Volume of products	= 0,4515317 cm^3/g
Exponent 'Gamma'	= 4,432355
Moles of gaseous products	= 7,975057 mol/mol explosive
Moles of condensed products	= 8,691205 mol/mol explosive
Volume of gas at STP	= 427,4786 dm^3/kg
Mean molecular mass of gas. prod.	= 33,33563 g/mol
Mean molecular mass of cond.prod.	= 21,90806 g/mol
Mean molecular mass of all prod.	= 27,37632 g/mol
Entropy of products	= 5,979245 kJ/kg K
Internal energy of products	= 5498,693 kJ/kg, i.e. 9,936138 kJ/cm^3
Compression energy	= 809,639 kJ/kg, i.e. 1,463018 kJ/cm^3
Total heat energy	= -4689,054 kJ/kg, i.e. -8,473121 kJ/cm^3

Composition of detonation products:

Products	mol/mol	mol/kg	Mol %
C(gr) =	6,431299	14,09593	38,58873
N_2 =	2,992699	6,55931	17,95663
CO_2 =	2,735446	5,995472	16,41308
C(d) =	1,260495	2,762716	7,563151
CO =	1,250929	2,74175	7,505755
H_2SO_4(l) =	0,9994115	2,190481	5,996614
H_2O =	0,6515798	1,428114	3,909574
CH_2O_2 =	0,3141219	0,6884832	1,884777
H_2 =	0,01257659	0,02756501	0,07546138
NH_3 =	0,00966649	0,02118673	0,05800035
HCN =	0,004917161	0,01077729	0,02950368
CH_4 =	0,002191769	0,004803856	0,01315093
SO_2 =	0,000304655	0,000667734	0,001827974
H_2S =	0,0002471838	0,0005417704	0,001483139
C_2H_4 =	0,0001805352	0,0003956919	0,001083238
C_2H_6 =	8,194115E-05	0,0001795962	0,0004916589
CH_3OH =	4,398813E-05	9,641191E-05	0,0002639352
SO =	2,075228E-05	4,548425E-05	0,0001245167
CH_2O =	1,170198E-05	2,564806E-05	7,021358E-05
CHNO =	1,071673E-05	2,348863E-05	6,430196E-05
COS =	6,818645E-06	1,494491E-05	4,091286E-05
H =	6,454679E-06	1,414718E-05	3,872902E-05
S =	6,280336E-06	1,376506E-05	3,768293E-05
NH_2 =	3,800892E-06	8,330684E-06	2,28059E-05
CNO =	1,85511E-06	4,065976E-06	1,113093E-05
N_2H_4 =	9,523343E-07	2,087299E-06	5,714144E-06
SO_3 =	7,425338E-07	1,627464E-06	4,455311E-06
S_2 =	7,166028E-07	1,570629E-06	4,299721E-06
NS =	3,485204E-07	7,638769E-07	2,091173E-06
H_2SO_4 =	2,421166E-07	5,306642E-07	1,452735E-06

N_2O =	2,917707E-08	6,394946E-08	1,750667E-07
N =	1,056298E-08	2,315164E-08	6,337945E-08
NO_2 =	7,991626E-09	1,751581E-08	4,795092E-08
CS =	2,315313E-10	5,074636E-10	1,389222E-09
S(l) =	2,112241E-13	4,629548E-13	1,267375E-12
S_8 =	2,032646E-18	4,455094E-18	1,219617E-17

3 Structure refinement data

3.1 Compound 1

Empirical formula	C_{12} H_6 N_4 O_9
Formula weight	350.21
Temperature	150(2) K
Wavelength	0.71073 Å
Crystal system	Triclinic
Space group	*P*-1
Unit cell dimensions	a = 7.9044(12) Å
	b = 8.0845(11) Å
	c = 11.3617(15) Å
	α = 81.224(11)°
	β = 69.815(13)°
	γ = 84.647(12)°
Volume	672.83(17) $Å^3$
Z	2
Density (calculated)	1.729 mg/m^3
Absorption coefficient	0.152 mm^{-1}
F(000)	356
Crystal size	0.2 x 0.04 x 0.04 mm^3
Theta range for data collection	2.552 - 28.282°
Index ranges	-10≤h≤10, -10≤k≤10, -15≤l≤15
Reflections collected	6048
Independent reflections	3342 [R_{int} = 0.0464]
Data / restraints / parameters	3342 / 0 / 226
Goodness-of-fit on F^2	1.006
Final R indices [I>2sigma(I)]	R_1 = 0.0644, wR_2 = 0.1334
R indices (all data)	R_1 = 0.1174, wR_2 = 0.1603
Largest diff. peak and hole	0.387 and -0.313 e.$Å^{-3}$

3.2 Compound 2

Empirical formula	$C_{12}\ H_4\ N_6\ O_{13}$
Formula weight	440.21
Temperature	143(2) K
Wavelength	0.71073 Å
Crystal system	Monoclinic
Space group	$P2_1$
Unit cell dimensions	a = 8.0043(3) Å
	b = 8.7613(3) Å
	c = 11.7424(5) Å
	α = 90°
	β = 105.700(4)°
	γ = 90°
Volume	792.75(5) $Å^3$
Z	2
Density (calculated)	1.844 Mg/m^3
Absorption coefficient	0.172 mm^{-1}
F(000)	444
Crystal size	0.4 x 0.2 x 0.05 mm^3
Theta range for data collection	3.521 - 30.504°
Index ranges	-11≤h≤11, -12≤k≤12, -16≤l≤16
Reflections collected	15900
Independent reflections	4833 [R_{int} = 0.0393]
Data / restraints / parameters	4833 / 1 / 280
Goodness-of-fit on F^2	1.038
Final R indices [I>2sigma(I)]	R_1 = 0.0388, wR_2 = 0.0779
R indices (all data)	R_1 = 0.0498, wR_2 = 0.0835
Absolute structure parameter	-0.2(5)
Largest diff. peak and hole	0.297 and -0.222 e.$Å^{-3}$

3.3 Compound 3

Empirical formula	C_{12} H_4 N_6 O_{12} S
Formula weight	456.27
Temperature	298(2) K
Wavelength	0.71073 Å
Crystal system	Monoclinic
Space group	$P2_1$
Unit cell dimensions	a = 10.9756(5) Å
	b = 11.0066(4) Å
	c = 14.0260(5) Å
	α = 90°
	β = 104.829(4)°
	γ = 90°
Volume	1637.96(12) $Å^3$
Z	4
Density (calculated)	1.850 Mg/m^3
Absorption coefficient	0.288 mm^{-1}
F(000)	920
Crystal size	0.2 x 0.05 x 0.05 mm^3
Theta range for data collection	4.172 - 28.278°
Index ranges	-14≤h≤14, -14≤k≤14, -18≤l≤10
Reflections collected	15113
Independent reflections	7871 [R_{int} = 0.0404]
Data / restraints / parameters	7871 / 1 / 559
Goodness-of-fit on F^2	1.032
Final R indices [I>2sigma(I)]	R_1 = 0.0424, wR_2 = 0.0755
R indices (all data)	R_1 = 0.0556, wR_2 = 0.0817
Largest diff. peak and hole	0.388 and -0.264 e.$Å^{-3}$

4 Enlarged View of the Figures

4.1 Figure 2

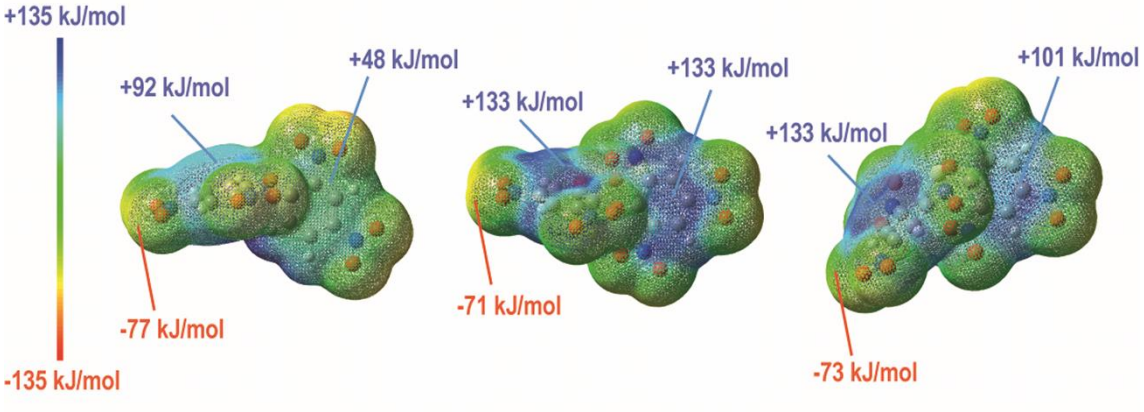

Figure 2. ESP of **1** (left), **2** (center) and **3** (right), calculated on the 0.02 electron bohr^{-3} hypersurface.

4.2 Figure 3

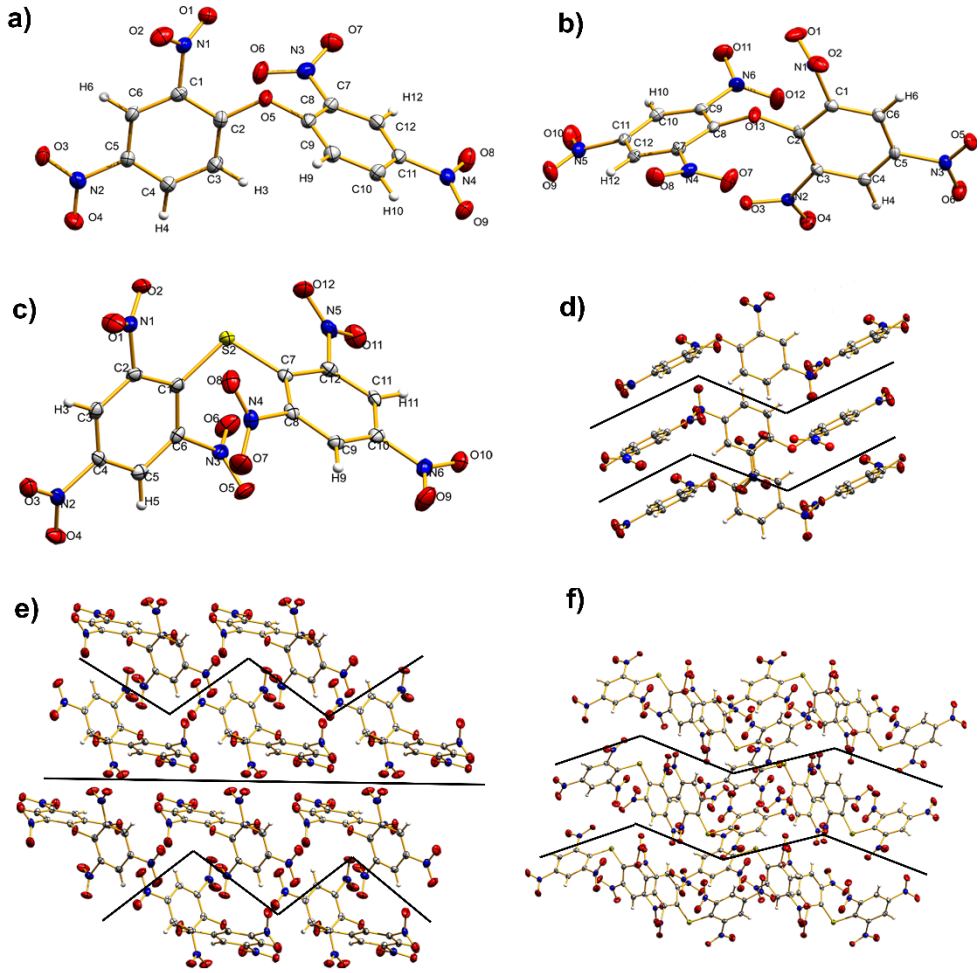

Figure 3. Single-crystal X-ray structure of **1** (a), **2** (b), **3** (c) and the crystal packing of **1** (d), **2** (e), **3** (f).

6 Investigation of Structure-Property Relationships of Three Nitroaromatic Compounds: 1-Fluoro-2,4,6-trinitrobenzene, 2,4,6-Trinitrophenyl methanesulfonate and 2,4,6-Trinitrobenzaldehyde

Reproduced with permission from *Cryst. Growth Des.* **2021**, *21*, 1, 243–248 (doi: 10.1021/acs.cgd.0c01049)

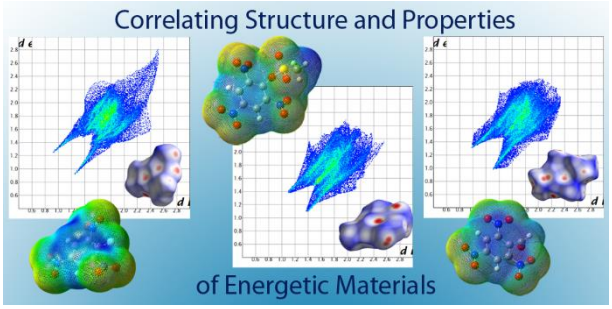

6.1 Abstract

Recently the investigation of the correlation between the crystal structure and important properties like sensitivity and thermostability of energetic materials has gained more and more interest among experts in the field. To contribute to this development, several models for the sensitivity prediction of energetic materials have been applied to the title compounds. Very often, older models that focus on bond dissociation enthalpy or electrostatic potential result in values that differ significantly from values of actual measurements. However, more recent models like Hirshfeld surface analysis or Fingerprint plot analysis offer an improved correlation between prediction and practical tests. We compared these methods with the mentioned older models and gained further insight into the structure-property relationships of energetic materials. The accuracy of predictions of structure-property relationships which can be deduced from a crystal structure increases with the sample size over time. Therefore, this method should be pursued and applied to different energetic materials in the future, for a better understanding of those relationships.

6.2 Introduction

In 1997 *Spackmann* communicated a novel concept for the definition and visualization of a molecule in a crystal based on Hirshfelds Stockholder partitioning scheme.[1-2] This method for crystal analysis and crystal engineering was further refined and became famous as the Hirshfeld surface in 1998.[3] In 2002 *McKinnon* and *Spackmann* complemented their method with 2D Fingerprint plot analysis for improved visualization of intermolecular close contacts in a crystal.[4] This work was followed by the initial development of the Crystal Explorer software in 2004 and 2005, which has been

continuously improved since then.[5] With the current version of Crystal Explorer, various interactions in the crystal can be easily visualized and quantified, including features like crystal surface mapping and close contact analysis, which makes it a valuable tool for crystal engineering and material design.[6] In 2014, Hirshfeld surface and Fingerprint plot analysis found their way into the analysis and development of energetic materials for the first time.[7] Since then various authors like *Gozin*[8], *Klapötke*[9], and *Shreeve*[10] have utilized this methodology and the Crystal Explorer software for the investigation and design of new energetic materials with the goal to achieve a deeper insight into structure-property relationships, especially with regard to sensitivity and thermal stability. Regarding synthesis and design of new energetic materials, the insensitivity towards external stimuli is one of the most important requirements among other characteristics like improved environmental compatibility, higher density, and thermal stability as well as increased detonation velocity and pressure.[11-12] One strategy to achieve an increased performance of HEDMs is to use compounds with a high heat of formation, but this is often related to a higher sensitivity towards external stimuli.[13] Due to this contrary behavior,[13-15] the molecular design, as well as the crystallographic design, have to be considered when creating new materials, to achieve a suitable balance between safety and performance.[10] For this purpose, we applied a combination of various methods to all title compounds, which form a group of 1-substituted derivatives of 2,4,6-trinitrobenzene. Those molecules are interesting building blocks for the synthesis of more sophisticated energetic materials and serve as model compounds for the analysis of structure-property relationships. The applied set of methods comprises both preceding predictive models like the computation of BDE and ESP values – as well as newer methods like Hirshfeld surface analysis and Fingerprint plot analysis.[7-10,16] By comparing the results of different prediction models with experimental values, we hope to achieve a better understanding of the energetic behavior regarding the aforementioned compounds and also a deeper insight into structure-property relationships of energetic materials in general.

6.3 Results and Discussion

***6.3.1 Spectroscopic Characterization*.** The three title compounds were prepared by modified and optimized methods and were intensively characterized by multinuclear NMR spectroscopy, vibrational spectroscopy (IR, Raman), elemental analysis as well as single-crystal X-ray diffraction. Found ^{1}H NMR chemical shifts of aromatic protons (**1**: 9.20, **2**: 9.24; **3**: 9.16) are in good agreement with other known 1-substituted trinitrobenzene derivatives like TNT (8.8 ppm) or picric acid (9.0 ppm).[17-18] The ^{13}C{^{1}H} NMR spectra reveal the corresponding chemical shifts between 120 ppm and 190 ppm. Compound **1** shows two distinct signals for the nitro groups in ortho and para positions in the ^{14}N NMR spectrum. In the case of molecules **2** and **3**, no distinct signals for the nitro groups were found due to the rather large signal width of 440 Hz and 500 Hz.

Typical Raman- and infrared vibration modes were found in the corresponding spectra and assigned according to available literature (**Table 1**).[19]

Table 1. Characteristic vibration modes of **1**, **2**, and **3**.

	1		**2**		**3**	
	IR	Raman	IR	Raman	IR	Raman
ν(C-H)	3063	3063	3095	3097	3096	3104
$\nu_{as}(NO_2)$	1541	1548	1543	1547	1554	1553
$\nu_{s}(NO_2)$	1342	1364	1343	1363	1343	1351
ν(C-N)	923	940	919	1089	919	938
$\delta(NO_2)$	737	817	730	823	729	826

$\nu_{as/s}$ asymmetric/ symmetric vibration mode δ: deformation vibration

All three compounds show very similar values for the symmetric-, asymmetric- and deformation modes of the nitro groups. The same applies to the C-H and C-N modes of the three title compounds, except for the Raman C-N mode of compound **2**. It has been previously shown by other researchers, that the bond dissociation enthalpy (BDE), can be directly linked to the sensitivity of energetic materials.[20-21] All three compounds are expected to have very similar BDE values and therefore similar sensitivities towards external stimuli using this particular model. In this work, the BDEs were calculated based on the respective crystal structure data and the B3LYP/6-311G+(d,p) method. According to various studies, the BDEs of a molecule can be considered as the most important factor in pyrogenic decomposition. The BDE correlates to a trigger bond which is first to break and can therefore be utilized to assess the sensitivity of a material.[10]

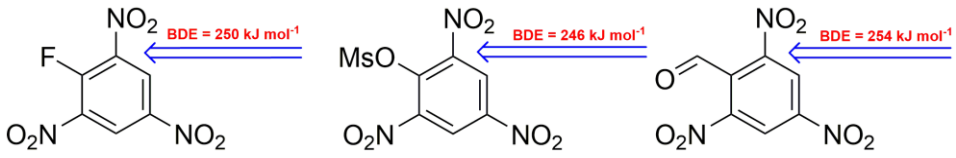

Figure 1. Calculated BDE Values of the weakest Bond in the molecule **1**, **2**, and **3**, considering all X-C bonds (X: C, O, N, F)

The C-N bond of the ortho nitro group was identified as the weakest bond in all investigated compounds. All BDE values of compounds **1**, **2**, and **3** fall in a range between RDX (161 kJ mol^{-1}) and TATB (355 kJ mol^{-1}), which is the reason for categorizing them as sensitive.[15,22-28] The calculation-based trend of BDEs is **2** < **1** < **3** but the relative difference is very small (<10 kJ mol^{-1}). Based on this model, very similar sensitivity values would be expected. The electrostatic potential (ESP) can be

utilized for the visualization of the bond strength inside a molecule and therefore as an indicator for the potential sensitivity.[11] In addition, the calculation of h_{50} values or the acquisition of *volume-based sensitivities* based on ESP is possible.[11]

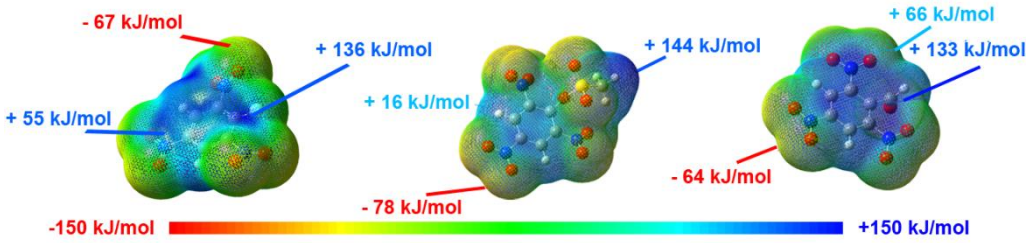

Figure 2. ESP of **1** (left), **2** (center) and **3** (right), calculated on the 0.02 electron bohr-3 hypersurface.

Regarding the ESP, all compounds show a significantly larger surface area in the positive range and the corresponding values are more pronounced in comparison to peak values of negative areas. This distribution and the strongly positive center of the investigated compounds is a typical indicator for sensitive materials.[26-28] The difference between the peak positive spot and the peak negative spot (**1**: +69 kJ mol^{-1}, **2**: +66 kJ mol^{-1}, **3**: +69 kJ mol^{-1}) is very similar for all three compounds. Therefore, a similar behavior towards external stimuli is expected.

***6.3.2 Structure-property relationship*.** Impact and friction resemble external mechanical stimuli which can cause the displacement of stabilizing layers in the crystal and therefore lead to internal strains. If the strain energy is below the lowest BDE, the integrity of the molecule is not affected. On the contrary, if the strain energy surpasses the energy necessary to break the weakest bond, the compound will decompose.[7] Besides the stacking and gearings of the individual layers, the strain caused by an interlayer slide also depends on other stabilizing interactions in the crystal, i.e. hydrogen bridges.[29] All three isolated molecules a, b and c show an almost planar benzene ring. When comparing the largest torsion angles of the ortho nitro groups (**1**: 41°, **2**: 45°, **3**: 41°), a very similar twisting behavior can be identified. This can be explained by sterical effects as well as by electronic repulsion between the substituents at 1-position and the neighboring nitro groups. Despite those similarities, each compound exhibits a unique packing behavior in the unit-cell of the crystal (d, e, f) and therefore a difference in the gearing of the individual layers. Compound **1** exhibits a wave-like pattern with a moderate gearing between each layer. Compound **3** exhibits a wave-like pattern with a higher gearing of the individual layers and compound **2** shows a layered structure with the lowest gearing of all investigated materials. For compound **3** the strain energy arising from mechanical stimuli is assumed to be the highest due to the high interlayer gearing and therefore the highest sensitivity is expected. Compound **2** exhibits the highest interlayer distance and therefore this material is expected to be the least sensitive towards mechanical stimuli, as it allows an easier sliding of adjacent layers without negative Oxygen-Oxygen repulsions or other detrimental interactions.

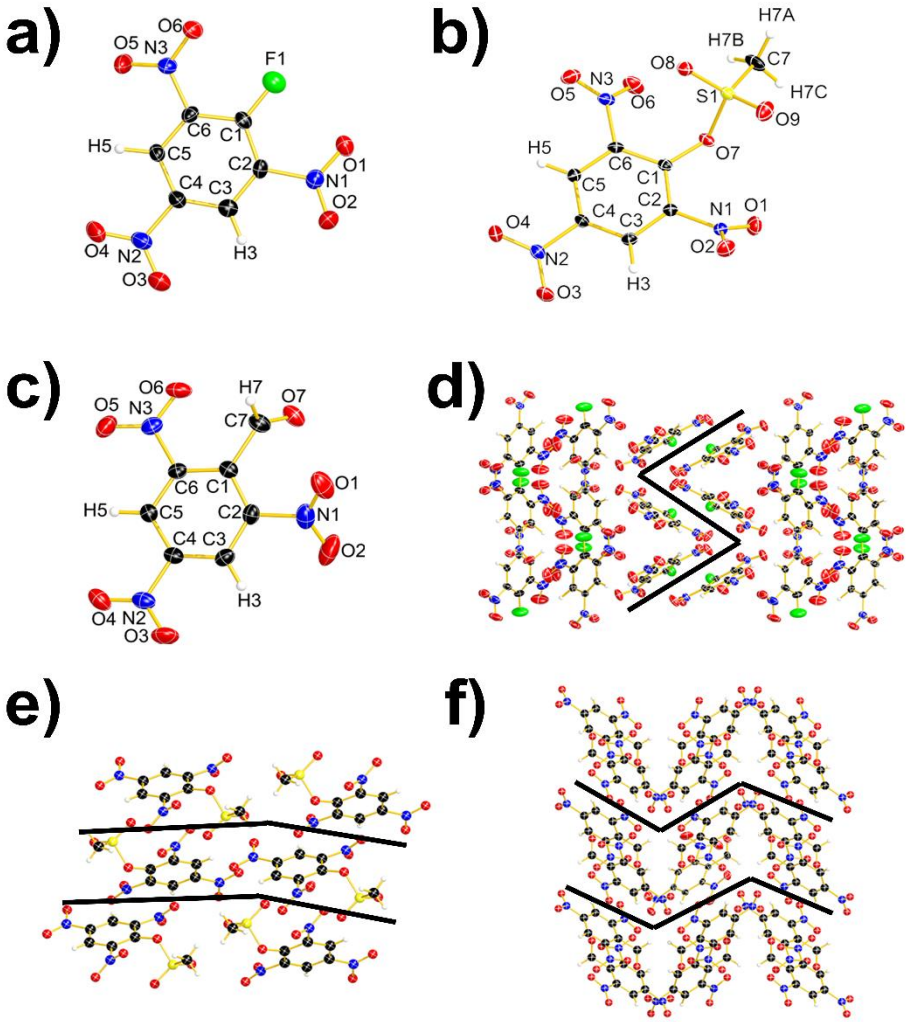

Figure 3. Single-crystal X-ray structure of **1** (a), **2** (b), **3** (c) and the crystal packing of **1** (d), **2** (e), **3** (f).

When this effect is very pronounced, the slip barrier can be reduced significantly enough to become smaller than the bond dissociation energy.[7] Next to crystal packing, a significant contribution to the extent of the slide barrier is made up of intermolecular interactions which therefore directly correlate with the sensitivity of a compound towards mechanical stimuli. In general, insensitive molecules exhibit a Hirshfeld surface in which the plane features the most red dots representing close contacts and fewer red dots between the individual layers.[29] Compounds **1**–**3** exhibit red dots and therefore close contacts which point out of the molecular plane (**Figure 4**) and can therefore be considered sensitive. Because none of these close contacts is arranged in a slidable plane, interlayer repulsion results from external stimuli, which is characteristic for sensitive materials.

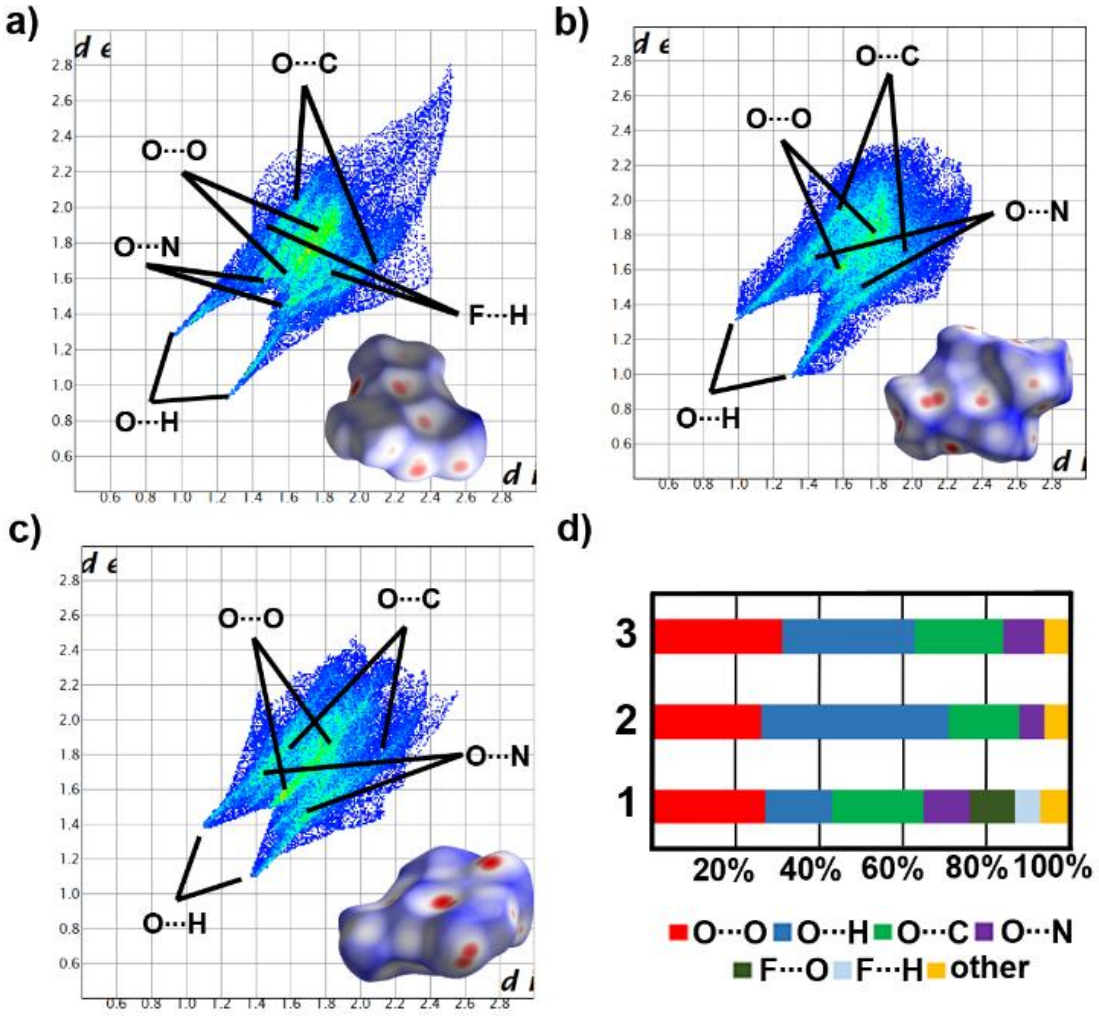

Figure 4. Two-dimensional Fingerprint plot in crystal stacking as well as the corresponding Hirshfeld surface (bottom right in the 2D plot) of **1** (a), **2** (b), and **3** (c) (color coding: white, distance d equals VDW distance; blue, d exceeds VDW distance, red, d, smaller than VDW distance). The population of close contacts of **1**, **2**, and **3** in crystal stacking (d).

The experimental sensitivity values for compounds **1**–**3** (IS: 9–10 J, FS: >360 N, ESD: 50–160 mJ) are very similar and the same would be expected for the distribution and intensity of stabilizing and destabilizing close-contacts in the Hirshfeld surface and Fingerprint plot analysis of the crystal structures. The compounds show a 3D network regarding their close contacts, represented by red dots on the surface in all three dimensions, which is typical for sensitive materials. The analysis of the 2D Fingerprint plots shows very interesting results as the distribution and intensity of the close contacts in the model compounds are very different. Less sensitive energetic materials are often designated by numerous and/or strong O···H and N···H interactions as they facilitate more rigid interlayers, which absorb energy more easily and are hence less likely to cause a detrimental sliding of the planes that induces a repulsion of these layers.[10] Compound **1** shows very few O···H contacts (22%) when compared to compound **2** (45%) and **3** (32%), but the number of strong O···H contacts (<2.5 Å) is significantly higher for compound **1**. Apparently, very few but strong O···H close

contacts in compound **1** are capable of stabilizing the molecule to the same extent as significantly more but weaker interactions in compounds **2** and **3**, as they show very similar sensitivities towards external stimuli. The stabilizing N···H close-contacts can be neglected in all three cases as their occurrence is low (0–0.9 %) and they can be regarded as weak (>3 Å). The same is true for the stabilizing F···H interactions (1.3%) in compound **1**. The O···O interaction is a particularly important close contact interaction, as a high occurrence of O···O contacts implies a high sensitivity. Increased exposure of nitro groups on the molecular surface causes the risk of explosion to rise due to the increased repulsion in the case of interlayer sliding.[7,10,15,29] The title compounds show significant amounts of O···O close-contacts (26–32%) and can therefore be considered sensitive. All O···N and C···N contacts are very weak (>3 Å), which is typical for sensitive materials.[29] The 2D Fingerprint plots exhibit two pronounced spikes that indicate strong O···H bonding in all investigated compounds.[10] With respect to di + de (di: the distance between the Hirshfeld surface to the nearest atom interior; de: distance from the Hirshfeld surface to the nearest atom exterior), the trend for the number of hydrogen bonds is **2** > **3** > **1**, but an inverse trend is found for the relative strength of the H-bonds. These results indicate, that not only the quantity but also the relative bond strength for stabilizing interactions must be considered when utilizing Hirshfeld surface and Fingerprint plot analysis for the sensitivity assessment of energetic materials.

***6.3.3 Heat of formation and detonation parameters*.** The performance of an energetic material depends directly on its density, which therefore is not only a decisive factor but most interestingly results from the packing behavior within the crystal. We observed the crystal densities of **1**, **2**, and **3** to be 1.89, 1.84, and 1.76 g cm^{-3} at 145 K. Hence, the calculated densities under ambient conditions are 1.84, 1.80, and 1.72 g cm^{-3}. To calculate the heat of formation (HOF), extremely precise theoretical methods must be applied, since experimental values are often inaccurate.[10] The calculation of the HOF was therefore performed using *ab-initio* calculations which make use of the optimized molecule geometry obtained by refining the obtained geometry from the X-ray diffraction experiment. According to Trouton´s Rule, the HOF was determined by the subtraction of the sublimation enthalpy from the HOF of the corresponding gas-phase species.[11] To obtain the HOF of the corresponding gas-phase species, the atomization energies were subtracted from the total enthalpy of the molecules.[30-31] All calculations were carried out on a CBS-4M level of theory in combination starting from the respective crystal structures. Applying the specific densities and the EXPLO5 (V6.05)[32] thermochemical code, the detonation properties of **1**, **2**, and **3** were determined and are given in **Table 2**. They were calculated at the Chapman−Jouguet point with the help of the stationary detonation model using a modified Becker−Kistiakowski−Wilson state equation for the system. The C−J point was found by the Hugoniot curve of the system by its first derivative.[32-33]

Table 2. Physical and calculated detonation parameters of compounds **1**, **2**, and **3** using the EXPLO5 computer code.

	(1)	**(2)**	**(3)**
formula	C6H2N3O6F1	C7H5N3O9S1	C7H3N3O7
Mr [g mol^{-1}]	231.09	307.19	241.11
IS[a] [J]	10	9	10
FS[b] [N]	>360	>360	>360
ESD [mJ]	160	50	120
N[c] [%]	18.18	13.68	17.43
N+O[d] [%]	59.72	60.55	63.88
ΩCO_2[e] [%]	-48.5	-39.1	-56.4
T_{melt}[f] [°C]	126.7	139.4	101.6
T_{dec}[g] [°C]	350.6	237.4	185.1
ρ25°C[h] [g cm^{-3}]	1.837	1.795	1.721
ΔH_f°[i] [kJ mol^{-1}]	-532.8	-386.1	-163.2
EXPLO5 V 6.05			
ΔU_f°[j] [kJ kg^{-1}]	-4070	-3904	-4391
T_{C-J}[k] [K]	3301	2240	3361
P_{C-J}[l] [GPa]	23.8	12.6	20.4
V_{det}[m] [ms^{-1}]	7376	5863	7062
V_o[n] [dm^3 kg^{-1}]	606.9	383.9	616.1

[a] Impact sensitivity[22] [b] friction sensitivity[23] [c] nitrogen content [d] combined nitrogen and oxygen content [e] absolute oxygen balance assuming the formation of CO or CO_2 [f] melting point from DTA [g] decomposition from DTA [h] calculated room temperature density [i] Heat of formation calculated at the CBS-4M level of theory for FMN, experimental determined for MN [j] detonation energy [k] detonation temperature [l] detonation pressure [m] detonation velocity [n] volume of detonation gases at standard temperature and pressure conditions

The HOF of the compounds can be ordered **3** > **1** > **2** whilst the densities are ordered **1** > **2** > **3**. According to these results, similar values for the detonation pressure and the detonation velocity can be expected. However, the mesyl substituent in compound **2** leads to a significantly lowered oxygen balance when compared to the other two compounds. It also exhibits significantly lower values for V_{det} and P_{C-J}. Regarding these values, compounds **1** and **3** slightly exceed TNT (6881 m s^{-1}, 18.9 GPa), whilst molecule **2** is unable to compete.[26-28]

6.4 Conclusions

1-Fluoro-2,4,6-trinitrobenzene, 2,4,6-trinitrophenyl methanesulfonate, and 2,4,6-trinitrobenzaldehyde have been prepared and intensively characterized. The molecular structures of all aforementioned compounds were elucidated by single-crystal X-ray diffraction. Older methods for the prediction of an energetic materials sensitivity (BDE, ESP) were compared with newer, current methods which are based on the crystal structure of a compound (Hirshfeld surface analysis & Fingerprint plot analysis). We found, that a combination of very few but strong stabilizing interactions in a crystal may result in the same sensitivity as numerous but significantly weaker stabilizing interactions. Another key result is the fact, that all investigated energetic materials had at least 25% of destabilizing O···O interactions as well as close contacts between the individual layers. The broader application of Hirshfeld surface analysis could lead to deeper insight and understanding of the relationship between structure and sensitivity of an energetic material. Sensitivity values could be predicted or even determined without the need to prepare large amounts of energetic material. This is not only environmentally friendly but also leads to a significant safety increase. The calculation using the EXPLO5 code showed that the performance of the investigated compounds decreases from **1** over **3** to **2**. Except for the latter compound, the values are comparable to TNT.

6.5 Experimental Section

General Information. 1-Fluoro-2,4-dinitrobenzene, pyridine, iodine *N*,*N*-dimethyl-p-nitrosoaniline, methanesulfonic anhydride, perchloric acid, nitric acid, sulfuric acid, oleum, and potassium nitrate are commercially available. Potassium picrate and TNT were used from a group internal stockpile.

For NMR spectroscopy the solvent DMSO-d_6 was dried using a 3 Å mole sieve. Spectra were recorded on a Bruker Avance III spectrometer operating at 400.1 MHz (^{1}H), 100.6 MHz (^{13}C), and 28.9 MHz (^{14}N). Chemical shifts are referred to TMS (^{1}H, ^{13}C) and $MeNO_2$ (^{14}N). Raman spectra were recorded with a Bruker MultiRam FT Raman spectrometer using a neodymium-doped yttrium aluminum garnet (Nd:YAG) laser (λ = 1064 nm) with 1074 mW. The samples for Infrared spectroscopy were placed under ambient conditions onto an ATR unit using a Perkin Elmer Spectrum BX II FT-IR System spectrometer. Melting and/or decomposition points were detected with a OZM DTA 552-Ex instrument. The scanning temperature range was set from 293 K to 673 K at a scanning rate of 5 K min^{-1}. Elemental analysis was performed with a Vario EL instrument and a Metrohm 888 Titrando device.

Caution! All investigated compounds are explosives, which show partly increased sensitivities toward various stimuli (e.g. higher temperatures, impact, friction, or electrostatic discharge). Therefore, proper safety precautions (safety glasses, Kevlar gloves, and earplugs) have to be applied while synthesizing and handling the described compounds.

***6.5.1 1-Fluoro-2,4,6-trinitrobenzene*.** 1-Fluoro-2,4-dinitrobenzene (13.6 g, 72.9 mmol) was slowly added to a nitration mixture consisting of 61.9 mL sulfuric acid, 50.8 mL Oleum (65%), and potassium nitrate (42.0 g, 415.4 mmol) at 0 °C. The reaction mixture was then stirred for 15 min at 0 °C and subsequently warmed to room temperature before the solution was finally heated to 125 °C for five days. The obtained suspension was allowed to cool to ambient temperature and afterward poured onto 750 mL of iced water. The solid was collected by suction filtration and washed with water (3 × 200 mL) until the filtrate ran clear. The filter cake was dried and recrystallized from boiling tetrachlorocarbon to afford the product upon cooling as pale yellow crystals (9.7 g, yield: 57%).

^{1}H NMR (Chloroform-d_1, 400 MHz): δ 9.20 (d, 2H, $^{4}J_{FH}$ = 5.6 Hz) ppm **^{13}C{^{1}H} NMR** (Chloroform-d_1, 100 MHz): δ 154.2 (d, $^{1}J_{FC}$ = 292.0 Hz), 142.4 (s, broad), 139.4 (s, broad), 125.9 (d, $^{3}J_{FC}$ = 0.8 Hz) ppm. **^{14}N NMR** (Chloroform-d_1, 29 MHz): δ -24 (s, NO_2) ppm. **^{19}F NMR** (Chloroform-d_1, 377 MHz): δ -113.2 (t, $^{4}J_{FH}$ = 5.6 Hz) ppm. **IR** (ATR, cm^{-1}): $\tilde{\nu}$ 3110 (w), 3089 (w), 3063 (m), 2887 (w), 1620 (s), 1541 (vs), 1482 (m), 1421 (m), 1342 (vs), 1319 (s), 1280 (m), 1258 (m), 1202 (m), 1089 (s), 948 (w), 938 (m), 923 (s), 827 (vw), 776 (w), 757 (w), 737 (s), 718 (s), 709 (vs), 672 (m), 649 (s), 551 (m), 519 (m), 481 (w), 462 (w), 406 (w). **Raman** (1064 nm, 1000 mW, 25 °C, cm^{-1}): $\tilde{\nu}$ 3063 (9), 2643 (2), 1621 (14), 1548 (36), 1364 (100), 1347 (51), 1279 (14), 1187 (4), 1090 (6), 940 (11), 927 (7), 826 (21), 817 (12), 741 (3), 522 (2), 377 (5), 354 (8), 333 (20), 313 (7), 205 (26), 149 (8), 105 (48), 90 (40). **Elemental Analysis** calcd (%) for $C_6H_2FN_3O_6$: C 31.18, H 0.87, F 8.22, N 18.18, O 41.54; found: C 31.42, H 1.13, N 18.23. **DTA**: 127 °C (m.p.), 351 °C (dec.) **IS**: 10 J. **FS**: >360 N. **ESD**: 160 mJ.

***6.5.2 2,4,6-Trinitrophenyl methanesulfonate*.** Potassium picrate (10.0 g, 37.4 mmol, 1.0 eq.) was suspended in 200 mL toluene. Methanesulfonic anhydride (6.5 g, 37.4 mmol, 1.0 eq.) was added to the yellow suspension in small portions. After adding perchloric acid (60% solution in acetic acid, 10 drops) the reaction mixture was stirred for 4 h at 120 °C with a $CaCl_2$ filled drying tube on top of the reflux condenser. After cooling to room temperature, the yellowish by-product potassium mesylate was separated by filtration and the filter residue was washed with ~150 mL toluene. The yellow filtrate phases were combined and the solvent was removed *in vacuo*. The resulting yellow-orange oil was treated with ~15 mL of ice-cold ether to precipitate the solid product. The solvents were removed *in vacuo* and a pale yellow solid was obtained. It was recrystallized from 150 mL chloroform to afford the product as a white solid 8.6 g (75%).

^{1}H NMR (Acetone-d_6, 400 MHz): δ 9.24 (s, 2H), 3.69 (s, 3H) ppm **^{13}C{^{1}H} NMR** (Acetone-d_6, 100 MHz): δ 146.3, 145.8, 138.8, 126.0, 40.4. ppm. **^{14}N NMR** (Acetone-d_6, 29 MHz): δ -22 (s, NO_2) ppm. **IR** (ATR, cm^{-1}): $\tilde{\nu}$ 3095 (w), 2163 (w), 2004 (w), 1614 (w), 1543 (m), 1373 (m), 1343 (s), 1243 (m), 1192 (m), 1169 (m), 1087 (w), 969 (w), 919 (m), 847 (s), 823 (m), 792 (m), 775 (s), 730 (s), 716 (s), 668 (s), 634 (m),

560 (m), 536 (s), 505 (s). **Raman** (1064 nm, 1000 mW, 25 °C, cm^{-1}): ṽ 3097 (18), 3035 (15), 2942 (46), 1616 (55), 1547 (42), 1363 (100), 1245 (50), 1089 (25), 823 (31), 636 (37), 565 (21), 367 (23), 330 (33), 250 (17). **Elemental Analysis** calcd (%) for $C_7H_5N_3O_9S$: C 27.37, H 1.64, S 10.44, N 13.68, O 46.87; found: C 27.34, H 1.69, N 13.60, S 10.99. **DTA**: 139 °C (m.p.), 237 °C (dec.) **IS**: 9 J. **FS**: >360 N. **ESD**: 50 mJ.

***6.5.3 2,4,6-Trinitrobenzaldehyde*.** Trinitrotoluene (10.0 g, 44.0 mmol, 1 eq) and *N*,*N*-dimethyl-p-nitrosoaniline (7.0 g, 47.0 mmol, 1.1 eq) were dissolved in 15 mL pyridine with 50 mg of iodine as a catalyst. The mixture was stirred for 7 days at 20–25 °C. The organic solid was separated by filtration and washed with cold acetone. The obtained crude product was dried *in vacuo* and then dissolved in 180 mL of aqueous HCl (36%) and stirred at 80 °C for two hours. The product was then separated by filtration and washed acid-free with water. This way 6.4 g (61%) of pure TNBA could be obtained as a black solid.

^{1}H NMR (DMSO-d6,400 MHz): δ 10.55 (s, 1H), 9.16 (s, 2H) ppm. **^{13}C{^{1}H} NMR** (DMSO-d6,100 MHz): δ 188.1, 148.1, 147.7, 134.2, 124.7 ppm. **^{14}N NMR** (DMSO-d6, 29 MHz): δ -20 (s, NO_2) ppm. **IR** (ATR, cm^{-1}): ṽ 3096 (w), 2916 (vw), 1714 (m), 1605 (m), 1554 (s), 1535 (vs), 1452 (w), 1405 (w), 1343 (vs), 1194 (m), 1185 (w), 1157 (m), 1075 (w), 979 (w), 935 (w), 919 (m), 839 (m), 826 (m), 772 (m), 742 (m), 729 (s), 701 (m), 570 (w), 538 (w), 475 (w), 435 (m). **Raman** (1064 nm, 1000 mW, 25 °C, cm^{-1}): ṽ 3104 (8), 2911 (7), 2903 (8), 1713 (16), 1623 (15), 1553 (29), 1382 (32), 1351 (81), 1274 (10), 1197 (12), 981 (8), 938 (7), 842 (13), 826 (18), 334 (22), 292 (8), 255 (7), 232 (19), 203 (34), 192 (26), 151 (36), 88 (100).**Elemental Analysis** calcd (%) for $C_7H_3N_3O_7$: C 34.87, H 1.25, N 17.43; found: C 34.87, H 1.38, N 17.12. **DTA**: 102 °C (m.p.), 185 °C (dec.) **IS**: 10 J. **FS**: 360 N. **ESD**: 120 mJ.

***6.5.4 X-Ray Measurements*.** 1-Fluoro-2,4,6-trinitrobenzene and 2,4,6-trinitrobenzaldehyde were solved in ethyl acetate and single crystals have been received after slow solvent evaporation. Single crystals of 2,4,6-trinitrophenyl methanesulfonate have been received after slow solvent evaporation of chloroform. Data collection was performed with an Oxford Xcalibur 3 diffractometer with a CCD area detector, equipped with a multilayer monochromator, a Photon 2 detector and a rotating-anode generator were employed for data collection using Mo-Kα radiation (λ= 0.7107 Å). Data collection and reduction were carried out using the Crysalispro software.[34] The structures were solved by direct methods (SIR-2014)[35] and refined (SHELXLE)[36] by full-matrix least-squares on F2 (ShelxL)[37-38] and finally checked using the platon software[39] integrated with the WinGX software suite.[40] The non-hydrogen atoms were refined anisotropically and the hydrogen atoms were located and freely refined. All Diamond 3 plots are shown with thermal ellipsoids at the 50% probability level and hydrogen atoms are shown as small spheres of arbitrary radius.

ASSOCIATED CONTENT

Supporting Information

The Supporting Information is available free of charge on the ACS Publication website.

^{1}H, ^{13}C, ^{19}F, ^{14}N NMR spectra; Crystallographic information, Detonation parameter calculations (output files) (PDF)

X-ray data for 1-Fluoro-2,4,6-trinitrobenzene (CIF)

CCDC: 2016176

X-ray data for 2,4,6-Trinitrophenyl methanesulfonate (CIF)

CCDC: 2016174

X-ray data for 2,4,6-Trinitrobenzaldehyde (CIF)

CCDC: 2016175

This material is available free of charge via the Internet at http://pubs.acs.org

AUTHOR INFORMATION

Corresponding Author

* tmk@cup.uni-muenchen.de

ORCID

Konstantin Karaghiosoff: 0000-0002-8855-730X

Thomas M. Klapötke: 0000-0003-3276-1157

Marco Reichel: 0000-0003-0137-4816

Dominik E. Dosch: 0000-0003-4804-6473

Max Born: 0000-0003-4807-0211

Author Contributions

‡ Dominik Dosch, Marco Reichel, and Max Born contributed equally to this work.

Notes

The authors declare no competing financial interests.

6.6 Acknowledgment

For financial support of this work by Ludwig−Maximilian University (LMU), the Office of Naval Research (ONR) under grant no. ONR.N00014-16-1-2062 and the Strategic Environmental Research and Development Program (SERDP) under contract no. WP19-1287 are gratefully acknowledged. The authors also thank Dr. Teresa Küblböck for her help with the graphics and F−Select GmbH for the generous donation of fluoro-chemicals.

6.7 References

[1] Hirshfeld F.L., Bonded-atom fragments for describing molecular charge densities. *Theoretica chimica acta* **1977**, *44*, 129-138.

[2] Spackman M. A. Byrom P. G., A novel definition of a molecule in a crystal. *Chem. Phys. Lett.* **1997**, *267*, 215-220.

[3] McKinnon J. J., Mitchell A. S., Spackman M. A., Hirshfeld Surfaces: A New Tool for Visualising and Exploring Molecular Crystals. *Chem. – Eur. J.* **1998**, *4*, 2136-2141.

[4] Spackman M. A., McKinnon J. J., Fingerprinting intermolecular interactions in molecular crystals. *CrystEngComm* **2002**, *4*, 378-392.

[5] McKinnon J. J., Spackman M. A., Mitchell A. S., Novel tools for visualizing and exploring intermolecular interactions in molecular crystals. *Acta Crystallogr, Sect. B: Struct. Sci.* **2004**, *60*, 627-668.

[6] McKinnon J. J., Jayatilaka D., Spackman M. A., Towards quantitative analysis of intermolecular interactions with Hirshfeld surfaces. *Chem. Commun.* **2007**, 3814-3816.

[7] Ma Y., Zhang A., Xue X., Jiang D., Zhu Y., Zhang C., Crystal Packing of Impact-Sensitive High-Energy Explosives. *Cryst. Growth & Des.* **2014**, *14*, 6101-6114.

[8] Li H., Zhang L., Petrutik N., Wang K., Ma Q., Shem-Tov D., Zhao F., Gozin M., Molecular and Crystal Features of Thermostable Energetic Materials: Guidelines for Architecture of "Bridged" Compounds. *ACS Cent. Sci.* **2020**, *6*, 54-75.

[9] Reichel M., Dosch D., Klapötke T., Karaghiosoff K., Correlation between Structure and Energetic Properties of Three Nitroaromatic Compounds: Bis(2,4-dinitrophenyl) Ether, Bis(2,4,6-trinitrophenyl) Ether, and Bis(2,4,6-trinitrophenyl) Thioether. *J. Am. Chem. Soc.* **2019**, *141*, 19911-19916.

[10] Zhang J., Zhang Q., Vo T. T., Parrish D. A., Shreeve J., Energetic Salts with π-Stacking and Hydrogen-Bonding Interactions Lead the Way to Future Energetic Materials. *J. Am. Chem. Soc.* **2015**, *137*, 1697-1704.

[11] Klapötke T.M., *Chemie der hochenergetischen Materialien*, 1st ed., De Gruyter: Berlin, **2009**.

[12] Gao H., Shreeve J., Azole-Based Energetic Salts. *Chem. Rev. (Washington, DC, U. S.)* **2011**, *111*, 7377.

[13] Zhi C. Y., Cheng X. L., Zhao F., The Correlation between Electric Spark Sensitivity of Polynitroaromatic Compounds and Their Molecular Electronic Properties. *Propellants, Explos., Pyrotech.* **2010**, *35*, 555.

[14] Thottempudi V., Gao H., Shreeve J., Trinitromethyl-substituted 5-nitro- or 3-azo-1,2,4-triazoles: synthesis, characterization, and energetic properties. *J. Am. Chem. Soc.* **2011**, *133*, 6464.

[15] Tang, Y.; Zhang, J.; Mitchell, L. A.; Parrish, D. A.; Shreeve,J. Taming of 3,4-Di(nitramino)furazan. *J. Am. Chem. Soc.* **2015**, *137*, 15984−15987.

[16] Spackman M. A., Jayatilaka D., Hirshfeld surface analysis. *CrystEngComm* **2009**, *11*, 19.

[17] Hussain I., Tariq M. I., Siddiqui H. L., Structure Elucidation of Chromogen Resulting from Jaffes´s Reaction. *J. Chem. Soc. Pak.* **2009**, *31*, 937.

[18] Soojhawon I., Lokhande P. D., Kodam K. M., Gawai K. R., Biotransformation of nitroaromatics and their effects on mixed function oxidase system. *Enzyme Microb. Technol.* **2005**, *37*, 527.

[19] Lewis I. R., Daniel N. W., Griffiths P. R., Interpretation of Raman Spectra of Nitro-Containing Explosive Materials. Part I: Group Frequency and Structural Class Membership. *Appl. Spectrosc.* **1997**, *51*, 1854.

[20] Li J., Relationships for the Impact Sensitivities of Energetic C-Nitro Compounds Based on Bond Dissociation Energy. *J. Phys. Chem. B,* **2010**, *114*, 2198.

[21] J. Li, *J.,* A quantitative relationship for the shock sensitivities of energetic compounds based on X–NO_2 (X = C, N, O) bond dissociation energy. *Hazard. Mater.* **2010**, *180*, 768.

[22] NATO. Standardization Agreement 4489 (STANAG 4489), *Explosives, Impact Sensitivity Tests*; Brussels, Belgium, **1999**.

[23] NATO. Standardization Agreement 4487(STANAG 4487), *Explosives, Friction Sensitivity Tests*; Brussels, Belgium, **2002**.

[24] www.reichel-partner.com.

[25] *Test methods according to the UN Manual of Tests and Criteria, Recommendations on the Transport of Dangerous Goods*,4th revised ed.; United Nations Publication: Geneva, **2003**. Impact: insensitive > 40 J, less sensitive≥35 J, sensitive≥4 J, very sensitive≤3 J; friction: insensitive > 360 N, less sensitive: 360 N, sensitive < 360N and > 80 N, very sensitive≤80 N, extremely sensitive≤10 N.

[26] Köhler J., Meyer R., Homburg A., *Explosivstoffe;* Wiley-CH: Weinheim, **2008**.

[27] Klapötke T.M., *Chemistry of High-Energy Materials*, 5th ed., DeGruyter: Boston, **2019**.

[28] Klapötke T. M., *Energetic Materials Encyclopedia*, 1st ed., DeGruyter: Boston, **2018**.

[29] Zhang C., Xue C., Cao Y., Zhou Y., Li H., Zhou J., Gao T., T., Intermolecular friction symbol derived from crystal information. *CrystEngComm* **2013**, *15*, 6837.

[30] Curtiss, L. A.; Raghavachari, K.; Redfern, P. C.; Pople, J. A., Assessment of Gaussian-2 and density functional theories for thecomputation of enthalpies of formation. *J. Chem. Phys.* **1997**, *106*, 1063.

[31] Byrd, E.; Rice, B. M. Improved Prediction of Heats of Formation of Energetic Materials Using Quantum Mechanical Calculations. *J. Phys. Chem. A* **2006**, *110*, 1005.

[32] Suceska M. Explo5 V6.05; Brodarski Institute: Zagreb **2018**;

[33] Klapötke, T. M.; Krumm, B.; Steemann, F. X.; Umland, K.-D. Bis(1,3-dinitratoprop-2-yl) nitramine, a new sensitive explosivecombining a nitrate ester with a nitramine. *Z. Anorg. Allg. Chem.* **2010**, *636*, 2343.

[34] CrysAlisPro (Version 171.33.41); Oxford Diffraction Ltd., **2009**.

[35] Burla, M. C.; Caliandro, R.; Carrozzini, B.; Cascarano, G. L.; Cuocci, C.; Giacovazzo, C.; Mallamo, M.; Mazzone, A.; Polidori, G.Crystal structure determination and refinement via SIR2014. *J. Appl. Crystallogr.* **2015**, *48*, 306-309.

[36] Hübschle, C. B.; Sheldrick, G. M.; Dittrich, B. ShelXle: a graphical user interface for SHELXL. *J. Appl. Crystallogr.* **2011**, *44*, 1281-1284.

[37] Sheldrick G. M., *SHELXL-97, Program for the Refinement of Crystal Structures*, University of Göttingen, Germany, **1997**.

[38] Sheldrick, G. M., A short history of SHELX. *Acta Crystallogr. Sect. A* **2008**, 112 - 122.

[39] Spek A. L., *PLATON, A Multipurpose Crystallographic Tool,* Utrecht University, The Netherlands **1999**.

[40] Farrugia, L. J., WinGX and ORTEP for Windows: an update. *J. Appl. Cryst.* **2012**, 849 - 854.

6.8 Supporting Information

1 NMR Spectra

1.1 Compound 1

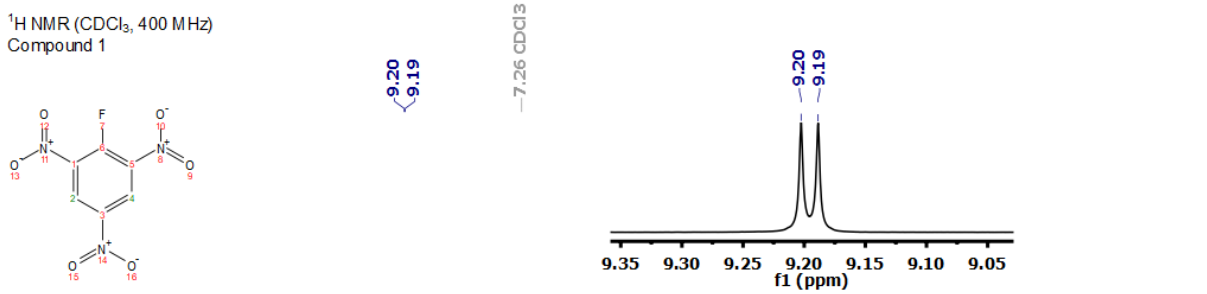

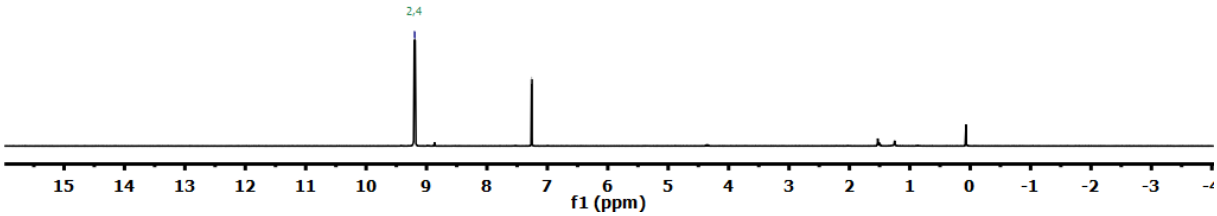

$^{13}C\{^{1}H\}$ NMR ($CDCl_3$, 101 MHz)
Compound 1

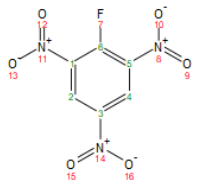

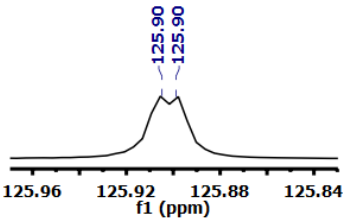

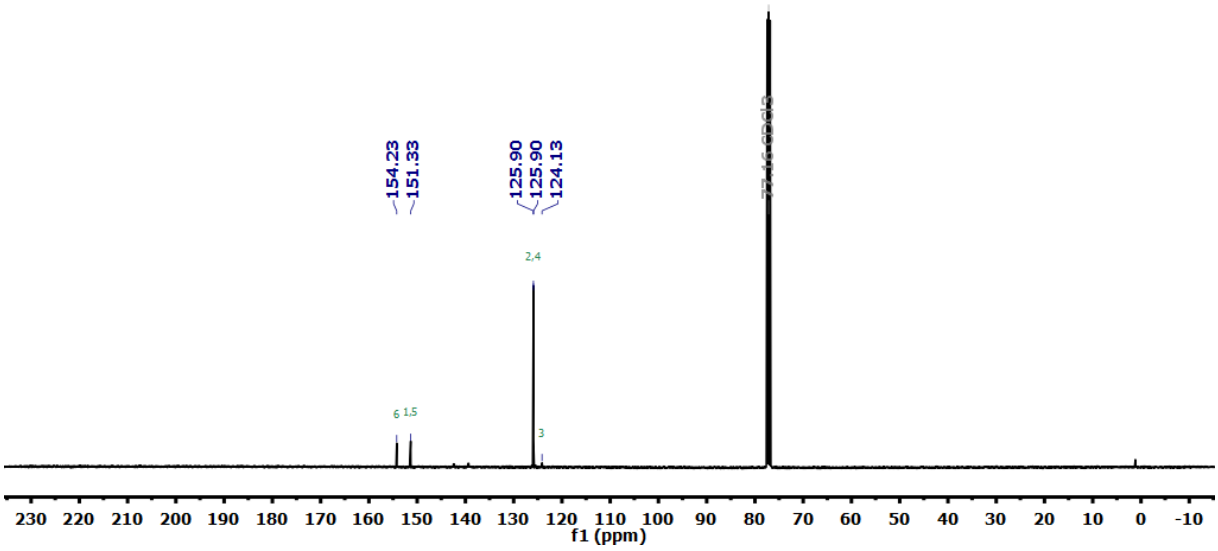

$^{14}N\{^{1}H\}$ NMR ($CDCl_3$, 29 MHz)
Compound 1

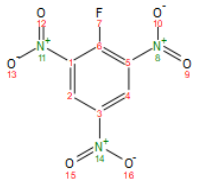

$^{19}F\{^{1}H\}$ NMR ($CDCl_3$, 376 MHz)
Compound 1

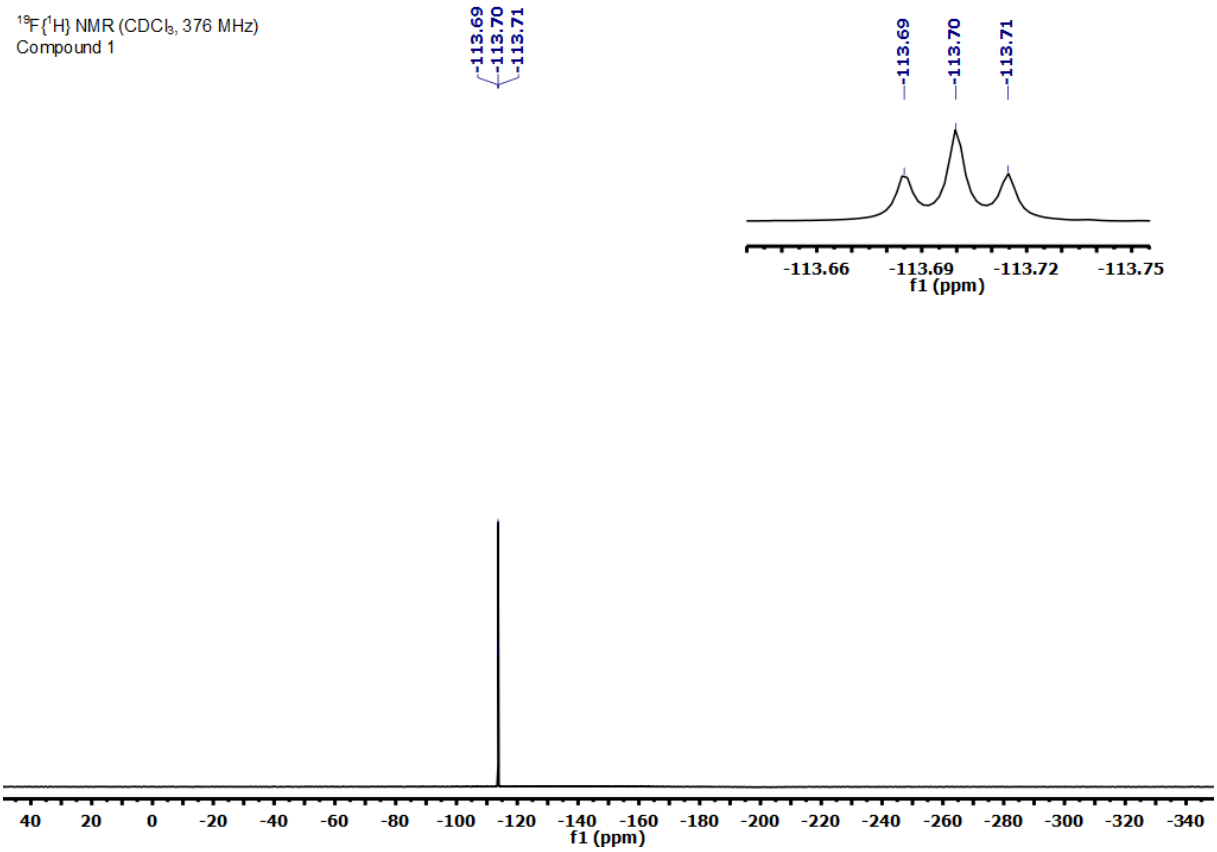

1.2 Compound 2

^{1}H NMR ($(CD_3)_2CO$, 400 MHz)
Compound 2

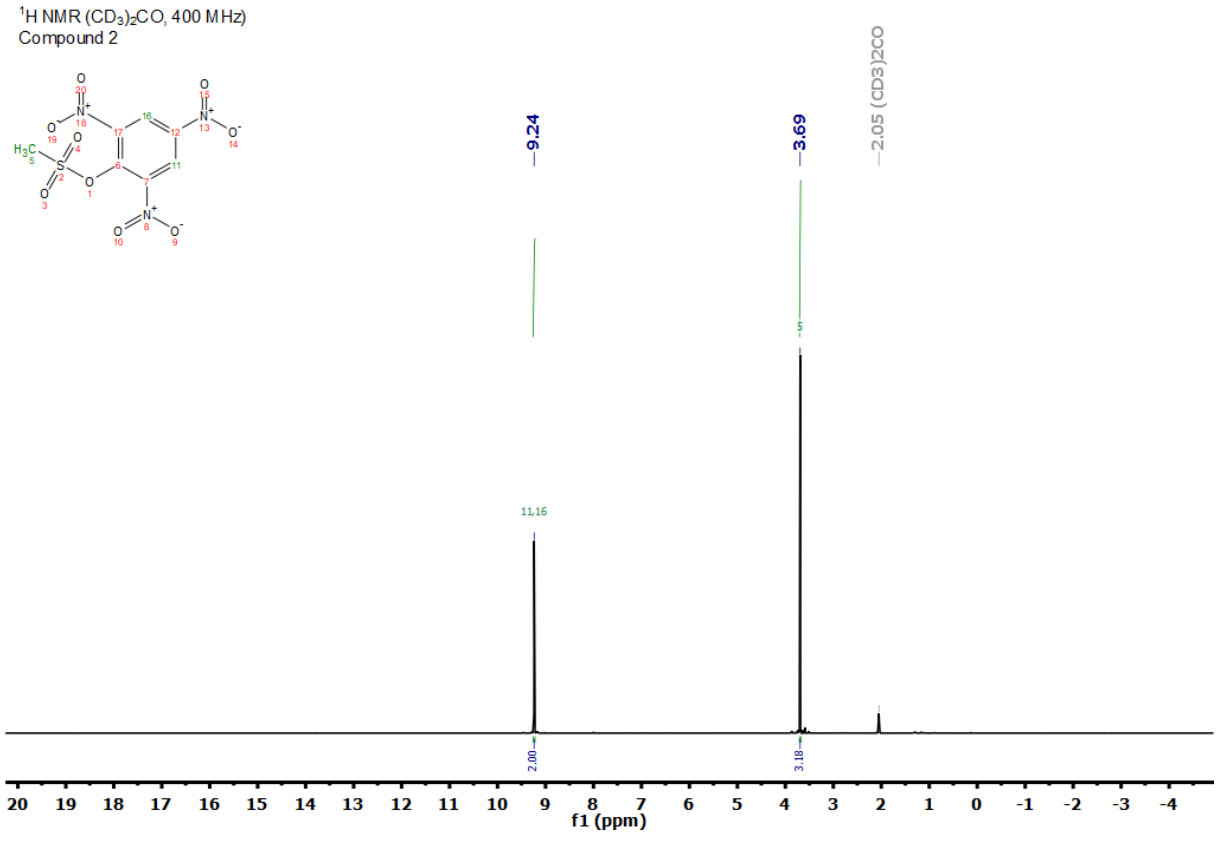

$^{13}C\{^{1}H\}$ NMR $(CD_3)_2CO$, 101 MHz)
Compound 2

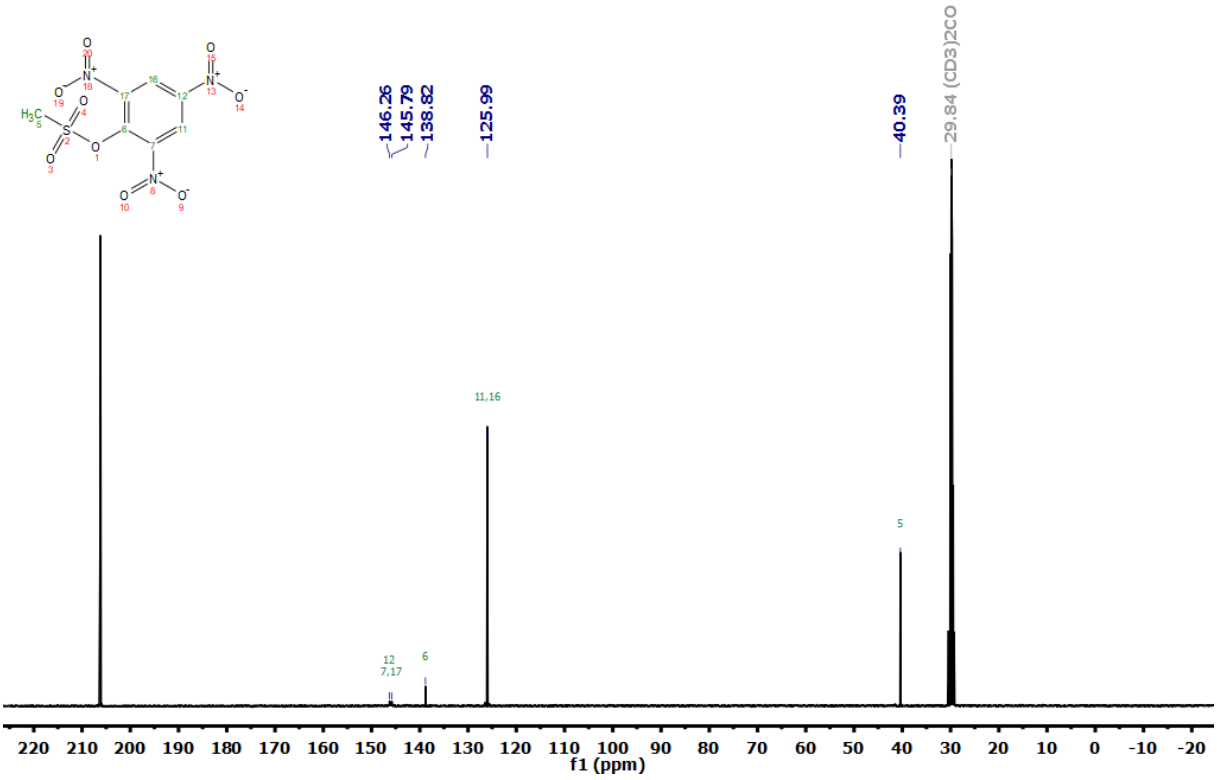

$^{14}N\{^{1}H\}$ NMR $(CD_3)_2CO$, 29 MHz)
Compound 2

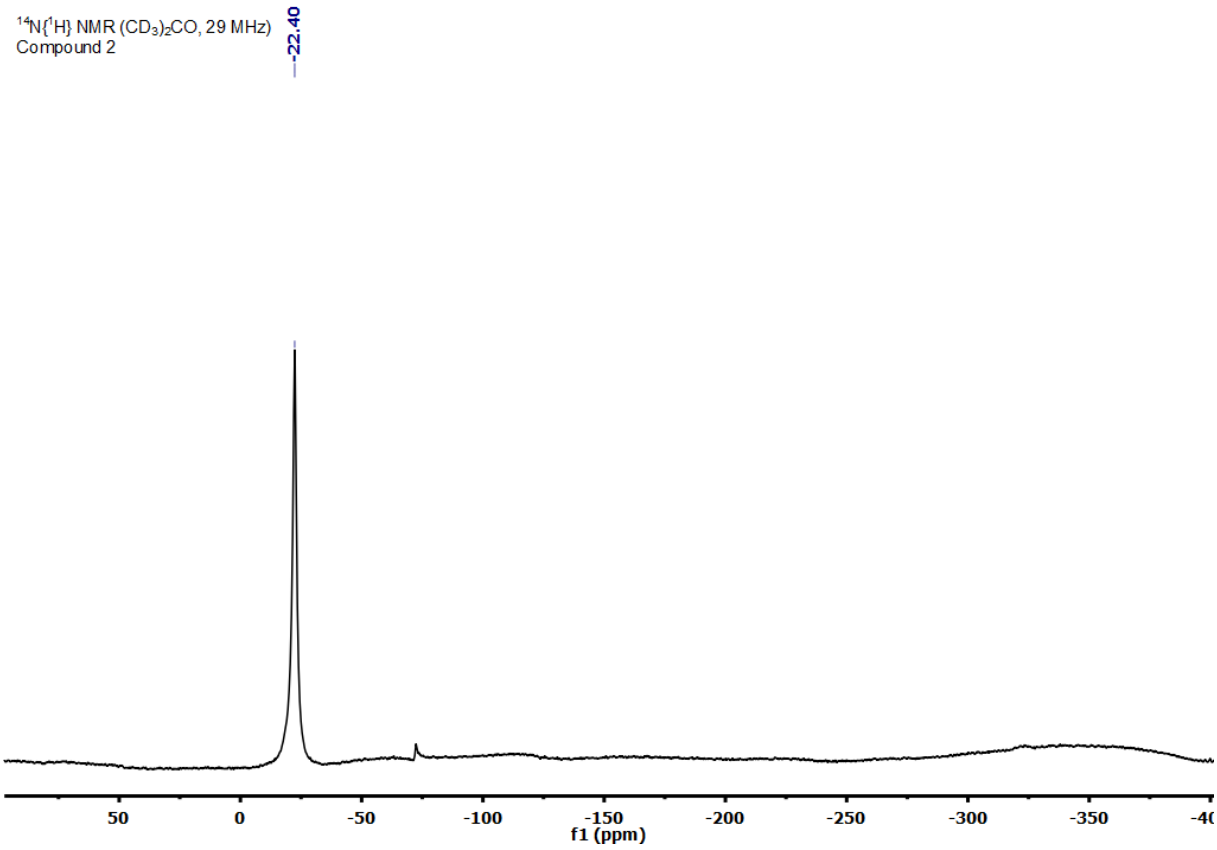

1.3 Compound 3

^{1}H NMR (DMSO-$_{d6}$, 400 MHz)
Compound 3

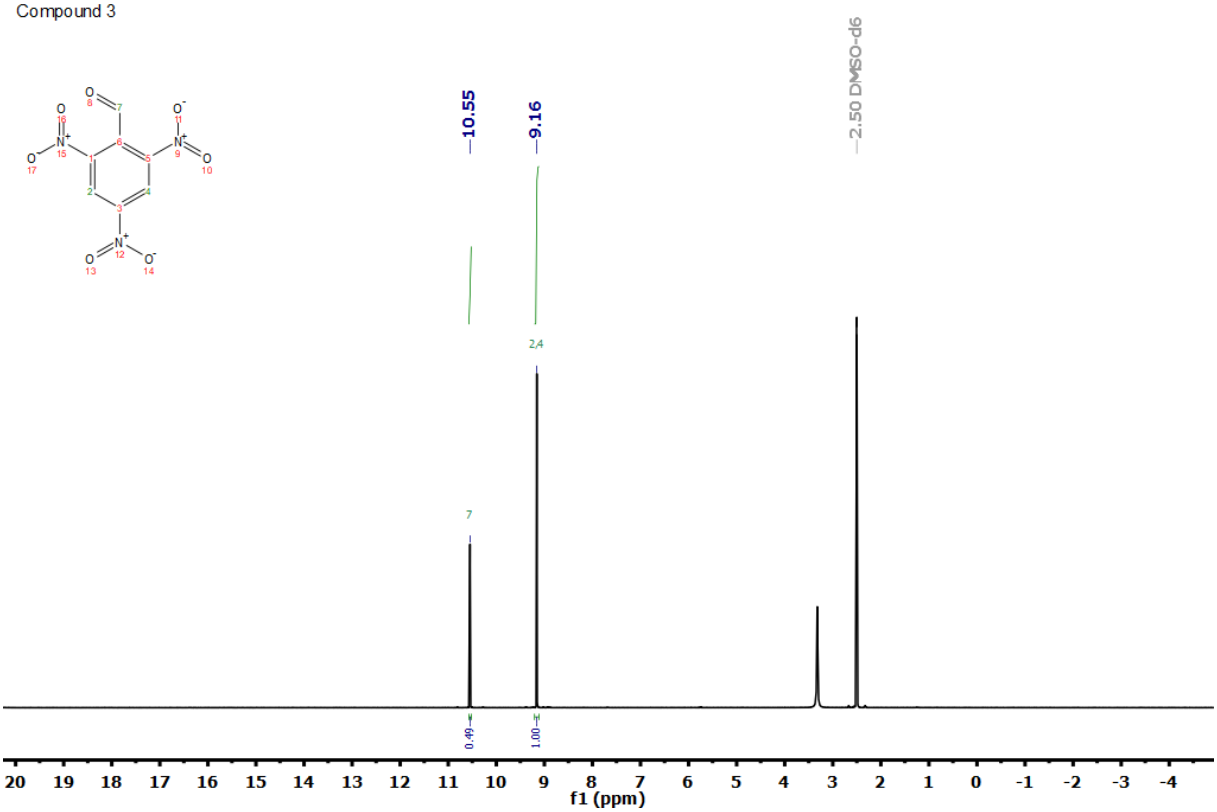

^{13}C{^{1}H} NMR (DMSO-$_{d6}$, 101 MHz)
Compound 3

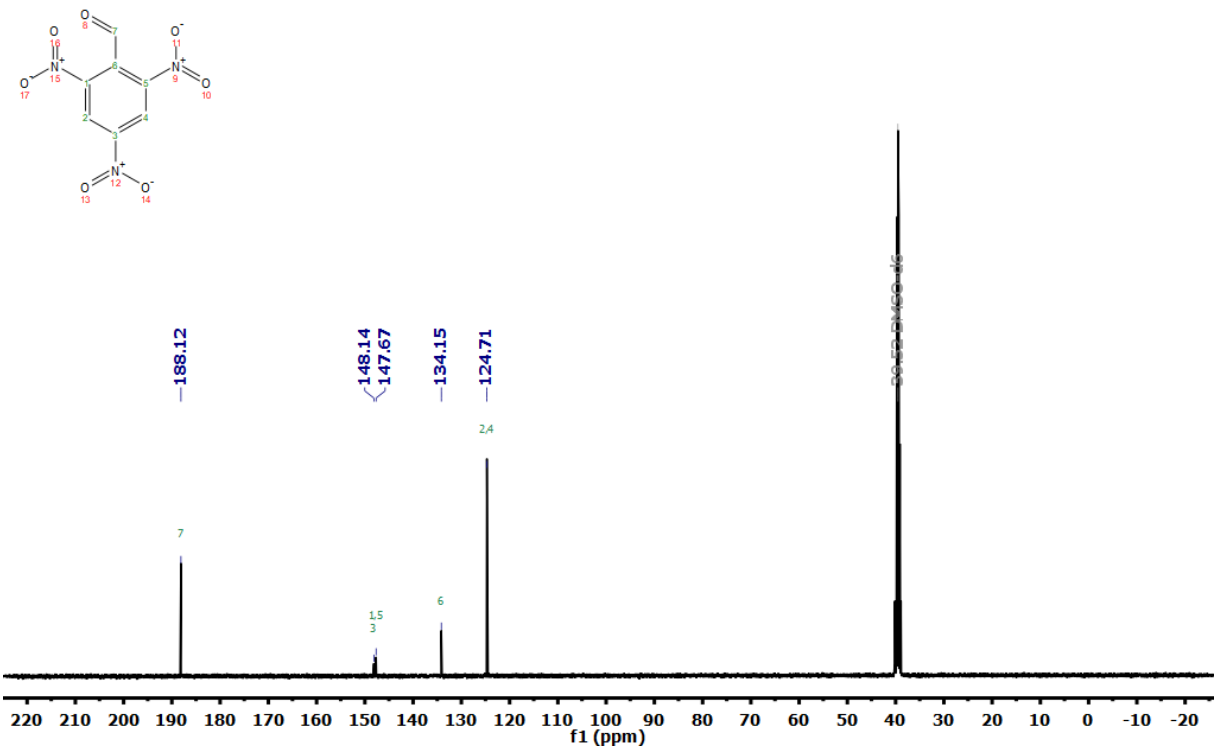

$^{14}N\{^{1}H\}$ NMR (DMSO-D_6, 29 MHz)
Compound 3

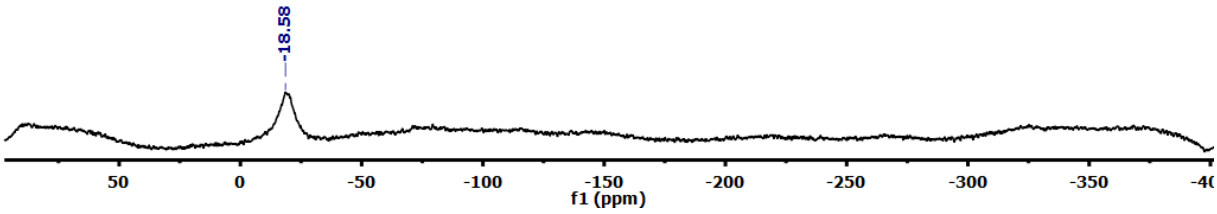

2 Detonation Parameter

2.1 Compound 1

C(6,000) H(2,000) N(3,000) O(6,000) F(1,000)

Molecular weight = 231,09

Density of reactant = 1,837 g/cm^3

Initial pressure = 0,1 MPa

Oxygen balance = -45,00052 %

Enthalpy of formation = -1670,75 kJ/kg

Internal energy of formation = -1603,71 kJ/kg

Detonation parameters (at the C-J point):

Heat of detonation = -4070,915 kJ/kg

Detonation temperature = 3301,012 K

Detonation pressure = 23,86535 GPa

Detonation velocity = 7376,067 m/s

Particle velocity = 1761,295 m/s

Sound velocity = 5614,772 m/s

Density of products = 2,413247 g/cm^3

Volume of products = 0,4143794 cm^3/g

Exponent 'Gamma' = 3,187853

Moles of gaseous products = 5,734581 mol/mol explosive

Moles of condensed products = 2,679472 mol/mol explosive

Volume of gas at STP = 606,8738 dm^3/kg

Mean molecular mass of gas. prod. = 34,6867 g/mol

Mean molecular mass of cond.prod.= 12,011 g/mol

Mean molecular mass of all prod. = 27,46557 g/mol

Entropy of products = 5,7983 kJ/kg K

Internal energy of products = 5622,008 kJ/kg, i.e. 10,32763 kJ/cm^3

Compression energy = 1551,093 kJ/kg, i.e. 2,849357 kJ/cm^3

Total heat energy = -4070,915 kJ/kg, i.e. -7,478271 kJ/cm^3

Composition of detonation products (47):

Products	mol/mol EM	mol/kg EM	Mol %	Mass %
C(d) =	2,679472E+00	1,159473E+01	31,8452	13,9264
CO2 =	2,142781E+00	9,272333E+00	25,4667	40,8075
N2 =	1,497698E+00	6,480902E+00	17,8000	18,1550
CO =	8,285554E-01	3,585361E+00	9,8473	10,0426
HF =	4,377052E-01	1,894057E+00	5,2021	3,7893
CH2O2 =	2,990076E-01	1,293879E+00	3,5537	5,9551
H2O =	2,876848E-01	1,244882E+00	3,4191	2,2427
H2F2 =	1,844428E-01	7,981289E-01	2,1921	3,1938
CF4 =	4,705893E-02	2,036354E-01	0,5593	1,7922
H2 =	2,905926E-03	1,257465E-02	0,0345	0,0025
HCN =	2,566023E-03	1,110381E-02	0,0305	0,0300
NH3 =	2,019898E-03	8,740591E-03	0,0240	0,0149
H3F3 =	1,490167E-03	6,448316E-03	0,0177	0,0387
CH2F2 =	2,035239E-04	8,806976E-04	0,0024	0,0046
CFO =	1,582283E-04	6,846926E-04	0,0019	0,0032
CH4 =	1,325425E-04	5,735436E-04	0,0016	0,0009
F =	1,046203E-04	4,527174E-04	0,0012	0,0009
C2H4 =	1,832081E-05	7,927862E-05	0,0002	0,0002
CNO =	1,054605E-05	4,563534E-05	0,0001	0,0002
H =	8,407203E-06	3,638002E-05	0,0001	0,0000
H4F4 =	8,134671E-06	3,520070E-05	0,0001	0,0003
CH3OH =	7,273919E-06	3,147602E-05	0,0001	0,0001
NH2 =	3,564576E-06	1,542479E-05	0,0000	0,0000

HCNO =	3,309321E-06	1,432024E-05	0,0000	0,0001
CH2O =	2,676408E-06	1,158147E-05	0,0000	0,0000
C2H6 =	2,567320E-06	1,110942E-05	0,0000	0,0000
H2O2 =	8,090705E-07	3,501045E-06	0,0000	0,0000
N2H4 =	6,373253E-07	2,757862E-06	0,0000	0,0000
N =	2,148729E-07	9,298074E-07	0,0000	0,0000
N2O =	1,371812E-07	5,936165E-07	0,0000	0,0000
F2 =	6,305020E-08	2,728336E-07	0,0000	0,0000
CFN =	5,508686E-08	2,383743E-07	0,0000	0,0000
H6F6 =	4,275934E-08	1,850301E-07	0,0000	0,0000
FO =	3,661208E-08	1,584294E-07	0,0000	0,0000
HFO =	3,420147E-08	1,479981E-07	0,0000	0,0000
H5F5 =	1,061634E-08	4,593947E-08	0,0000	0,0000
NF =	8,485902E-09	3,672056E-08	0,0000	0,0000
CF2 =	3,814907E-09	1,650803E-08	0,0000	0,0000
CHF =	2,935616E-09	1,270312E-08	0,0000	0,0000
NF3 =	1,007263E-09	4,358673E-09	0,0000	0,0000
CF =	2,293456E-10	9,924344E-10	0,0000	0,0000
CHF3 =	2,278122E-10	9,857989E-10	0,0000	0,0000
CF2O =	1,499837E-10	6,490161E-10	0,0000	0,0000
F2O =	1,336626E-11	5,783905E-11	0,0000	0,0000
CF3 =	2,299087E-12	9,948709E-12	0,0000	0,0000
C(gr) =	7,169055E-17	3,102225E-16	0,0000	0,0000
C2HF =	1,574275E-19	6,812273E-19	0,0000	0,0000

2.2 Compound 2

C(7,000) H(5,000) N(3,000) O(9,000) S(1,000)

Molecular weight = 307.19

Density of explosive = 1.795 g/cm^3

Oxygen balance = -49,47784 %

Enthalpy of formation = -1734,44 kJ/kg

Internal energy of formation = -1655,76 kJ/kg

Detonation parameters (at the C-J point):

Heat of detonation = -3904,681 kJ/kg

Detonation temperature = 2240,498 K

Detonation pressure = 12,57338 GPa

Detonation velocity = 5862,976 m/s

Particle velocity = 1194,72 m/s

Sound velocity = 4668,256 m/s

Density of products = 2,254384 g/cm^3

Volume of products = 0,4435802 cm^3/g

Exponent 'Gamma' = 3,907376

Moles of gaseous products = 4,82162 mol/mol explosive

Moles of condensed products = 5,870428 mol/mol explosive

Volume of gas at STP = 383,86 dm^3/kg

Mean molecular mass of gas. prod. = 31,24055 g/mol

Mean molecular mass of cond.prod. = 26,67034 g/mol

Mean molecular mass of all prod. = 28,73129 g/mol

Entropy of products = 5,9155 kJ/kg K

Internal energy of products = 4618,37 kJ/kg, i.e. 8,289973 kJ/cm^3

Compression energy = 713,688 kJ/kg, i.e. 1,281072 kJ/cm^3

Total heat energy = -3904,681 kJ/kg, i.e. -7,008902 kJ/cm^3

Composition of detonation products:

Products	mol/mol	mol/kg	Mol %	Mass %
C(gr) =	4,870561E+00	1,585526E+01	45,5531	19,0437
N2 =	1,487744E+00	4,843091E+00	13,9145	13,5670
CO2 =	1,474806E+00	4,800973E+00	13,7935	21,1291
H2O =	1,162167E+00	3,783232E+00	10,8695	6,8156
H2SO4(l) =	9,998671E-01	3,254892E+00	9,3515	31,9237
CO =	3,860281E-01	1,256647E+00	3,6104	3,5199
CH2O2 =	2,512905E-01	8,180321E-01	2,3503	3,7650
NH3 =	2,342778E-02	7,626505E-02	0,2191	0,1299
H2 =	1,991075E-02	6,481597E-02	0,1862	0,0131
CH4 =	1,371934E-02	4,466091E-02	0,1283	0,0716
HCN =	1,079142E-03	3,512959E-03	0,0101	0,0095
C2H6 =	9,113819E-04	2,966844E-03	0,0085	0,0089
C2H4 =	2,912388E-04	9,480769E-04	0,0027	0,0027
H2S =	1,155614E-04	3,761900E-04	0,0011	0,0013
CH3OH =	1,012711E-04	3,296703E-04	0,0009	0,0011
SO2 =	1,607743E-05	5,233724E-05	0,0002	0,0003
CH2O =	6,274240E-06	2,042469E-05	0,0001	0,0001
HCNO =	2,517524E-06	8,195359E-06	0,0000	0,0000
H =	8,063507E-07	2,624933E-06	0,0000	0,0000
NH2 =	7,235816E-07	2,355493E-06	0,0000	0,0000
N2H4 =	5,472519E-07	1,781483E-06	0,0000	0,0000
COS =	5,225123E-07	1,700947E-06	0,0000	0,0000
SO =	4,870590E-07	1,585535E-06	0,0000	0,0000
S =	8,669488E-08	2,822200E-07	0,0000	0,0000
CNO =	2,646984E-08	8,616794E-08	0,0000	0,0000
H2SO4 =	1,779389E-08	5,792489E-08	0,0000	0,0000

H2O2 =	1,261897E-08	4,107885E-08	0,0000	0,0000
SO3 =	1,161260E-08	3,780279E-08	0,0000	0,0000
S2 =	9,768153E-09	3,179851E-08	0,0000	0,0000
NS =	3,991198E-09	1,299265E-08	0,0000	0,0000
N2O =	6,494896E-10	2,114300E-09	0,0000	0,0000
N =	8,409478E-11	2,737558E-10	0,0000	0,0000
CS =	2,622255E-12	8,536292E-12	0,0000	0,0000
C(d) =	2,686988E-14	8,747018E-14	0,0000	0,0000
S(l) =	5,109685E-24	1,663368E-23	0,0000	0,0000

2.3 Compound 3

C(7,000) H(3,000) N(3,000) O(7,000)

Molecular weight = 241,11

Density of reactant = 1,721 g/cm3

Initial pressure = 0,1 MPa

Oxygen balance = -56,40203 %

Enthalpy of formation = -676,87 kJ/kg

Internal energy of formation = -602,33 kJ/kg

Detonation parameters (at the C-J point):

Heat of detonation = -4391,028 kJ/kg

Detonation temperature = 3361,192 K

Detonation pressure = 20,43825 GPa

Detonation velocity = 7062,668 m/s

Particle velocity = 1681,48 m/s

Sound velocity = 5381,188 m/s

Density of products = 2,258767 g/cm^3

Volume of products = 0,4427193 cm^3/g

Exponent 'Gamma' = 3,200252

Moles of gaseous products = 6,073771 mol/mol explosive

Moles of condensed products = 3,279312 mol/mol explosive

Volume of gas at STP = 616,0655 dm^3/kg

Mean molecular mass of gas. prod. = 33,21294 g/mol

Mean molecular mass of cond.prod. = 12,011 g/mol

Mean molecular mass of all prod. = 25,77926 g/mol

Entropy of products = 6,1434 kJ/kg K

Internal energy of products = 5804,73 kJ/kg, i.e. 9,989941 kJ/cm^3

Compression energy = 1413,702 kJ/kg, i.e. 2,432981 kJ/cm^3

Total heat energy = -4391,028 kJ/kg, i.e. -7,55696 kJ/cm^3

Composition of detonation products:

Products	mol/mol	mol/kg	Mol %	Mass %
C(d) =	3,279251E+00	1,360059E+01	35,0606	16,3357
CO2 =	1,841066E+00	7,635760E+00	19,6841	33,6050
N2 =	1,488687E+00	6,174281E+00	15,9165	17,2960
CO =	1,249791E+00	5,183469E+00	13,3624	14,5189
H2O =	8,341380E-01	3,459560E+00	8,9183	6,2325
CH2O2 =	6,168757E-01	2,558472E+00	6,5954	11,7754
H2 =	1,720835E-02	7,137107E-02	0,1840	0,0144
NH3 =	1,360286E-02	5,641740E-02	0,1454	0,0961
HCN =	8,953327E-03	3,713363E-02	0,0957	0,1004
CH4 =	2,576904E-03	1,068763E-02	0,0276	0,0171
C2H4 =	4,559740E-04	1,891137E-03	0,0049	0,0053
C2H6 =	1,652431E-04	6,853405E-04	0,0018	0,0021
CH3OH =	1,227484E-04	5,090948E-04	0,0013	0,0016
C(gr) =	6,114367E-05	2,535914E-04	0,0007	0,0003
H =	3,718788E-05	1,542355E-04	0,0004	0,0000
CH2O =	2,582675E-05	1,071156E-04	0,0003	0,0003
NH2 =	2,155524E-05	8,939968E-05	0,0002	0,0001
CNO =	1,718879E-05	7,128993E-05	0,0002	0,0003
HCNO =	1,710196E-05	7,092983E-05	0,0002	0,0003
N2H4 =	6,513339E-06	2,701386E-05	0,0001	0,0001
H2O2 =	2,417571E-06	1,002680E-05	0,0000	0,0000
N =	3,764218E-07	1,561197E-06	0,0000	0,0000
N2O =	1,914663E-07	7,941001E-07	0,0000	0,0000

3 Structure refinement data

3.1 Compound 1

Empirical formula	C6 H2 F N3 O6
Formula weight	231.11
Temperature	123(2) K
Wavelength	0.71073 Å
Crystal system	Trigonal
Space group	R-3
Unit cell dimensions	a = 21.7651(3) Å α = 90°.
	b = 21.7651(3) Å β = 90°.
	c = 8.9198(2) Å γ = 120°.
Volume	3659.37(13) $Å^3$
Z	18
Density (calculated)	1.888 Mg/m^3
Absorption coefficient	0.185 mm^{-1}
F(000)	2088
Crystal size	0.400 x 0.400 x 0.300 mm^3
Theta range for data collection	2.526 to 30.502°.
Index ranges	-31<=h<=31, -31<=k<=31, -12<=l<=12
Reflections collected	24440
Independent reflections	2477 [R(int) = 0.0224]
Completeness to theta = 25.242°	99.3 %
Absorption correction	Semi-empirical from equivalents
Max. and min. transmission	1.00000 and 0.89869
Refinement method	Full-matrix least-squares on F^2
Data / restraints / parameters	2477 / 0 / 147
Goodness-of-fit on F^2	1.035
Final R indices [I>2sigma(I)]	R1 = 0.0316, wR2 = 0.0851
R indices (all data)	R1 = 0.0358, wR2 = 0.0885
Extinction coefficient	n/a
Largest diff. peak and hole	0.456 and -0.177 $e.Å^{-3}$

3.2 Compound 2

Empirical formula	C7 H5 N3 O9 S
Formula weight	307.20
Temperature	143(2) K
Wavelength	0.71073 Å
Crystal system	Monoclinic
Space group	$P2_1$
Unit cell dimensions	a = 8.3195(6) Å α = 90°.
	b = 7.9947(5) Å β = 103.585(7)°.
	c = 8.5747(6) Å γ = 90°.
Volume	554.36(7) $Å^3$
Z	2
Density (calculated)	1.840 Mg/m^3
Absorption coefficient	0.349 mm^{-1}
F(000)	312
Crystal size	0.450 x 0.400 x 0.050 mm^3
Theta range for data collection	3.531 to 28.275°.
Index ranges	-11<=h<=11, -10<=k<=10, -11<=l<=10
Reflections collected	4825
Independent reflections	2522 [R(int) = 0.0170]
Completeness to theta = 25.242°	99.7 %
Absorption correction	Semi-empirical from equivalents
Max. and min. transmission	1.00000 and 0.69252
Refinement method	Full-matrix least-squares on F^2
Data / restraints / parameters	2522 / 1 / 201
Goodness-of-fit on F^2	1.056
Final R indices [I>2sigma(I)]	R1 = 0.0267, wR2 = 0.0656
R indices (all data)	R1 = 0.0285, wR2 = 0.0678
Absolute structure parameter	0.32(4)
Extinction coefficient	n/a
Largest diff. peak and hole	0.277 and -0.334 e.$Å^{-3}$

3.3 Compound 3

Empirical formula	C7 H3 N3 O7	
Formula weight	241.12	
Temperature	143(2) K	
Wavelength	0.71073 Å	
Crystal system	Orthorhombic	
Space group	Pbcn	
Unit cell dimensions	a = 10.5782(10) Å	α = 90°.
	b = 14.2749(16) Å	β = 90°.
	c = 12.0267(13) Å	γ = 90°.
Volume	1816.1(3) $Å^3$	
Z	8	
Density (calculated)	1.764 Mg/m^3	
Absorption coefficient	0.162 mm^{-1}	
F(000)	976	
Crystal size	0.200 x 0.100 x 0.050 mm^3	
Theta range for data collection	4.151 to 28.281°.	
Index ranges	-11<=h<=14, -19<=k<=18, -16<=l<=14	
Reflections collected	15402	
Independent reflections	2245 [R(int) = 0.0616]	
Completeness to theta = 25.242°	99.5 %	
Absorption correction	Semi-empirical from equivalents	
Max. and min. transmission	1.00000 and 0.90557	
Refinement method	Full-matrix least-squares on F^2	
Data / restraints / parameters	2245 / 0 / 166	
Goodness-of-fit on F^2	1.032	
Final R indices [I>2sigma(I)]	R1 = 0.0432, wR2 = 0.0950	
R indices (all data)	R1 = 0.0748, wR2 = 0.1110	
Extinction coefficient	n/a	
Largest diff. peak and hole	0.247 and -0.208 $e.Å^{-3}$	

4 Enlarged View of the Figures

4.1 Figure 2

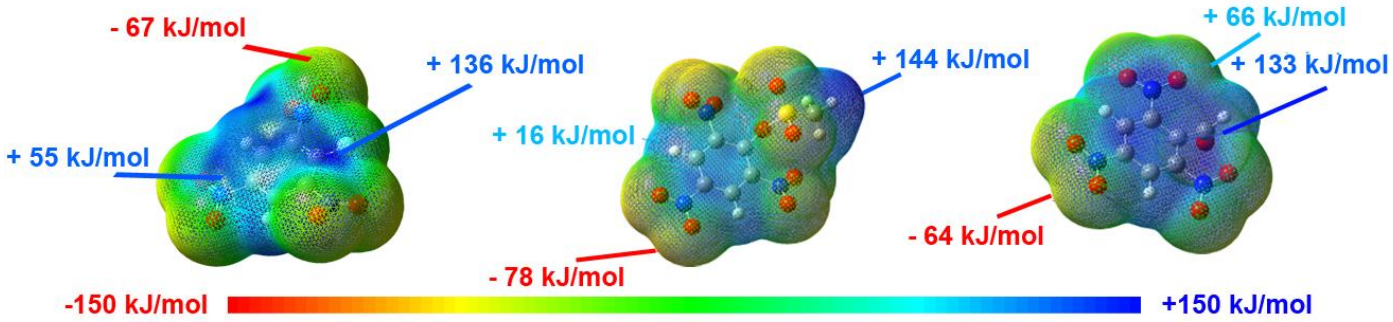

Figure 2. ESP of **1** (left), **2** (center) and **3** (right), calculated on the 0.02 electron bohr^{-3} hypersurface.

4.2 Figure 3

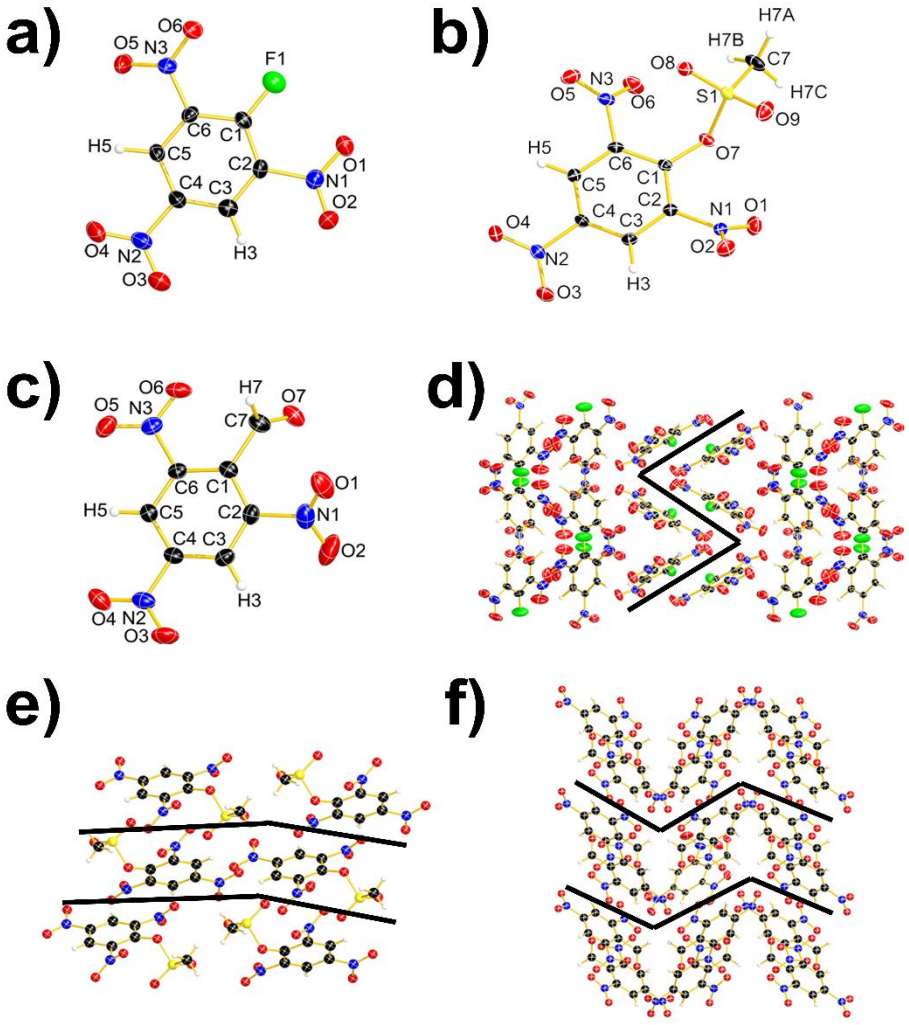

Figure 3. Single-crystal X-ray structure of **1** (a), **2** (b), **3** (c) and the crystal packing of **1** (d), **2** (e), **3** (f).

4.3 Figure 4

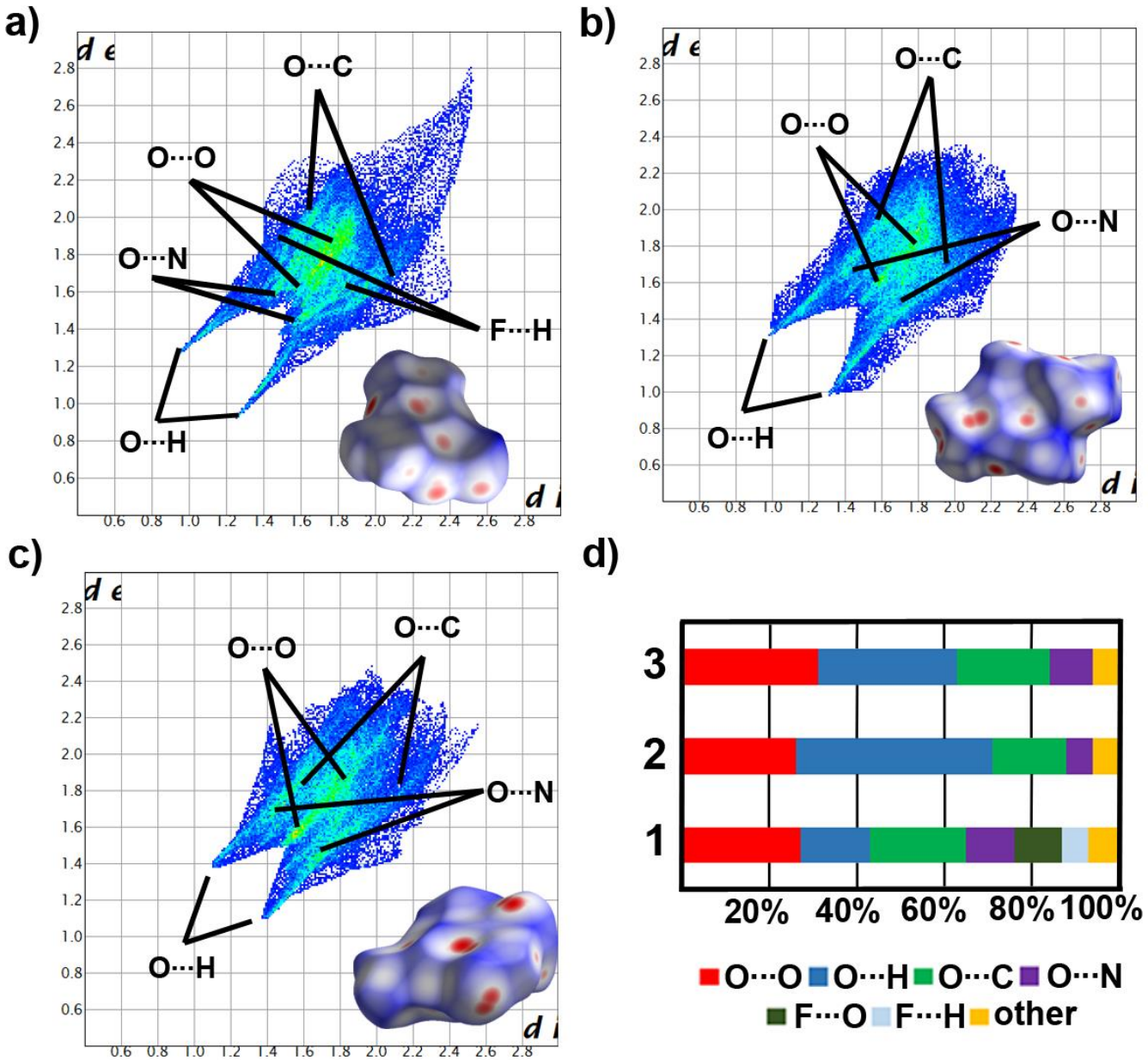

Figure 4. Two-dimensional Fingerprint plot in crystal stacking as well as the corresponding Hirshfeld surface (bottom right in 2D plot) of **1** (a), **2** (b), and **3** (c) (color coding: white, distance d equals VDW distance; blue, d exceeds VDW distance, red, d, smaller than VDW distance). The population of close contacts of **1**, **2**, and **3** in crystal stacking (d).

7 A Study of 3,5-Dinitro-1-(2,4,6-trinitrophenyl)-1*H*-pyrazol-4-amine (PicADNP) as a New High Energy Density Booster Explosive

published in *Eur. J. Org. Chem.* **2021**, *2021*, 1964–1970. (doi: 10.1002/ejoc.202100159)

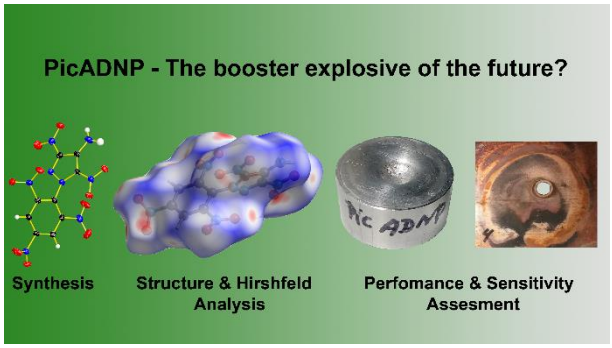

7.1 Abstract

Two improved fast, feasible, scalable, and economic synthetic protocols for the laboratory scale manufacturing of 3,5-dinitro-1-(2,4,6-trinitrophenyl)-1H-pyrazol-4-amine (PicADNP) are described. The previous set of analytical data from an earlier publication could be verified and complemented by additional measurements. The material was fully characterized by multinuclear NMR, spectroscopic methods, elemental analysis, DSC and DTA as well as X-ray diffraction. The crystal structure was elucidated and Hirshfeld surface analysis, as well as 2D Fingerprint plot analysis for the assessment of sensitivities towards external stimuli was applied. The sensitivity towards shock, friction, and electrostatic discharge was also determined experimentally. The performance of the title compound was calculated by applying the EXPLO5 computer code and the theoretical results were compared with the results of SSRT and booster testing experiments. The title compound combines good energetic properties with improved safety characteristics and could find its way into an application as a new booster explosive to replace the state-of-the-art material PETN. The optimizations of the synthetic protocol comprise a greener solvent system, shorter reaction times, higher yields for the pure material, and a nontoxic byproduct to make the manufacturing process more attractive and better suitable for a subsequent scale up to the technical and industrial scale.

KEYWORDS: HEDM, Booster Explosive, Green Chemistry, Hirshfeld surface analysis.

7.2 Introduction

Over the last decade, the development of new high energy density materials (HEDMs), which exhibit superior performance, a greener and economic synthesis, and an

increased safety profile has been of major interest to the energetic materials community.[1-3] One specific area is the development of new materials for booster explosives, as the energy generated by the initiation of a small amount of a primary explosive like lead azide is often insufficient for the safe and proper initiation of various high explosives such as TATB or HNS.[4] A solution for this problem are booster explosives, which are applied to transfer and enhance the energy of the initial shockwave of a primary explosive for successful initiation of the respective high explosive.[1,3] For this application new energetic materials need to balance a shock sensitivity that is low enough for initiation via a primary explosive with sufficient explosive performance for the safe initiation of the high explosive while maintaining a safe application for the user.[1] Another important requirement for booster explosives is high thermal stability, especially for the application in insensitive munitions, deep-well drilling, and stage separation for space exploration.[1,3] Examples for developments in this area of HEDM research are polymer-bonded explosive formulations based on LLM-105[5] or CL-20/FOX-7[6], which have been published in recent years. However, since 1912[7] the most common component in booster charges has been PETN due to its high explosive performance and easy synthesis. The two main drawbacks of PETN are the high sensitivity (IS: 4 J, FS: 73 N, ESD: 30 mJ) and a comparably low melting point of 142 °C.[2,8-10] To mitigate those problems it can be applied in a formulation with TNT ("pentolite").[1] To overcome the drawbacks of PETN and PETN-based formulation we started our research for a potential replacement material for PETN, which should combine high energetic performance with an increased safety profile for energy transfer applications.

The title compound 3,5-dinitro-1-(2,4,6-trinitrophenyl)-1*H*-pyrazol-4-amine (PicADNP) was first synthesized via a nucleophilic substitution reaction of 4-amino-3,5-dinitropyrazol (ADNP, LLM-116) with picryl chloride and sodium fluoride in NMP by *Wang et al.* in 2009.[11] However, the synthetic protocol proposed by the authors has various drawbacks for manufacturing exceeding the laboratory scale. The analytical data for PicADNP given in the publication of *Wang et al.* comprises ^{1}H and ^{13}C NMR, elemental analysis, melting point, and infrared spectroscopy.[11]

This work proposes two new and optimized synthetic protocols for the manufacturing of PicADNP on a laboratory scale starting from potassium 4-amino-3,5-dinitropyrazol-1-ide (KADNP) and picryl derivatives. Both protocols are scalable, time-efficient, and more environmentally benign. A complete characterization of the title compound was conducted and new results for thermal analysis, structural elucidation via X-ray, and calculated as well as experimental values for various energetic properties could be obtained.

7.3 Results and Discussion

***7.3.1 Optimization of the Synthesis*.** As mentioned in the introduction, the initial synthesis for PicADNP proposed by *Wang et al.* shows some significant drawbacks for manufacturing exceeding the laboratory scale. The synthetic protocol takes 16 h and only a comparably low yield of 53% is obtained in the process. The applied solvent N-methyl-2-pyrrolidone (NMP) is considered toxic for reproduction and can damage the unborn child and is as such part of the REACH candidate list of “substances of very high concern for authorization”.[12] Also, the very toxic byproduct hydrogen fluoride is formed in the reaction process.[13]

To overcome those drawbacks, a screening of various picrylating agents for the nucleophilic substitution of potassium 4-amino-3,5-dinitropyrazol-1-ide (KADNP) was performed in an initial study for this work. In addition, various solvents were evaluated to replace NMP with a more environmentally benign alternative. The best results were achieved when utilizing picryl chloride (PicCl) or picryl mesylate (PicMs) as the picrylation agents, HPLC grade acetonitrile as the solvent, and a temperature of 70 °C for the reaction. In a subsequent study, the reaction time was varied between 4 and 72 h for the best two systems to further optimize the manufacturing process. The two most promising synthetic protocols for a fast, easy and scalable synthesis of PicADNP are depicted in **Schemes 1** and **2**.

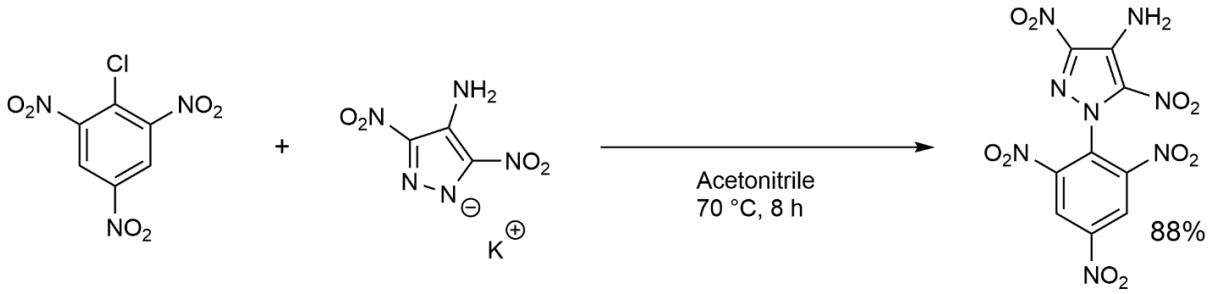

Scheme 1. Reaction Scheme for Synthetic Protocol 1.

By following the first protocol, a yield of 88% could be realized within a reaction time of only 8 hours at 70 °C, starting from KADNP and PicCl. This resembles a significant improvement over the state-of-the-art synthesis proposed by *Wang et al.* because the synthesis is faster, cheaper, less toxic, and exhibits a higher yield.

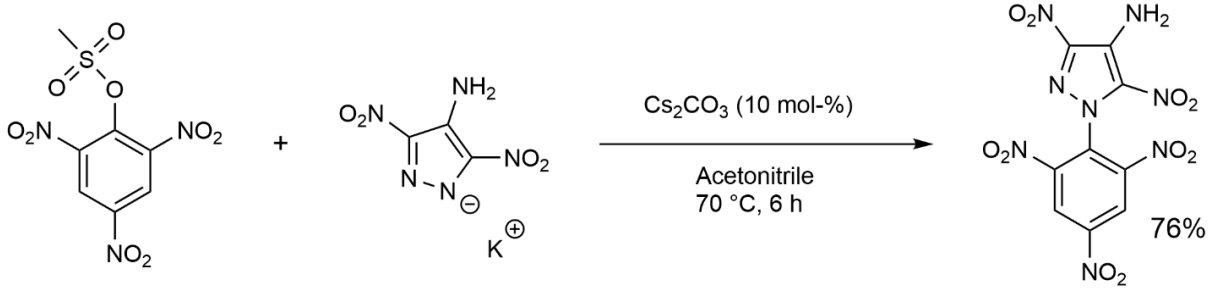

Scheme 2. Reaction Scheme for Synthetic Protocol 2.

For the second protocol utilizing KADNP and PicMs as the starting materials and cesium carbonate as a catalyst, a slightly lower yield of 76% was obtained however, the time required for the maximum yield at 70 °C could be lowered by another 25% to 6 hours. Despite this improvement regarding reaction time, the second protocol has two minor drawbacks as the starting material picryl mesylate is very hygroscopic and not commercially available.

Another improvement that was employed for both protocols is the cheap, feasible, and scalable workup process. The respective non-toxic byproduct (KMs, KCl) precipitates from the reaction mixture during the synthesis and can be easily separated by filtration. Adding an excess of water to the acetonitrile phase precipitates the product with high purity.

***7.3.2 Spectroscopic Characterization*.** The material obtained by both synthetic protocols was completely characterized by multinuclear NMR spectroscopy, vibrational spectroscopy (IR, Raman), and elemental analysis. No notable differences were found for the purified materials from both synthetic protocols. The chemical shifts found in the ^{1}H NMR measurements (9.36, 7.89 ppm) are in good agreement with the previously reported signals of *Wang et al.* (9.36, 7.88 ppm). The same is true for the results of the ^{13}C{^{1}H} NMR measurements, which revealed chemical shifts between 125 and 150 ppm as expected. In the ^{14}N NMR spectrum, no distinct signals for the nitro groups were found due to the rather large signal width of over 800 Hz. The values for the IR spectroscopy are in good agreement with the values given by *Wang et al.*. In **Table 1** an overview of various characteristic Raman- and infrared vibration modes is given. They were assigned according to the available literature.[14]

Table 1. Characteristic vibration modes of PicADNP.

	PicADNP	
	IR	Raman
ν(N-H)	3362	3364
ν(C-H)	3096	3087
$\nu_{as}(NO_2)$	1542	1556
$\nu_{s}(NO_2)$	1337	1364
ν(C-N)	912	824
δ(NO2)	742	773

$\nu_{as/s}$: asymmetric/symmetric vibration mode *δ*: deformation vibration

The results of the elemental analysis proof a successful synthesis of high purity PicADNP with very low deviations from the calculated values for the elemental composition of the title compound.

***7.3.3 Thermal Analysis*.** The observed values for thermal analysis (DTA & DSC) are in good agreement with the melting range given by *Wang et al.* (234–236°C). In the DTA measurements, a melting point was observed at 234.6 °C as well as a subsequent decomposition starting at 238.2 °C **(Figure 1)**.

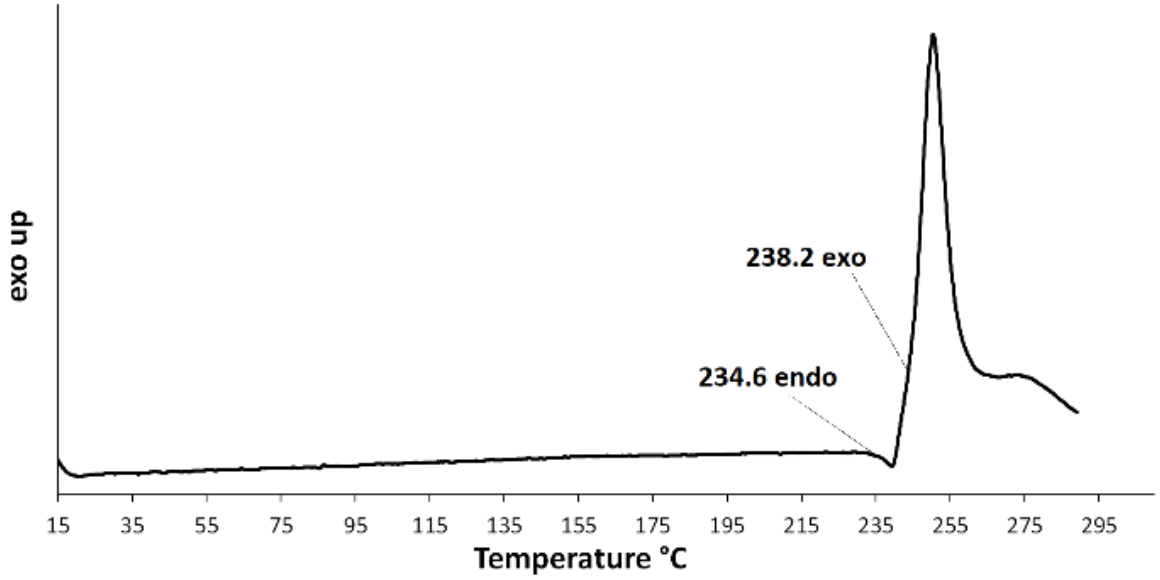

Figure 1. Differential thermal analysis at 5 K/min.

In the DSC measurements, a melting point was observed at 233.6 °C as well as a subsequent decomposition starting at 237.5 °C (**Figure 2**).

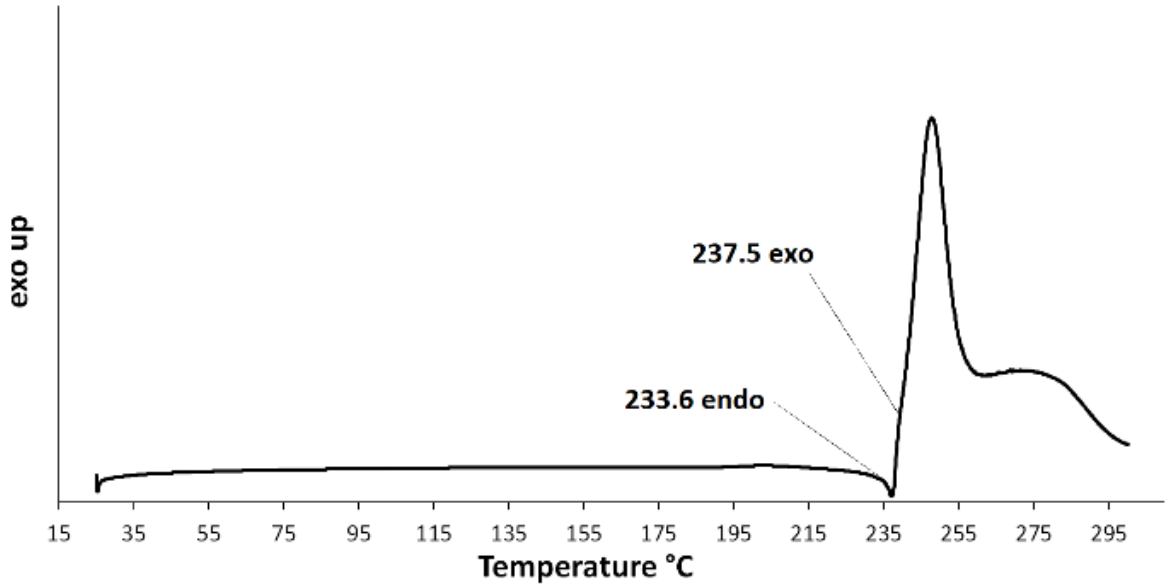

Figure 2. Differential scanning calorimetry at 5 K/min

***7.3.4 Structure-property relationship*.** External mechanical stimuli like impact or friction can lead to a displacement of stabilizing crystal layers in a crystal, which subsequently results in internal strains. The energy of such strains can surpass the required energy to break the weakest bond of the molecule, which leads to the decomposition of a material.[15] The strain energy caused by an interlayer slide is not only dependent on factors like the stacking and gearing of the individual layers, but also on other stabilizing interactions like hydrogen bridges.[16] Therefore the combination of crystal structure analysis and the analysis of the close-contact population via Hirshfeld surface analysis is required for an assessment of the sensitivity towards external stimuli of an energetic material.

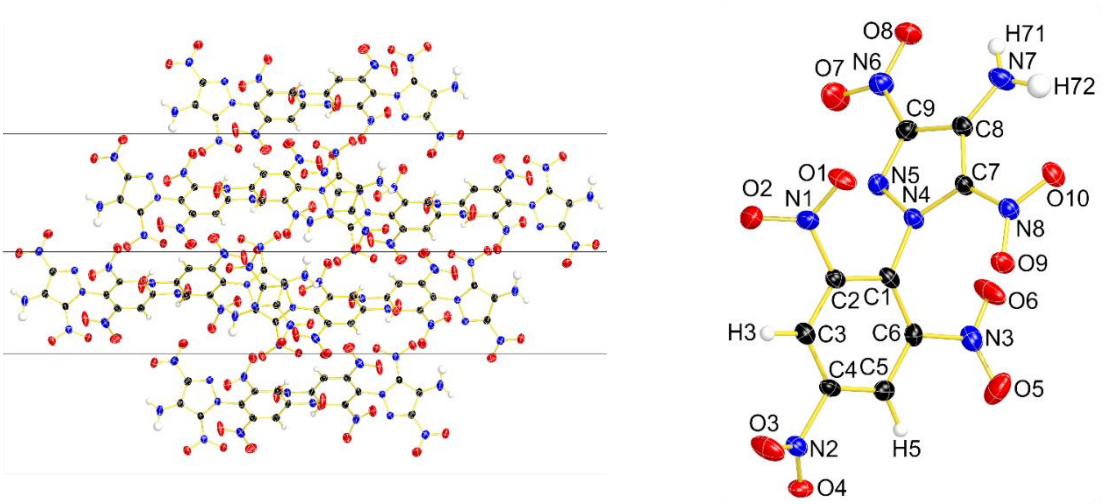

Figure 3. Single-crystal X-ray structure and the layered crystal packing of PicADNP.

In the crystal, PicADNP exhibits a planar benzene ring and a planar pyrazole ring, which is twisted out of the benzene plane by 78.2°. The ortho nitro groups of the benzene ring show torsion angles of 38.9° (C2-nitro) and 18.8° (C6-nitro), which is a very common observation for trinitrobenzene derivatives.[17,18] This behavior is usually explained by a combination of steric effects and electronic repulsion between the substituent at the 1-position and the ortho nitro groups.[17,18] For PicADNP, the discussed torsion of the substituents facilitates minimization of the repulsion between neighboring nitro groups and reduces the repulsion between the pyrazole ring and the C2-nitro group. The lowest intramolecular oxygen-oxygen distance is observed for O6···O9 and is comparably high with 3.152 Å. The distance between the pyrazole ring and the ortho-nitro group is 2.940 Å (N5···O1). All other intramolecular interactions are within typical ranges and as expected. The atypical and surprisingly strong twisting of the para-nitro group 31.8° (C4-nitro) can be explained by strong intermolecular hydrogen bonds between O4···H71′ (2.387 Å) and two weaker hydrogen bonds between N2···H71′ (2.927 Å) and O3···H71′ (2.866 Å). These three interactions are also essential for the stabilization of the molecular structure and the unit-cell structure. PicADNP exhibits a layered structure in the unit-cell with little to no gearing and moderately strong, stabilizing interlayer hydrogen bonds i.e. H5···O7′ (2.727 Å), H5···O9′ (2.612 Å), H3···O3′ (2.589 Å), and H3···O6′ (2.793 Å).

However, if those stabilizing interactions are destroyed by external stimuli like impact or friction an easy interlayer slide is facilitated, which results in negative oxygen-oxygen repulsions and other detrimental interactions between the individual layers. When the resulting strain energies surpass the lowest bond dissociation energy (BDE) of the molecule the material will decompose.[15] Besides the discussed crystal packing effects the amount and intensity of stabilizing and destabilizing intermolecular interactions in each layer of the structure is important for the extend of the energy that is required for a decomposition of the structure, which correlates directly with the sensitivity of the material.[15] They can be assessed by applying a combined method of Hirshfeld surface analysis and 2D Fingerprint plotting.

As a general trend for insensitive molecules, it was found, that the individual planes of their Hirshfeld surface feature red dots which represent close contacts that are located within the plane of the molecule and therefore in a stabilized layer.[15,17,18] On the contrary, an increased amount of red dots that point out of the molecular plane is typical for more sensitive materials.[15,17,18]

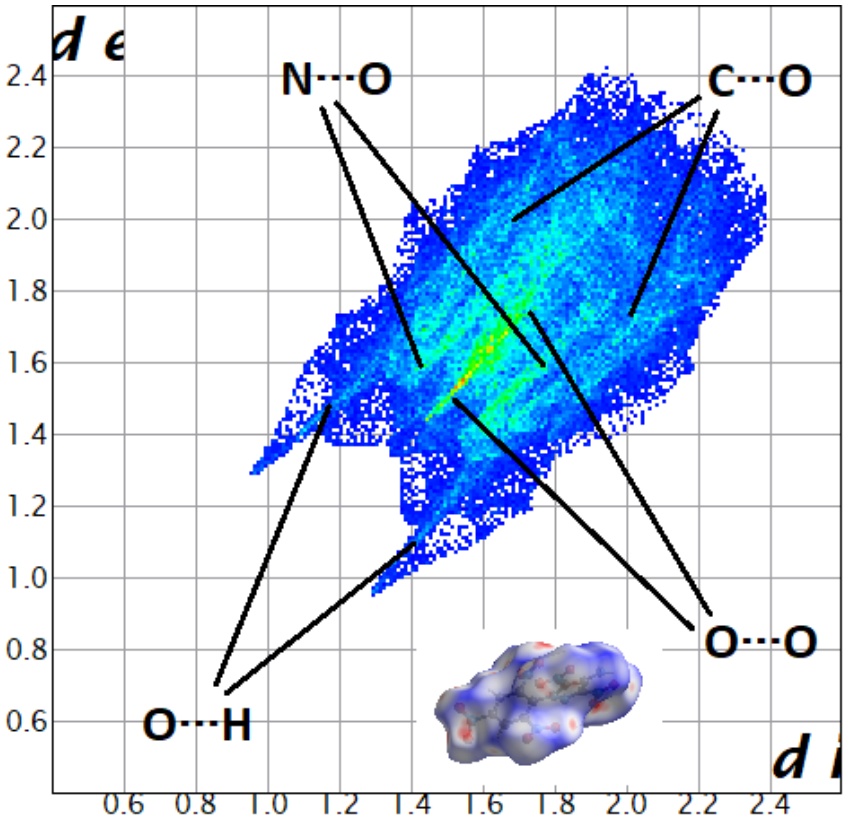

Figure 4. Two-dimensional Fingerprint plot in crystal stacking as well as the corresponding Hirshfeld surface (bottom right in the 2D plot) of PicADNP (color coding: white, distance d equals VDW distance; blue, d exceeds VDW distance; red, d smaller than VDW distance).

PicADNP exhibits various of those red dots, which point out of the molecular plane (**Figure 4**) and therefore the material is considered sensitive. Due to the arrangement of those close contacts in a nonslidable plane, a loss of stabilization and a subsequent

interlayer repulsion will occur if the material is exposed to external stimuli, which is common for sensitive materials. The title compound shows a 3D network with regard to its close contacts, which are represented by red dots on the surface in all three dimensions. This is a characteristic pattern for sensitive materials.

The analysis of the 2D Fingerprint plots shows very interesting results regarding the distribution as well as the intensity of those close contacts observed for PicADNP. A high occurrence and/or very strong stabilizing interactions, especially O···H and N···H interactions, lead to more rigid interlayers that are capable of higher energy absorption and therefore are found in less sensitive materials. Such compounds can be exposed to stronger external mechanical stimuli before they undergo an interlayer slide and the subsequent repulsion of the layers and decomposition occurs.[19] An overview of the complete population of all close contacts for PicADNP is given in **Figure 5**.

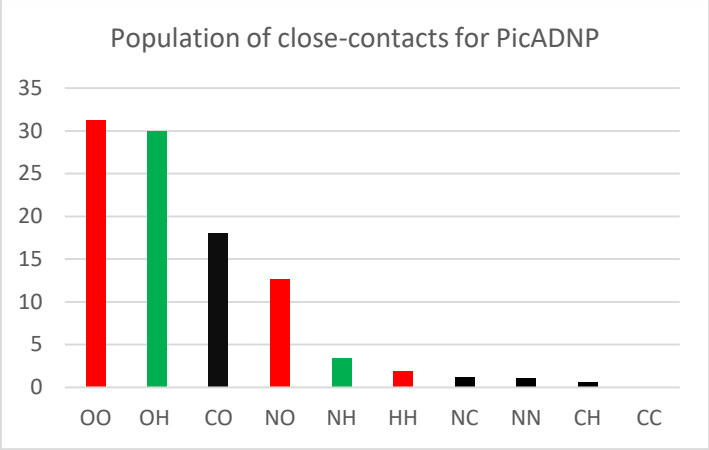

Figure 5. Population of close contacts for PicADNP (color coding: green = stabilizing interaction, red = destabilizing interaction, black = neutral interaction).

PicADNP shows a high amount of stabilizing O···H contacts (30.0%) with a high relative strength ranging from 2.3–3.0 Å. The amount of stabilizing N···H contacts is very low (3.4%) and weak (>3.3 Å) and can therefore be neglected. The same is true for the C···C, C···H, N···N, N···C, and H···H interactions as they all range between 0 and 1.9%. Another particularly important close contact interaction for sensitivity assessment is the O···O repulsion, as a high occurrence of this destabilizing interaction is typical for a material with a high sensitivity. The nitro groups of PicADNP are exposed on the molecular surface and the distance between the oxygen atoms is maximized in the layered crystal structure. However, when the layers slide after an exposure to external stimuli closer oxygen-oxygen contacts lead to a repulsion of the layers, which results in strains and subsequent decomposition.[15,16,19,20] The title compound shows a very high amount of destabilizing O···O (31.3%) and N···O close-contacts (12.6%), which is typical for a sensitive material.[16-18]

The 2D Fingerprint plot of PicADNP (**Figure 4**) exhibits two pronounced spikes that represent the strongest O···H bonds in the structure.[19] In this plot di + de (di: the

distance between the Hirshfeld surface to the nearest atom interior; de: distance from the Hirshfeld surface to the nearest atom exterior) combine to values between 2.2 and 3.6 Å, which is a typical range for hydrogen bonds. The 2D plot of the oxygen-oxygen interactions reveals, that the majority of those destabilizing close contacts range from 2.9 to 3.6 Å, which is a typical observation for sensitive materials. A similar observation is made for the destabilizing N···O close contacts, which range from 3.0–3.6 Å in the 2D plot. The majority of C···O interactions range between 2.9–4 Å and can therefore be considered medium to weak. It can be stated, that the amount of destabilizing close-contacts is higher than the amount of stabilizing interactions and PicADNP must be considered a sensitive material.

***7.3.5 Heat of formation and calculated detonation parameters*.** The performance of an energetic material is directly dependent on its density and the density of a solid material results from its packing behavior in the crystal. For PicADNP a crystal density of 1.876 g cm^{-3} was observed at 145 K. The calculated density for ambient conditions is 1.82 g cm^{-3} and exceeds the density of PETN (1.77 g cm^{-3}).[2] A requirement for the exact calculation of the heat of formation (HOF) is the application of very precise theoretical methods because experimental values are often too inaccurate.[19] Therefore the calculation of the HOF is based on *ab-initio* calculations that utilized optimized molecular geometries which were obtained by refining the geometry that was obtained from the X-ray diffraction experiments in this work. Following Trouton´s rule, the subtraction of the sublimation enthalpy from the HOF of the corresponding gas-phase species yields the HOF of the molecule.[1] The HOF of the gas-phase species was obtained by subtracting the atomization energies from the total enthalpy of the molecule.[21,22] Those calculations were carried out on a CBS-4M level of theory in combination with the crystal structures as starting points for the structure optimization. The detonation properties of PicADNP given in **Table 2** were calculated with the EXPLO5 (V6.05)[23] computer code from the extrapolated room temperature densities. The properties were calculated at the Chapman−Jouguet point with the help of the stationary detonation model using a modified Becker−Kistiakowski−Wilson state equation for the system. The C−J point was found by the Hugoniot curve of the system by its first derivative.[23,24]

The calculated energetic properties for PicADNP range between 82–93% of the values for PETN and therefore a similar explosive performance would be expected for both materials. The title compound exhibits a detonation energy of -4952 kJ kg^{-1} compared to the -5995 kJ kg^{-1} and the respective detonation temperatures are 3692 K and 3958 K. Concerning detonation pressure PicADNP shows a value of 27.2 GPa, whilst PETN exhibits a value of 31.6 GPa. The respective detonation velocities are 7993 m s^{-1} and 8525 m s^{-1}, whilst their volume of formed gas is 654.5 dm^3 kg^{-1} and 746 dm^3 kg^{-1}.

Table 2. Physical and calculated detonation parameters of PicADNP using the EXPLO5 computer code.

	PicADNP	**PETN**
formula	$C_9H_4N_8O_{10}$	$C_5H_8N_4O_{12}$
M_r [g mol^{-1}]	384.18	316.14
IS [a] [J]	7	4
FS [b] [N]	>360	73
ESD [mJ]	270	30
N[c] [%]	29.17	17.72
N + O[d] [%]	70.81	78.45
Ω_{CO2}[e] [%]	-41.6	-10.12
T_{melt}[f] [°C]	234.6	142
T_{dec}[g] [°C]	238.2	210
$\rho_{25°C}$[h] [g cm^{-3}]	1.82	1.77
ΔH_f°[i] [kJ mol^{-1}]	119	-481
EXPLO5 V 6.05		
ΔU_f°[j] [kJ kg^{-1}]	-4952	-5995
T_{C-J}[k] [K]	3692	3958
P_{C-J}[l] [GPa]	27.2	31.6
V_{det}[m] [ms^{-1}]	7993	8525
V_o[n] [dm^3 kg^{-1}]	654.5	746

[a] Impact sensitivity[25] [b] friction sensitivity[26] [c] nitrogen content [d] combined nitrogen and oxygen content [e] absolute oxygen balance assuming the formation of CO or CO_2 [f] melting point from DTA [g] decomposition from DTA [h] calculated room temperature density [i] heat of formation calculated at the CBS-4M level of theory for FMN, experimental determined for MN [j] detonation energy [k] detonation temperature [l] detonation pressure [m] detonation velocity [n] volume of detonation gases at standard temperature and pressure conditions.

Regarding the thermal stability of both materials, PicADNP surpasses PETN by over 90 °C, as the title compound melts at 234.6 °C, whilst PETN already melts at 142 °C. The same trend is observed for the sensitivities towards external stimuli, as the title compound is less sensitive towards impact (7 J compared to 4 J), insensitive towards friction (>360 N compared to 73 N), and less sensitive towards electrostatic discharge (270 mJ compared to 30 mJ). Therefore, PicADNP is considered a suitable replacement for PETN for the application in booster explosives with an increased safety profile.

***7.3.6 Small-scale shock reactivity test and booster testing*.** For the evaluation of the explosive performance of PicADNP, a small-scale shock reactivity test (SSRT) was performed to compare it with PETN. This test is suitable for the assessment of the shock reactivity (explosiveness) of potential energetic materials, often even below the corresponding critical diameter.[27,28] For this purpose samples of PicADNP and PETN were pressed into perforated steel blocks with a specific volume (V_s) and a pressure of 3 tons for five seconds. The initiation of the evaluated material was performed by using a commercially available detonator (**Figures 6** and **7**).

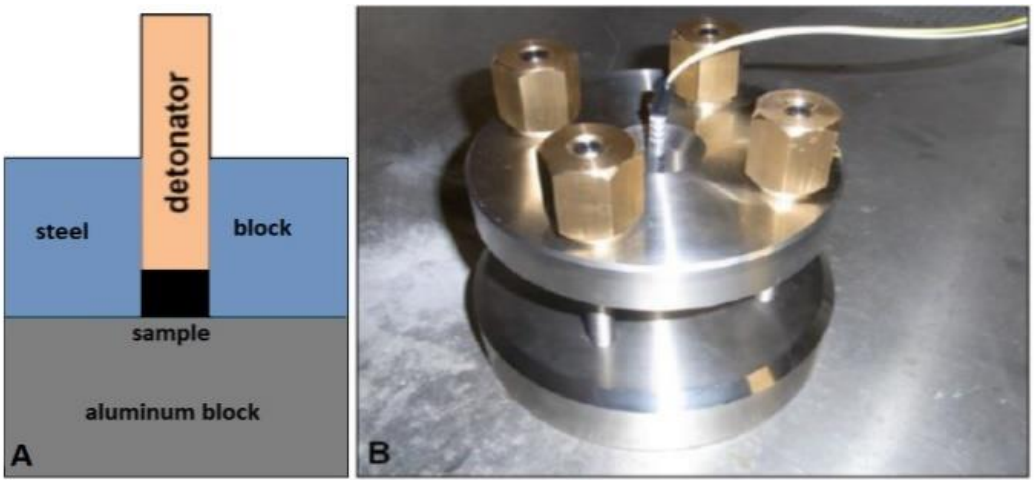

Figure 6. Details of the SSRT setup: schematic drawing (A); photograph of the test setup (B).

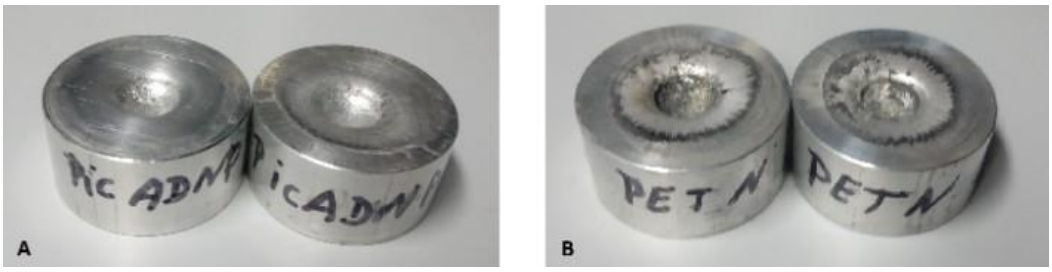

Figure 7. The SSRT results for PicADNP (A) and PETN (B): dented aluminum blocks after initiation.

The dent sizes were measured by filling them 30 times with finely powdered SiO_2 and measuring the resulting average weight from both experiments for each material. The mass of explosive and the average mass of SiO_2 required to fill the volumes of the dents are given in **Table 3**.

Table 3. SSRT values for PicADNP and PETN.

	SSRT Values	
	PicADNP	PETN
m_E[a] [mg]	491	482
m_{SiO2}[b] [mg]	514	556

[a] Mass of the explosive: $m_E = V_s \cdot \rho \cdot 0.95$, ($V_s$ = 284 mm^3) [b] Mass of SiO_2

The results of the small-scale shock reactivity test indicate, that PicADNP exhibits a slightly lower performance than PETN, which equals 92%. This result fits very well with the calculated EXPLO5 values for both materials.

In a subsequent test, the suitability of PicADNP as a booster explosive was investigated. For this purpose, four copper tubes were each filled with 200 mg of 2,2′,4,4′,6,6′-Hexanitrophenylethylen (HNS) that was pressed with 3 tons for 5 seconds. The reference samples 1 and 2 were filled with 50 mg and 100 mg of non-phlegmatized, unpressed lead azide. Samples 3 and 4 were filled with 50 and 100 mg of PicADNP, which was also pressed with 3 tons for 5 seconds. The top layers of samples 3 and 4 were 50 and 100 mg of non-phlegmatized, unpressed lead azide. The details of the experimental setup are depicted in **Figure 8**.

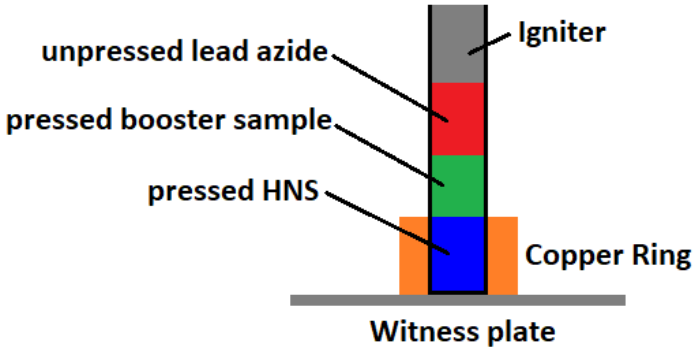

Figure 8. Schematic drawing of the booster test setup.

The reference samples 1 and 2 which contained no booster explosive show only a minor fragmentation and the witness plates are intact because the HNS could not be initiated. Sample 3 which contained 50 mg LA and 50 mg of PicADNP exhibits a significantly fragmented tube and a strong dent on the witness plate, which indicates a partial initiation of the pressed HNS. Sample 4 which contained 100 mg LA and 100 mg PicADNP shows a complete destruction of the tube and the witness plate was perforated (C), which proves the successful initiation of the pressed HNS. The samples before (A) and after the initiation (B) are depicted in **Figure 9**.

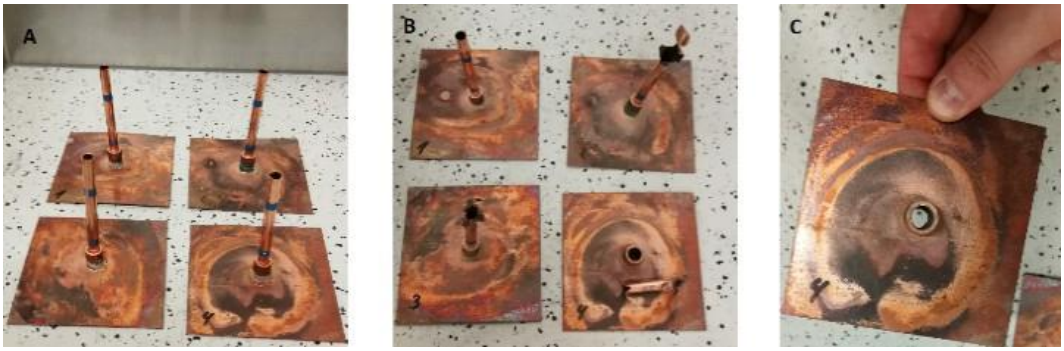

Figure 9. Filled copper tubes before the test (A); Copper tubes and witness plates after the test (B); Successful initiation for sample 4 (C).

The preparation of the samples for the booster testing shows, that PicADNP can be pressed and processed like PETN. Apparently, the material features no press dead point at 3 tons, which is an important feature for processing and application. The successful initiation of HNS in sample 4 proves the capability of PicADNP to replace PETN as a high-performing booster explosive with an increased safety profile.

7.4 Conclusions

It was shown, that the two proposed optimized synthetic protocols for the manufacturing of PicADNP are faster, greener, and scalable options for the synthesis of the target molecule. They facilitate excellent yields and a high purity among various other improvements over the previous synthesis. The older set of analytical data could be complemented with thermal analysis, Raman spectroscopy, sensitivity measurements, calculation of energetic properties, X-ray diffraction, and Hirshfeld surface analysis. The SSRT test revealed a performance similar to PETN and the sensitivities towards external stimuli are lower for PicADNP. Its thermal stability is over 90 °C higher, which makes the material safer for handling. The booster test of the title compound revealed the capability to initiate pressed HNS. Therefore, PicADNP must be considered a potential replacement for PETN and a suitable candidate for future application as a booster explosive.

7.5 Experimental Section

General Information.

HPLC grade Acetonitrile was purchased from Fisher Chemicals and Caesiumcarbonate was purchased from Merck Millipore. Picryl chloride, picryl mesylate, and KADNP were used from group internal stockpiles.

For NMR spectroscopy the solvent DMSO-d_6 was dried using a 3 Å mole sieve. Spectra were recorded on a Bruker Avance III spectrometer operating at 400.1 MHz (^{1}H), 100.6 MHz (^{13}C), and 28.9 MHz (^{14}N). Chemical shifts are referred to TMS (^{1}H, ^{13}C) and $MeNO_2$ (^{14}N). Raman spectra were recorded with a Bruker MultiRam FT Raman spectrometer using a neodymium-doped yttrium aluminum garnet (Nd:YAG) laser (λ = 1064 nm) with 1074 mW. The samples for Infrared spectroscopy were placed under ambient conditions onto an ATR unit using a Perkin Elmer Spectrum BX II FT-IR System spectrometer. Melting and/or decomposition points were detected with a OZM DTA 552-Ex instrument. The scanning temperature range was set from 293 K to 673 K at a scanning rate of 5 K min^{-1}. DSC values were determined on a Mettler-Toledo DSC 822e with an Intracooler (Julabo FT900) and a heating rate of 5 K min^{-1}. Elemental analysis was performed with a Vario EL instrument and a Metrohm 888 Titrando device.

Caution! All investigated compounds are explosives, which show partly increased sensitivities toward various stimuli (e.g. higher temperatures, impact, friction, or electrostatic discharge). Therefore, proper safety precautions (safety glasses, Kevlar gloves, and earplugs) have to be applied while synthesizing and handling the described compounds.

7.5.1 Synthetic protocol 1 – *Starting from picryl chloride.* Potassium 4-amino-3,5-dinitropyrazol-1-ide (1.00 g, 4.36 mmol) was added to a solution of picryl chloride (2.70 g, 10.91 mmol) in acetonitrile (150 mL). The reaction mixture was stirred at 70 °C for 8 h before it was allowed to cool to ambient temperature. The precipitated beige solid was filtered off and the dark red solution was poured into 300 mL of ice water and stirred for 2 hours. The precipitated yellow solid was filtered off, washed with water until the filtrate was colorless, and dried under ambient conditions (1.47 g, yield: 88%).

7.5.2 Synthetic protocol 2 – *Starting from picryl mesylate.* Potassium 4-Amino-3,5-dinitropyrazol-1-ide (0.75 g, 3.26 mmol) was added to a solution of picryl mesylate (2.00 g, 6.51 mmol) in acetonitrile (150 mL). Cesium carbonate (0.11 g, 326 µmol, 10 mol-%) was added and the reaction mixture was stirred at 70 °C for 6 h before it was allowed to cool to ambient temperature. The precipitated beige solid was filtered off and the bright orange solution was poured into 250 mL of ice water and stirred until a yellow solid precipitated. The yellow solid was filtered off, washed with water until the filtrate was colorless, and dried under ambient conditions (966 mg, yield: 77%).

^{1}H NMR (DMSO-d_6, 400 MHz): δ 9.24 (s, 2H), 7.89 (s, 2H) ppm. **^{13}C{^{1}H} NMR** (DMSO-d_6, 100 MHz): δ 148.3, 145.9, 144.5, 132.5, 130.2, 128.7, 125.7 ppm. **^{14}N NMR** (DMSO-d_6, 29 MHz): δ -23.5 (s, NO_2) ppm. **IR** (ATR): $\tilde{\nu}$ = 3477 (w, NH_2), 3362 (w, NH_2), 3096 (w, C_{arom}-H), 1644 (w, C=N), 1612 (w, C=C_{arom}), 1560 (m, C=C_{arom}), 1542 (m, NO_2), 1519 (m, NO_2), 1459 (m, C=C_{arom}), 1409 (w), 1395 (w), 1362 (w), 1337 (m, C-NO_2), 1318 (m, C-NO_2), 1278 (m), 1226 (m), 1193 (m), 1169 (m), 1089 (w), 982 (w), 935 (w), 912 (m, C-NO_2), 865 (m), 820 (m), 786 (w), 772 (m), 754 (m), 742 (m), 724 (m), 715 (m), 685 (w), 660 (m), 633 (w), 613 (w), 571 (w), 478 (m), 442 (m), 408 (m) cm^{-1}. **Raman** (300 mW): $\tilde{\nu}$ = 3364 (3), 3087 (3), 1643 (8), 1621 (16), 1556 (10), 1488 (10), 1410 (10), 1398 (28), 1364 (100), 1319 (5), 1277 (20), 824 (27), 773 (11), 727 (6), 351 (7), 285 (7), 205 (5), 92 (49) cm^{-1}. **Elemental Analysis** calcd (%) for $C_9H_4N_8O_{10}$: C 28.14; H 1.05; N 29.17 Experimental: C 28.08; H 1.04; N 29.16. **DTA**: 234.6 °C (m.p.), 238.2 °C (dec.) **DSC**: 233.6 °C (m.p.), 237.5 °C (dec.) **IS**: 7 J. **FS**: >360 N. **ESD**: 270 mJ.

7.5.3 X-Ray Measurements. Single crystals of 3,5-dinitro-1-(2,4,6-trinitrophenyl)-1*H*-pyrazol-4-amine were obtained after slow solvent evaporation of acetone. Data collection was performed with an Oxford Xcalibur 3 diffractometer with a CCD area detector, equipped with a multilayer monochromator, a Photon 2 detector and a rotating-anode generator were employed for data collection using Mo-Kα radiation (λ = 0.7107 Å). Data collection and reduction were carried out using the Crysalispro software.[29] The structures were solved by direct methods (SIR-2014)[30] and refined

(SHELXLE)[31] by full-matrix least-squares on F2 (ShelxL)[32,33] and finally checked using the platon software[34] integrated with the WinGX software suite.[35] The non-hydrogen atoms were refined anisotropically and the hydrogen atoms were located and freely refined. All Diamond 3 plots are shown with thermal ellipsoids at the 50% probability level and hydrogen atoms are shown as small spheres of arbitrary radius. The crystal structure of PicADNP has been deposited under CCDC number 2058636.

ASSOCIATED CONTENT

Supporting Information

The Supporting Information is available free of charge on the ACS Publication website.

^{1}H, ^{13}C, ^{14}N NMR spectra; DSC & DTA graphs; Detonation parameter calculations (output files); Crystallographic information; Enlarged pictures (PDF)

X-ray data for PicADNP (CIF)

CCDC: 2058636

This material is available free of charge via the Internet at http://pubs.acs.org

AUTHOR INFORMATION

Corresponding Author

* tmk@cup.uni-muenchen.de

ORCID

Prof. Dr. Thomas M. Klapötke: 0000-0003-3276-1157

Prof. Dr. Konstantin Karaghiosoff: 0000-0002-8855-730X

Dominik E. Dosch: 0000-0003-4804-6473

Veronika Fuchs: 0000-0003-4035-9387

Daniel Bauer: 0000-0002-3727-2857

Notes

The authors declare no competing financial interests.

7.6 Acknowledgment

For financial support of this work by Ludwig−Maximilian University (LMU), the Office of Naval Research (ONR) under grant no. ONR.N00014-16-1-2062 and the Strategic Environmental Research and Development Program (SERDP) under contract no. WP19-1287 are gratefully acknowledged. The authors would like to thank Mr. Max Born and Mr. Maximilian Benz for help with the SSRT and booster testing.

7.7 References

[1] T. M. Klapötke, In *Chemistry of High-Energy Materials*, 5th ed., De Gruyter: Berlin/Boston, **2019**.

[2] T. M. Klapötke, In *Energetic Materials Encyclopedia*, De Gruyter: Berlin/Boston, **2018**.

[3] R. Hollands, P. Barnes, R. Moss, M. Sharp, *Explosive booster selection criteria for insensitive munitions applications*, Insensitive Munitions and Energetic Materials Technology Symposium, Bristol, **2006**.

[4] J. Akhavan, In *The Chemistry of Explosives*, 2nd ed., The Royal Society of Chemistry: Cambridge, **2004**, p. 118-148.

[5] B. Wu, H. Yang, Z. Wang, Q. Lin, X. Ju, C. Lu, G. Cheng, *RSC Adv.* **2014**, *4* (95), 53282-53290.

[6] X. Li, X. Zhang, W. Yang, C. Song, H. Sun, J. Wang, *Propellants Explos. Pyrotech.* **2019**, *44* (5), 550-556.

[7] C. Claessen, DE265025A, **1912**.

[8] T. M. Klapötke, G. Lemarchand, T. Lenz, M. Mühlemann, J. Stierstorfer, R. Weber, *PETN - a sensitivity study*, New Trends in Research of Energetic Materials Conference, Pardubice, **2020**.

[9] J. Šelešovsky, J. Pachmaň, M. Hanus, *Proceedings of the Sixth Seminar New Trends in Research of Energetic Materials*, New Trends in Research of Energetic Materials Conference, Pardubice, **2003**, 309–321.

[10] R. K. Wharton, J. Harding, *J. Energ. Mater.* **1993**, *11* (1), 51-65.

[11] B. Z. Wang, Y. I. Wang, Z. Z. Zhang, C. I. Xiong, Y. G. Zhang, *Hanneng Cailiao* **2009**, *17* (3), 293-295.

[12] European Chemicals Agency Candidate List of Substances of Very High Concern for Authorisation. https://echa.europa.eu/candidate-list-table (accessed Dec 30, 2020).

[13] European Chemicals Agency Substance Infocard: Hydrogen Fluoride. https://echa.europa.eu/de/substance-information/-/substanceinfo/100.028.759 (accessed Jan 17, 2021).

[14] I. R. Lewis, N. W. Daniel, P. R. Griffiths, *Appl. Spectrosc.* **1997**, *51* (12), 1854-1867.

[15] Y. Ma, A. Zhang, X. Xue, D. Jiang, Y. Zhu, C. Zhang, *Cryst. Growth Des.* **2014**, *14* (11), 6101-6114.

[16] C. Zhang, X. Xue, Y. Cao, Y. Zhou, H. Li, J. Zhou, T. Gao, *CrystEngComm* **2013**, *15* (34), 6837-6844.

[17] M. Reichel, D. E. Dosch, T. M. Klapötke, K. Karaghiosoff, *J. Am. Chem. Soc.* **2019**, *141* (50), 19911-19916.

[18] D. E. Dosch, M. Reichel, M. Born, T. M. Klapötke, K. Karaghiosoff, *Cryst. Growth Des.* **2021,** *21* (1), 243-248.

[19] J. Zhang, Q. Zhang, T. T. Vo, D. A. Parrish, J. n. M. Shreeve, *J. Am. Chem. Soc.* **2015**, *137* (4), 1697-1704.

[20] Y. Tang, J. Zhang, L. A. Mitchell, D. A. Parrish, J. n. M. Shreeve, *J. Am. Chem. Soc.* **2015**, *137* (51), 15984-15987.

[21] L. A. Curtiss, K. Raghavachari, P. C. Redfern, J. A. Pople, *J. Chem. Phys.* **1997**, *106* (3), 1063-1079.

[22] E. F. C. Byrd, B. M. Rice, *J. Phys. Chem. A* **2006**, *110* (3), 1005-1013.

[23] M. Suceska, Explo5 V6.05; Brodarski Institute: Zagreb, **2018**.

[24] T. M. Klapötke, B. Krumm, F. X. Steemann, K.-D. Umland, *Z. Anorg. Allg. Chem.* **2010**, *636* (13-14), 2343-2346.

[25] NATO. Standardization Agreement 4489 (STANAG 4489), Explosives, Impact Sensitivity Tests; Brussels, Belgium, **1999**.

[26] NATO. Standardization Agreement 4487 (STANAG 4487), Explosives, Friction Sensitivity Tests; Brussels, Belgium, **2002**.

[27] H. W. Sandusky, R. H. Granholm, D. G. Bohl, IHTR 2701, Naval Surface Warfare Center, Indian Head Division, MD, USA, **2005**.

[28] J. E. Felts, H. W. Sandusky, R. H. Granholm, *AIP Conf. Proc.* **2009**, *1195* (1), 233–236.

[29] CrysAlisPro (Version 171.33.41); Oxford Diffraction Ltd., **2009**.

[30] M. C. Burla, R. Caliandro, B. Carrozzini, G. L. Cascarano, C. Cuocci, C. Giacovazzo, M. Mallamo, A. Mazzone, G. Polidori, *J. Appl. Crystallogr.* **2015**, *48* (1), 306-309.

[31] C. B. Hubschle, G. M. Sheldrick, B. Dittrich, *J. Appl. Crystallogr.* **2011**, *44* (6), 1281-1284.

[32] G. M. Sheldrick, SHELXL-97, Program for the Refinement of Crystal Structures, University of Göttingen, Germany, **1997**.

[33] G. A. Sheldrick, *Acta Crystallogr., Sect. A* **2008**, *64* (1), 112-122.

[34] A. L. Spek, PLATON, A Multipurpose Crystallographic Tool, Utrecht University, The Netherlands, **1999**.

[35] L. J. Farrugia, *J. Appl. Crystallogr.* **2012**, *45* (4), 849-854.

7.8 Supporting Information

1 NMR spectra

1.1 ^{1}H NMR spectrum of PicADNP

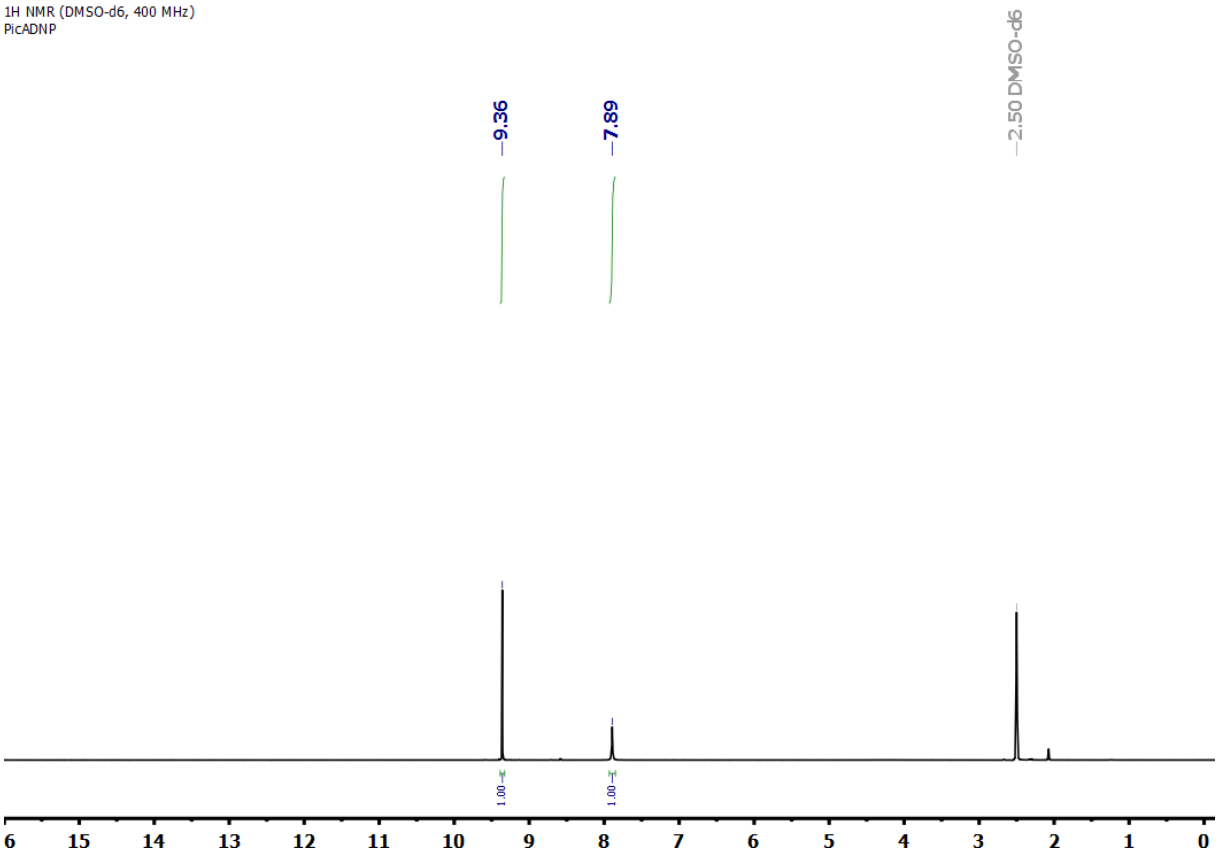

1.2 $^{13}C\{^{1}H\}$ NMR spectrum of PicADNP

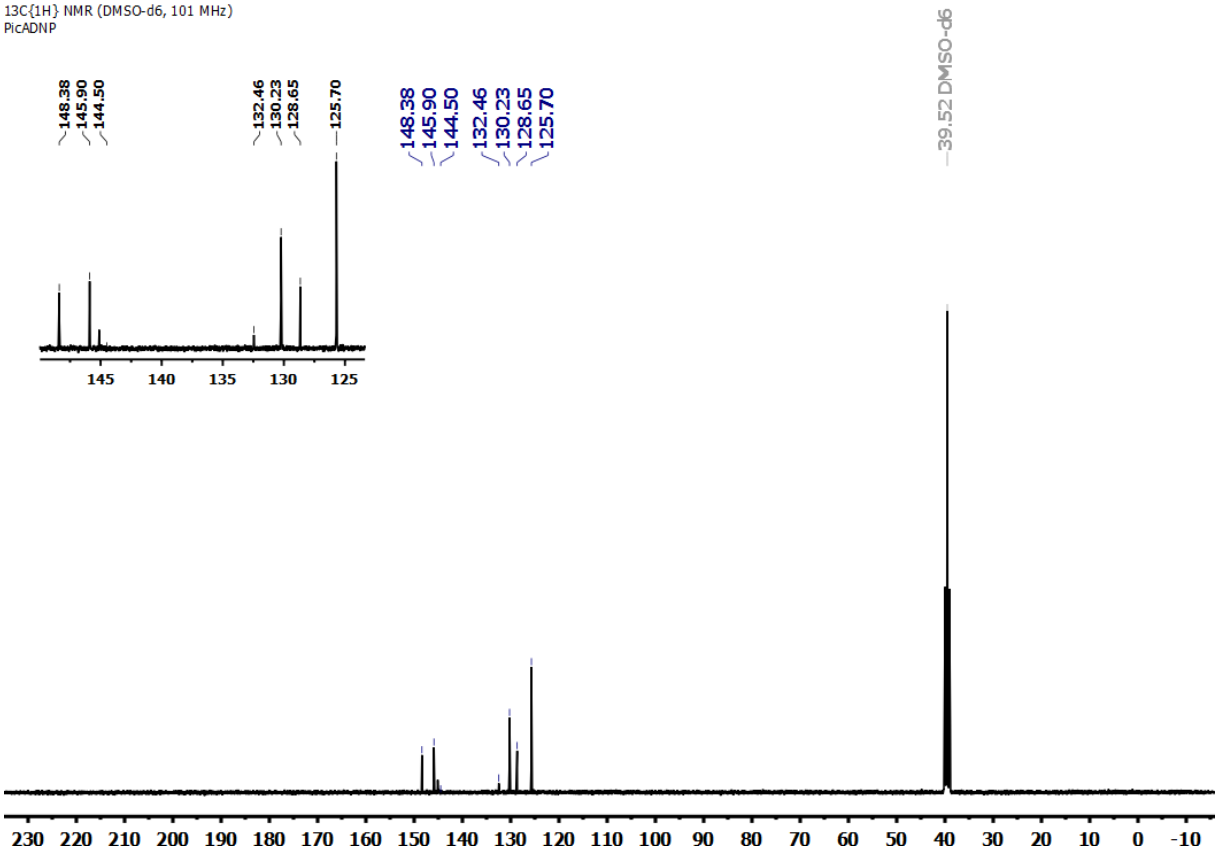

1.3 $^{14}N\{^{1}H\}$ NMR spectrum of PicADNP

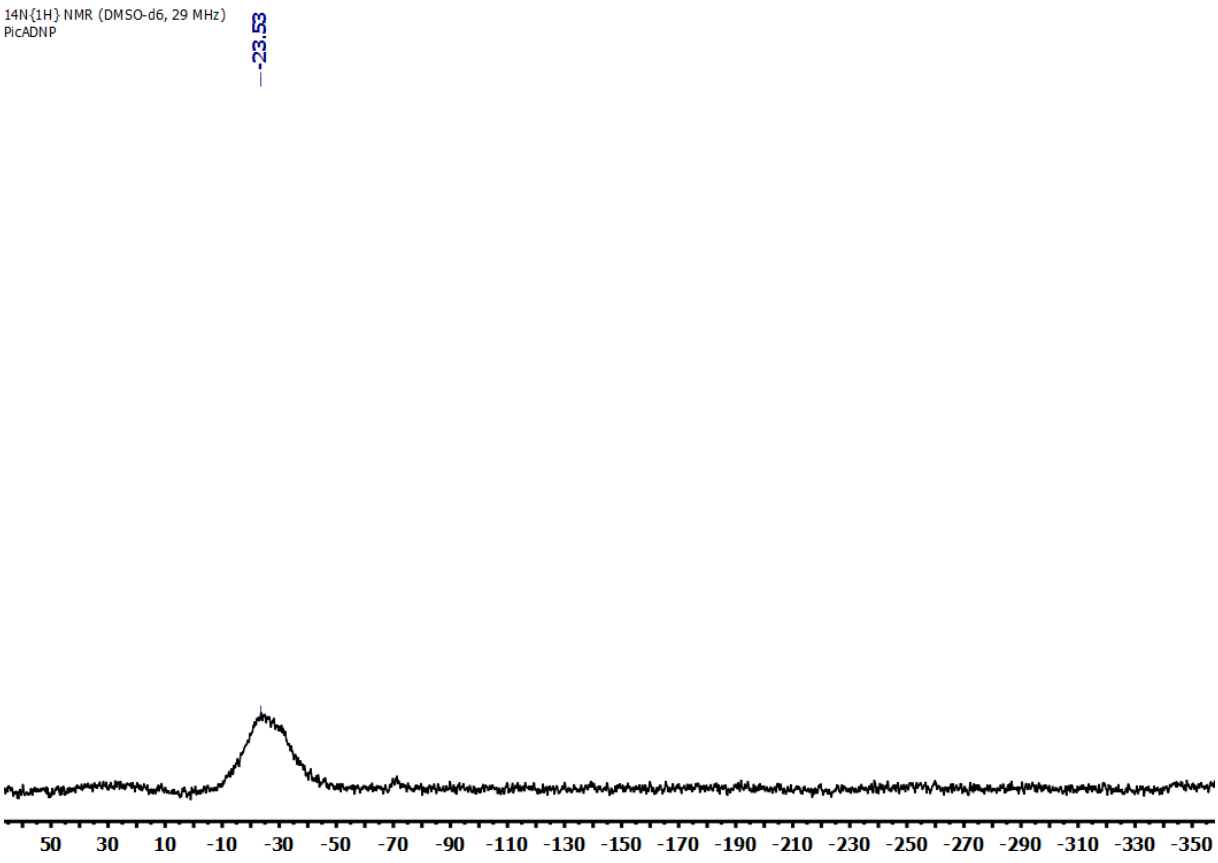

2. IR and Raman data of PicADNP

2.1 IR data of PicADNP

IR (ATR): $\tilde{\nu}$ = 3477 (w, NH_2), 3362 (w, NH_2), 3096 (w, C_{arom}-H), 1644 (w, C=N), 1612 (w, $C=C_{arom}$), 1560 (m, $C=C_{arom}$), 1542 (m, NO_2), 1519 (m, NO_2), 1459 (m, $C=C_{arom}$), 1409 (w), 1395 (w), 1362 (w), 1337 (m, C-NO_2), 1318 (m, C-NO_2), 1278 (m), 1226 (m), 1193 (m), 1169 (m), 1089 (w), 982 (w), 935 (w), 912 (m, C-NO_2), 865 (m), 820 (m), 786 (w), 772 (m), 754 (m), 742 (m), 724 (m), 715 (m), 685 (w), 660 (m), 633 (w), 613 (w), 571 (w), 478 (m), 442 (m), 408 (m) cm^{-1}.

2.1 Raman data of PicADNP

Raman (300 mW): $\tilde{\nu}$ = 3364 (3), 3087 (3), 1643 (8), 1621 (16), 1556 (10), 1488 (10), 1410 (10), 1398 (28), 1364 (100), 1319 (5), 1277 (20), 824 (27), 773 (11), 727 (6), 351 (7), 285 (7), 205 (5), 92 (49) cm^{-1}.

3. Elemental analysis of PicADNP

Calculated PicADNP: C 28.14; H 1.05; N 29.17 Experimental: C 28.08; H 1.04; N 29.16 (%).

4. Sensitivity values of PicADNP

BAM drop hammer: 7 J; Friction tester: >360 N; ESD: 270 mJ (grain size: 100–500 µm).

5. DSC and DTA data of PicADNP

5.1 DTA data of PicADNP

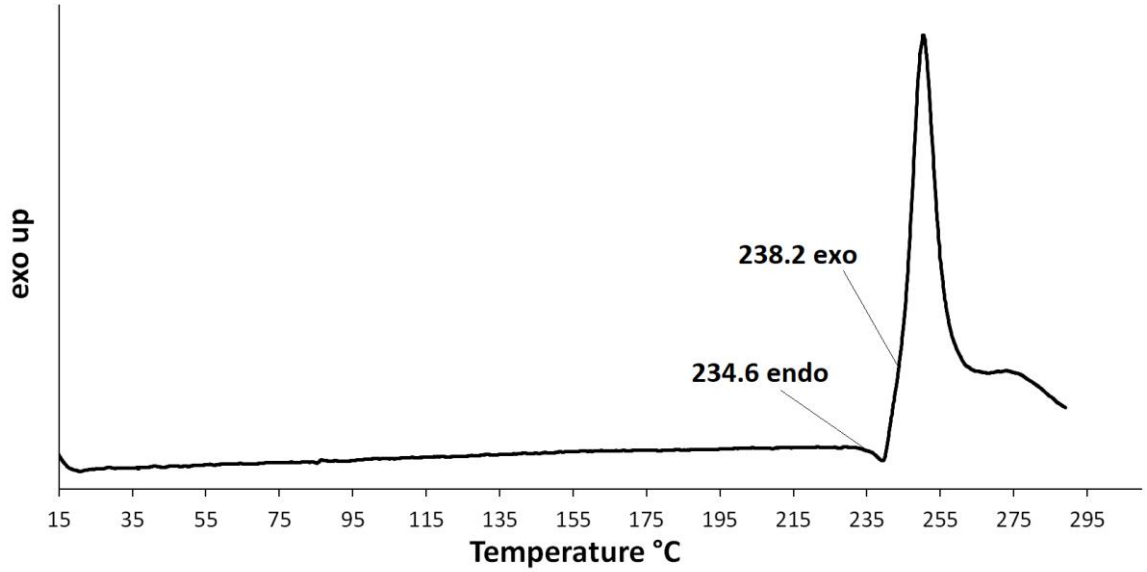

$T_{(melt)}$ (DTA): 234.6 °C, **$T_{(dec.)}$ (DTA)**: 238.2 °C.

5.2 DSC data of PicADNP

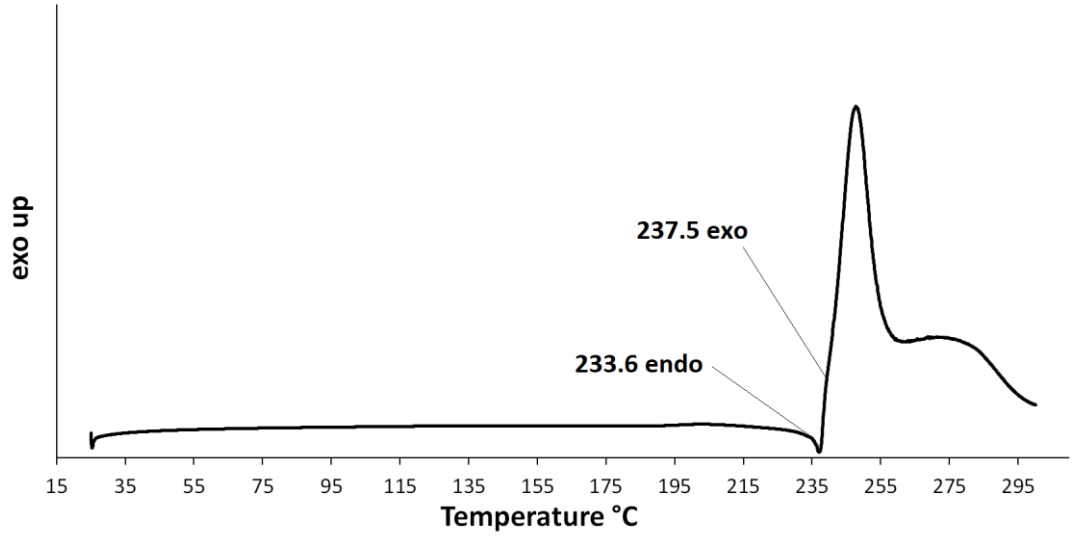

$T_{(melt)}$ (DSC): 233.6 °C, **$T_{(dec.)}$ (DSC):** 237.5 °C

6. Detonation Parameters of PicADNP

Reactant information:

---

1. 3,5-dinitro-1-(2,4,6-trinitrophenyl)-1H-pyrazol-4-amine (PicADNP), 100 %

C(9,000) H(4,000) N(8,000) O(10,000)

Molecular weight	= 384,18
Density of reactant	= 1,8212 g/cm^3
Initial pressure	= 0,1 MPa
Oxygen balance	= -41,64498 %
Enthalpy of formation	= 309,75 kJ/kg
Internal energy of formation	= 387,18 kJ/kg

Detonation parameters (at the C-J point):

Heat of detonation	= -4952,135 kJ/kg
Detonation temperature	= 3692,85 K
Detonation pressure	= 27,15533 GPa
Detonation velocity	= 7993,311 m/s
Particle velocity	= 1865,388 m/s
Sound velocity	= 6127,923 m/s
Density of products	= 2,375588 g/cm^3
Volume of products	= 0,4209485 cm^3/g
Exponent 'Gamma'	= 3,285054
Moles of gaseous products	= 10,28134 mol/mol explosive
Moles of condensed products	= 3,677468 mol/mol explosive
Volume of gas at STP	= 654,4929 dm^3/kg
Mean molecular mass of gas. prod.	= 33,0702 g/mol
Mean molecular mass of cond.prod.	= 12,011 g/mol
Mean molecular mass of all prod.	= 27,52212 g/mol
Entropy of products	= 6,214 kJ/kg K
Internal energy of products	= 6691,984 kJ/kg, i.e. 12,18744 kJ/cm^3
Compression energy	= 1739,849 kJ/kg, i.e. 3,168613 kJ/cm^3
Total heat energy	= -4952,134 kJ/kg, i.e. -9,018827 kJ/cm^3

Composition of detonation products (23):

Products	mol/mol EM	mol/kg EM	Mol %	Mass %
N2 =	3,986517E+00	1,037680E+01	28,5592	29,0685
C(d) =	3,677468E+00	9,572353E+00	26,3451	11,4974
CO2 =	2,733362E+00	7,114869E+00	19,5816	31,3125
CO =	1,562918E+00	4,068233E+00	11,1966	11,3951
CH2O2 =	1,011816E+00	2,633730E+00	7,2486	12,1217
H2O =	9,465551E-01	2,463858E+00	6,7811	4,4387
NH3 =	1,380082E-02	3,592318E-02	0,0989	0,0612
HCN =	1,300441E-02	3,385014E-02	0,0932	0,0915
H2 =	1,202942E-02	3,131227E-02	0,0862	0,0063
CH4 =	8,492831E-04	2,210662E-03	0,0061	0,0035
C2H4 =	1,773163E-04	4,615496E-04	0,0013	0,0013
CNO =	7,456259E-05	1,940845E-04	0,0005	0,0008
CH3OH =	5,756598E-05	1,498427E-04	0,0004	0,0005
H =	5,523641E-05	1,437789E-04	0,0004	0,0000
NH2 =	3,745026E-05	9,748205E-05	0,0003	0,0002
C2H6 =	3,572050E-05	9,297951E-05	0,0003	0,0003
N2H4 =	1,506050E-05	3,920210E-05	0,0001	0,0001
HCNO =	1,279110E-05	3,329489E-05	0,0001	0,0001
CH2O =	1,182619E-05	3,078325E-05	0,0001	0,0001
H2O2 =	7,112425E-06	1,851346E-05	0,0001	0,0001
N =	3,013166E-06	7,843193E-06	0,0000	0,0000
N2O =	1,016965E-06	2,647132E-06	0,0000	0,0000
C(gr) =	6,902717E-19	1,796759E-18	0,0000	0,0000

Excluded products (11):

C; C(Liq.1); C(Liq.2); H2O(l); N2O3; NO;

NO2; O; O2; O3; OH;

7. Structure Refinement Data of PicADNP

Empirical formula	C9 H4 N8 O10	
Formula weight	384.20	
Temperature	123(2) K	
Wavelength	0.71073 Å	
Crystal system	Monoclinic	
Space group	$P2_1/c$	
Unit cell dimensions	a = 10.1535(6) Å	α = 90°.
	b = 9.6147(8) Å	β = 91.842(5)°.
	c = 13.9425(9) Å	γ = 90°.
Volume	1360.40(16) $Å^3$	
Z	4	
Density (calculated)	1.876 Mg/m^3	
Absorption coefficient	0.173 mm^{-1}	
F(000)	776	
Crystal size	0.300 x 0.300 x 0.050 mm^3	
Theta range for data collection	2.007 to 28.275°.	
Index ranges	-13<=h<=12, -12<=k<=10, -18<=l<=17	
Reflections collected	9420	
Independent reflections	3162 [R(int) = 0.0492]	
Completeness to theta = 25.242°	99.8 %	
Absorption correction	Semi-empirical from equivalents	
Max. and min. transmission	1.00000 and 0.94650	
Refinement method	Full-matrix least-squares on F^2	
Data / restraints / parameters	3162 / 0 / 254	
Goodness-of-fit on F^2	1.039	
Final R indices [I>2sigma(I)]	R1 = 0.0534, wR2 = 0.0912	
R indices (all data)	R1 = 0.1047, wR2 = 0.1113	
Extinction coefficient	n/a	
Largest diff. peak and hole	0.289 and -0.244 $e.Å^{-3}$	

8. Enlarged Figures from the Manuscript

8.1 Enlarged Figures

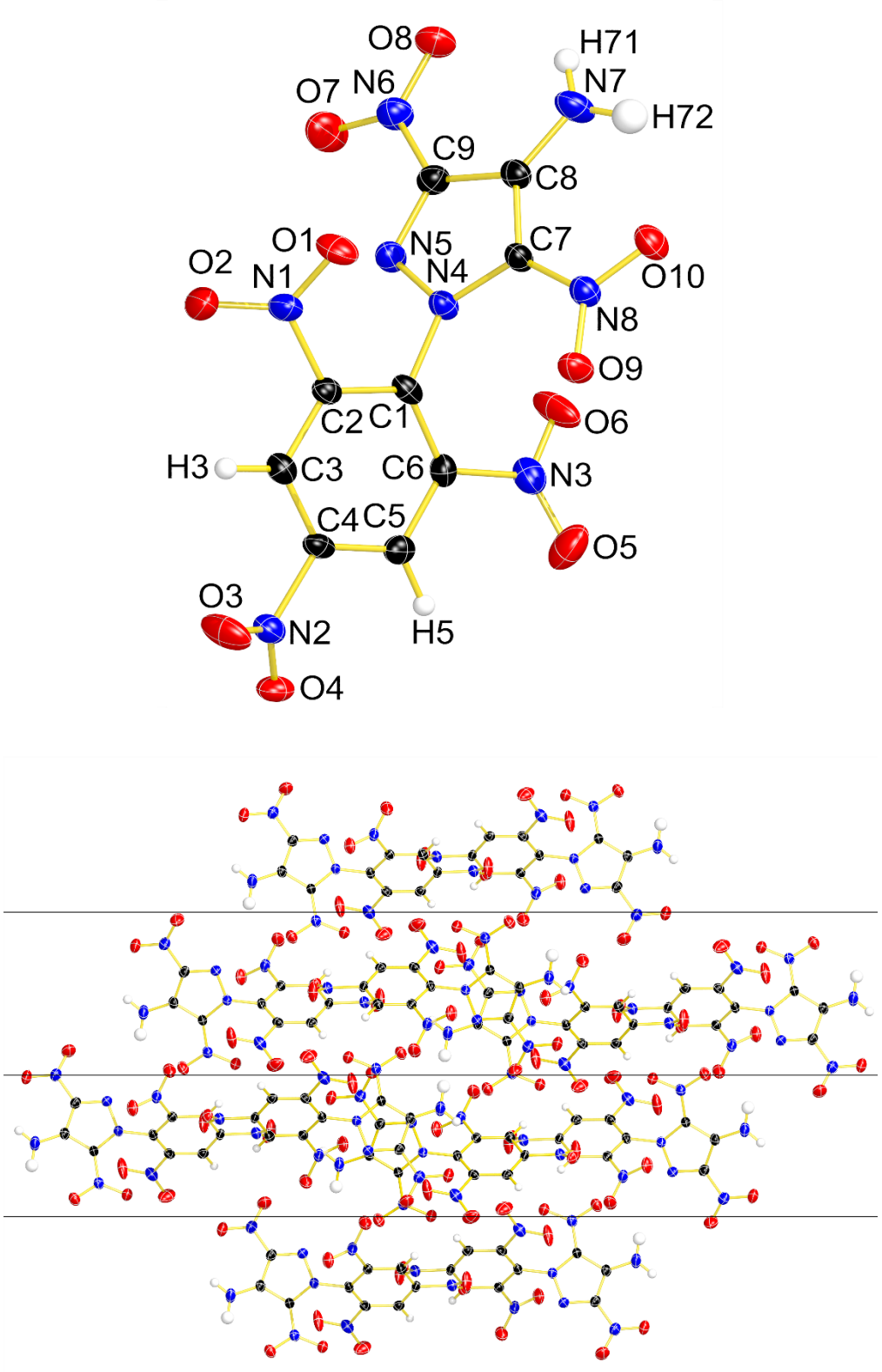

Enlarged Pictures for **Figure 3.**

8.2 Enlarged Hirshfeld surface picture & detailed 2D Fingerprint plot graphics

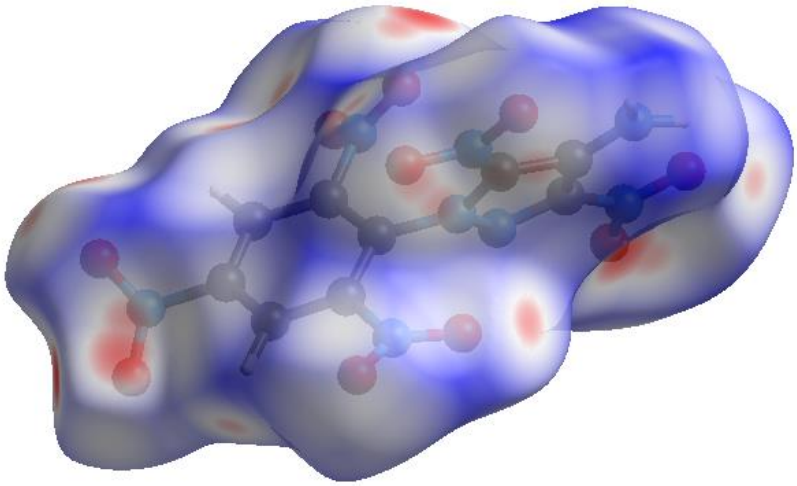

Enlarged Picture of the calculated Hirshfeld surface for PicADNP. Red dots represent close contacts.

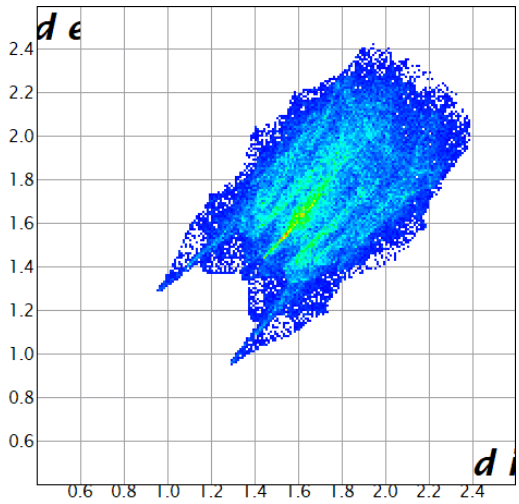

Complete 2D Fingerprint plot of PicADNP.

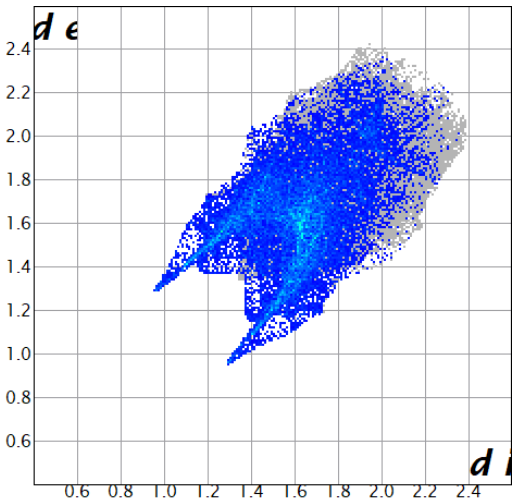

Fingerprint plot of the O···H Interactions.

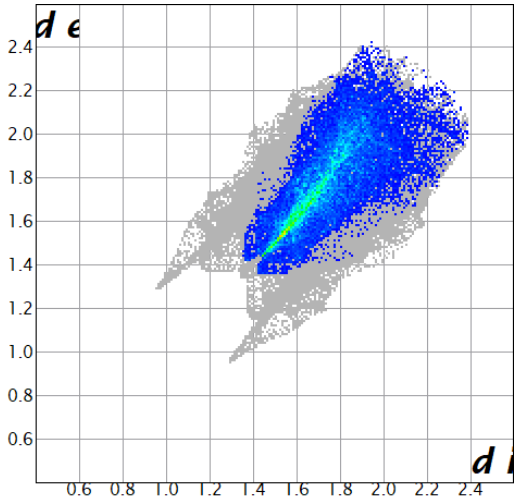

Fingerprint plot of the O···O interactions.

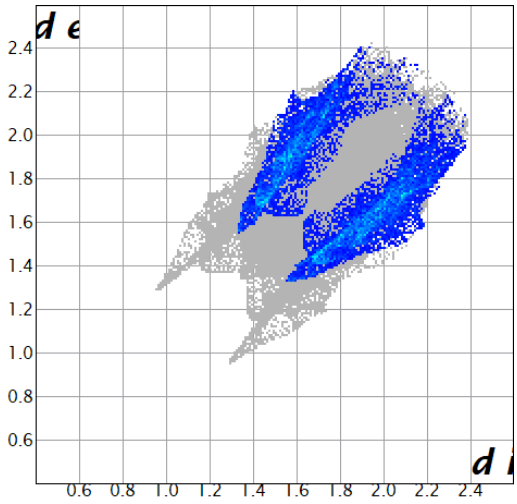

Fingerprint plot of the C···O Interactions.

Appendix

Appendix I – List of Publications

[1] D. E. Dosch, K. Andrade, B. Krumm, T.M. Klapötke, An Optimized & Scaled-Up Synthetic Procedure for Trinitroethyl Formate TNEF, Accepted and prepublished in *Propellants, Explos., Pyrotech.* **2021**

(doi: 10.1002/prep.202000323)

[2] D. E. Dosch, T. M. Klapötke, Scalability of a Time- and Cost-Effective Procedure for the Synthesis of Picryl Bromide, *Org. Process Res. Dev.* **2019**, *23*, 9, p. 2096–2098.

(doi: 10.1021/acs.oprd.9b00313)

[3] M. Reichel, D. E. Dosch, K. Karagiosoff, T. M. Klapötke, Correlation between Structure and Energetic Properties of Three Nitroaromatic Compounds: *Bis(2,4-dinitrophenyl) Ether,* Bis(2,4,6-trinitrophenyl) Ether *and* Bis(2,4,6-trinitrophenyl) Thioether *J. Am. Chem. Soc.* **2019**, 141, 50, p. 19911–19916.

(doi: 10.1021/jacs.9b11086)

[4] D. E. Dosch, M. Reichel, M. Born, K. Karaghiosoff, T. M. Klapötke, Investigation of Structure-Property Relationships of Three Nitroaromatic Compounds: *1-Fluoro-2,4,6-trinitrobenzene, 2,4,6-Trinitrophenyl methanesulfonate and 2,4,6-Trinitrobenzaldehyde*, *Cryst. Growth Des.* **2021**, *21*, 1, p**.** 243–248**.**

(doi: 10.1021/acs.cgd.0c01049)

[5] D. Bauer, D. E. Dosch, V. Fuchs, K. Karaghiosoff, T. M. Klapötke, A Study of *3,5-Dinitro-1-(2,4,6-trinitrophenyl)-1H-pyrazol-4-amine* (PicADNP) as a New High Energy Density Booster Explosive, *Eur. J. Org. Chem.* **2021**, *2021*, 1964–1970.

(doi: 10.1002/ejoc.202100159)

[6] Cover Feature – *Eur. J. Org. Chem.* (doi:10.1002/ejoc.202100321)